Государственный научный центр
Российской Федерации
ИНСТИТУТ ЯДЕРНОЙ ФИЗИКИ
им. Г.И. Будкера СО РАН

ОБЪЕДИНЕННАЯ USA–CERN–JAPAN УСКОРИТЕЛЬНАЯ ШКОЛА – ВЧ ТЕХНИКА ДЛЯ УСКОРИТЕЛЕЙ

(9–18 сетября 1996 г., Япония)

ЛЕКЦИИ, ПРОЧИТАННЫЕ СОТРУДНИКАМИ
ИЯФ СО РАН

НОВОСИБИРСК

Content

Тематика этих лекций была предложена сотрудникам ИЯФ организаторами школы. Все лекции данной школы будут опубликованы в конце 1997 – начале 1998 г. Институт, по-видимому, получит несколько экземпляров, которые будут доступны для ознакомления.

BEAM – CAVITY INTERACTION BEAM LOADING

M.M. KARLINER
Budker Institute of Nuclear Physics
630090 Novosibirsk, Russia

The interaction of a beam with a cavity and a generator in cyclic accelerators or storage rings is investigated. Application of Maxwell's equations together with the nonuniform boundary condition allows one to get an equivalent circuit for a beam loaded cavity. The general equation for beam loading is obtained on the basis of the equivalent circuit, and the beam admittance is calculated. Formulas for power consumption by a beam loaded cavity are derived, and the optimal tuning and coupling factor are analyzed.

1 Introduction

In this lecture we shall discuss the beam-cavity interaction in cyclic accelerators or storage rings. One or more cavities are used to impart some energy to particles during each revolution in order to accelerate them or to compensate for radiation losses. In proton storage rings RF cavities are used mainly to maintain bunching during collision (and acceleration during the process of energy rise).

f_0 — particle revolution frequency,
$f = h \cdot f_0$ — frequency of an accelerating field,
h — harmonic number,
$f_B = q \cdot f_0$ — recurrence frequency of bunches,
q — number of bunches.

The frequency of the accelerating field is usually a multiple of the recurrence frequency of bunches as well as of revolution frequency. As a limit, the number of bunches can equal the harmonic number.

Further, we assume the bunches to be uniformly distributed along the orbit. The beam at the cavity is seen as a succession of short current pulses. In the simplest case all pulses are equally spaced and equal in amplitude (see Fig. 1).

The frequency spectrum of such a current represents a sequence of harmonics spaced at intervals equal to the recurrence frequency of bunches $f_B = q \cdot f_0$ (see Fig. 2). The upper limit of this spectrum is determined by current pulse length.

The amplitudes of all harmonics having a time period much greater than

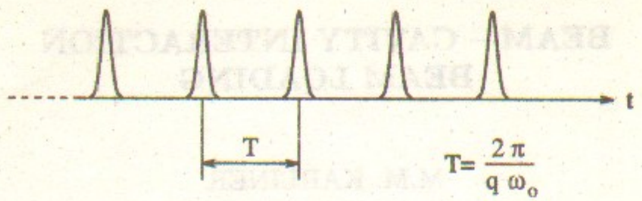

Figure 1: Beam current.

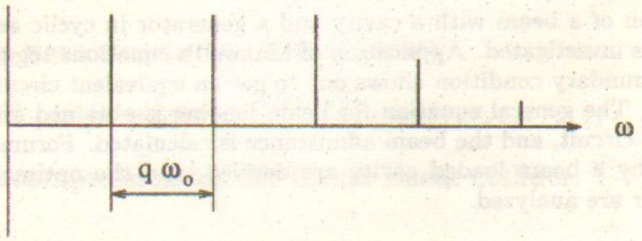

Figure 2: Beam current spectrum.

the pulse length are equal to $I_m = 2I_0$, where I_0 is the average current in an accelerator.

Among the current harmonics is the one whose frequency is equal to the accelerating frequency. The beam–cavity interaction occurs mainly at this frequency.

The beam crossing the cavity induces some voltage on it. Thus the voltage across an accelerating gap is the sum of the beam-induced voltage and the voltage produced by a generator. The phase relation between these voltages is determined by the condition that the energy gained by the particle during each crossing is equal to a specified value eV. The last is equal to radiation energy losses or an acceleration per revolution.

The object of the beam–cavity interaction theory is to establish an equation for an equilibrium in order to obtain relation that allows the calculation and optimization of the basic parameters of a cavity and its coupling to a generator.

2 Equivalent Circuit for a Cavity Exited by a Generator and a Beam

The electromagnetic field in a cavity is excited by a generator and by a beam. In this case Maxwell's equations and the boundary conditions are nonuniform; they contain the current terms

$$\mathrm{rot}\vec{E} = -j\omega\mu\vec{H}\,, \qquad \mathrm{rot}\vec{H} = j\omega\varepsilon\vec{E} + \vec{J}$$

$$\vec{n}\times\vec{E} = \begin{cases} \vec{K}_m \text{ on } A\,, \\ 0 \quad \text{on } S-A\,. \end{cases} \tag{1}$$

Here $\vec{J}$ is the beam current density, S is the surface enclosing a cavity, A is some portion of S on which the so-called surface magnetic current $\vec{K}_m$ is given, and $\vec{n}$ is the outside normal to surface S. Surface magnetic current is the way to specify the tangential component of an electric field on a part of a surface. In this way the action of a generator can be described.

The surface magnetic current is equal to $\vec{K}_m = -\vec{E}_g \times \vec{n}$, where $\vec{E}_g$ is an electric field produced on a surface by a generator. For example, if a cavity is excited through a waveguide, then an electric field exists at its intersection with a cavity surface. This electric field determines surface magnetic current etc.

The excited electromagnetic field can be expanded into a series

$$\vec{E} = \sum_n A_n\cdot\vec{E}_n - \mathrm{grad}\varphi_e\,, \quad \vec{H} = \sum_n B_n\cdot\vec{H}_n - \mathrm{grad}\varphi_m\,. \tag{2}$$

Here $\vec{E}_n$ and $\vec{H}_n$ are eigenfunctions of fundamental and higher modes; A_n and B_n are unknown coefficients of expansion; and $-\mathrm{grad}\varphi_e$ and $-\mathrm{grad}\varphi_m$ are potential terms that appear because possibly $\mathrm{div}\vec{E} \neq 0$ and $\mathrm{div}\vec{H} \neq 0$ in view of the presence of electric and magnetic charges. Note that the potential terms are orthogonal to all of the eigenfunctions.

To find A_n and B_n let us calculate the following expressions:

$$\begin{aligned} \mathrm{div}\left(\vec{E}_n^*\times\vec{H}\right) &= \vec{H}\cdot\mathrm{rot}\vec{E}_n^* - \vec{E}_n^*\cdot\mathrm{rot}\vec{H}\,, \\ \mathrm{div}\left(\vec{E}\times\vec{H}_n^*\right) &= \vec{H}_n^*\cdot\mathrm{rot}\vec{E} - \vec{E}\cdot\mathrm{rot}\vec{H}_n^*\,, \end{aligned} \tag{3}$$

taking into account that $\vec{E}_n$ and $\vec{H}_n$ satisfy the equations

$$\mathrm{rot}\vec{E}_n = -j\omega_n\mu\vec{H}_n\,, \qquad \mathrm{rot}\vec{H}_n = j\omega_n\varepsilon\vec{E}_n \tag{4}$$

and $\vec{E}$ and $\vec{H}$ satisfy Maxwell's equations given above.

As a result we obtain

$$\begin{aligned}
\mathrm{div}\left(\vec{E}_n^* \times \vec{H}\right) &= j\omega_n\mu\vec{H}_n^* \cdot \vec{H} - j\omega\varepsilon\vec{E} \cdot \vec{E}_n^* - \vec{J} \cdot \vec{E}_n^* \,, \\
\mathrm{div}\left(\vec{E} \times \vec{H}_n^*\right) &= -\, j\omega\mu\vec{H} \cdot \vec{H}_n^* + j\omega_n\varepsilon\vec{E}_n^* \cdot \vec{E} \,. \qquad (5)
\end{aligned}$$

Now let us integrate these equalities over the cavity volume. When we integrate the left side, volume integrals of divergence convert into surface integrals:

$$\begin{aligned}
\oint_S \left(\vec{E}_n^* \times \vec{H}\right) \cdot \vec{n} dS &= \int_V \left(j\omega_n\mu\vec{H}_n^* \cdot \vec{H} - j\omega\varepsilon\vec{E} \cdot \vec{E}_n^* - \vec{J} \cdot \vec{E}_n^*\right) \cdot dV, \\
\oint_S \left(\vec{E} \times \vec{H}_n^*\right) \cdot \vec{n} dS &= \int_V \left(-j\omega\mu\vec{H} \cdot \vec{H}_n^* + j\omega_n\varepsilon\vec{E}_n^* \cdot \vec{E}\right) \cdot dV. \qquad (6)
\end{aligned}$$

In place of $\vec{E}$ and $\vec{H}$, their expressions through the series given above should be substituted to the right side. Because of orthogonality, all volume integrals that contain eigenfunctions with different indexes or potential terms vanish.

Tangential components of $\vec{E}$ and $\vec{E}_n$ are equal to zero everywhere on S except for portion A of the surface S, where $\vec{E} = \vec{E}_g$. Therefore the first surface integral vanishes and the second would be taken over A only. As a result we obtain rearranging terms in the left and right sides:

$$\begin{aligned}
A_n \cdot j\omega\varepsilon \int_V \vec{E}_n \cdot \vec{E}_n^* dV - B_n \cdot j\omega_n\mu \int_V \vec{H}_n \cdot \vec{H}_n^* dV &= -\int_V \vec{J} \cdot \vec{E}_n^* dV, \qquad (7) \\
A_n \cdot j\omega_n\varepsilon \int_V \vec{E}_n \cdot \vec{E}_n^* dV - B_n \cdot j\omega\mu \int_V \vec{H}_n \cdot \vec{H}_n^* dV &= \int_A \left(\vec{E}_g \times \vec{H}_n^*\right) \cdot \vec{n} dS.
\end{aligned}$$

As stored electric and magnetic energy for free oscillation are equal to each other, eigenfunctions can be normalized so that

$$\varepsilon \int_V \vec{E}_n \cdot \vec{E}_n^* \, dV = \mu \int_V \vec{H}_n \cdot \vec{H}_n^* \, dV \,. \qquad (8)$$

Substitution into the equations obtained above yields

$$\begin{aligned}
j\omega \cdot A_n - j\omega_n \cdot B_n &= a_n \,, \\
j\omega_n \cdot A_n - j\omega_n \cdot B_n &= b_n \,, \qquad (9)
\end{aligned}$$

where

$$a_n = -\frac{\int_V \vec{J} \cdot \vec{E}_n^* \, dV}{\mu \int_V \vec{H}_n \cdot \vec{H}_n^* \, dV} \,, \qquad b_n = \frac{\int_A \left(\vec{E}_g \times \vec{H}_n^*\right) \cdot \vec{n} \, dS}{\mu \int_V \vec{H}_n \cdot \vec{H}_n^* \, dV} \,. \qquad (10)$$

Solving the system of linear equations relative to A_n and B_n one obtains

$$A_n = \frac{\omega \cdot a_n - \omega_n \cdot b_n}{j(\omega^2 - \omega_n^2)} \,, \qquad B_n = \frac{\omega_n \cdot a_n - \omega \cdot b_n}{j(\omega^2 - \omega_n^2)} \,. \qquad (11)$$

In this way the amplitudes of all modes can be found.

For a lossless cavity ω_n are real. Therefore A_n and B_n grow to infinity when ω tends to ω_n, i.e. at resonance. In reality the growth of amplitude is limited by losses in a cavity and radiation into the coupling line.

In the presence of losses eigenfrequency acquires an imaginary part

$$\omega_n^2 = \omega_n'^2 \left(1 + \frac{j}{Q_n}\right) . \qquad (12)$$

and

$$\omega^2 - \omega_n^2 = \omega^2 - \omega_n'^2 - j\frac{\omega_n'^2}{Q_n} \qquad (13)$$

Therefore the denominator in expressions for A_n and B_n cannot become zero because ω is real. At the resonance ($\omega = \omega_n'$)

$$A_n = Q_n \frac{a_n - b_n}{\omega_n'} \,, \qquad B_n = Q_n \frac{a_n - b_n}{\omega_n'} \,, \qquad (14)$$

i.e. $A_n = B_n$.

From the relations obtained one can see that, if the frequency is close to one of the eigenfrequencies, the amplitude of the corresponding mode is especially large. Further we will assume that only the fundamental mode is near resonance. As the quality factor Q_n is usually very large, all higher modes and potential fields can be neglected in the vicinity of the resonance ω_n. They can, however, introduce some beam energy losses.

Let us write the dependence of the amplitudes on frequency near the resonance. In this case it is possible to assume $\omega \cong \omega'_n$ everywhere except for the frequency difference in the denominator. Then

$$A_n \cong B_n \cong \frac{\omega'_n(a_n - b_n)}{j(\omega^2 - \omega'^2_n) + \omega'^2_n/Q_n} =$$

$$\frac{Q_n(a_n - b_n)}{1 + jQ_n/\omega'^2_n(\omega^2 - \omega'^2_n)} = = \frac{Q_n(a_n - b_n)/\omega'_n}{1 + jQ_n x}, \qquad (15)$$

where

$$x = \frac{\omega}{\omega'_n} - \frac{\omega'_n}{\omega} \cong \frac{2\Delta\omega}{\omega'_n} \qquad (16)$$

is relative detuning.

This is the resonant dependence with the narrow bandwidth determined by the Q_n value.

Let the frequency of the fundamental harmonic of the beam current be exactly equal to the cavity eigenfrequency used for acceleration (ω_n for example). Then

$$A_n = \frac{Q_n}{\omega_n} a_n = - \frac{Q_n}{\omega_n} \frac{\int_V \vec{J} \cdot \vec{E}^*_n \, dV}{\mu \int_V \vec{H}_n \cdot \vec{H}^*_n \, dV} . \qquad (17)$$

If the beam is thin enough, one can assume that $\vec{E}_n = \text{const}$ in its cross section. Then

$$\int_V \vec{J} \cdot \vec{E}^*_n \, dV = \int_L \vec{E}^*_n \cdot \vec{I}_B \, dl , \qquad (18)$$

where $\vec{I}_B = \int \vec{J} \cdot dS$ is the beam current (integral over the beam cross section).

Let us assume that the accelerating gap is so short that the beam current can be considered as constant along it: $I_B = \text{const}$. Then

$$\int_L \vec{E}^*_n \cdot \vec{I}_B \, dz = I_B \cdot \int_L \vec{E}^*_n \cdot d\vec{z} = - I_B \cdot U^*_n . \qquad (19)$$

Here

$$U = - \int_L \vec{E}_n \cdot d\vec{z} \qquad (20)$$

is a voltage at the gap for $A_n = 1$.

As a result one obtains

$$A_n = \frac{Q_n}{\omega_n} \cdot \frac{U^*_n}{\int_V \mu |H_n|^2 \, dV} \cdot I_B . \qquad (21)$$

The electric field is

$$\vec{E} = A_n \cdot \vec{E}_n \qquad (22)$$

and the voltage across the gap is

$$U = - \int_L \vec{E} \cdot d\vec{z} = A_n \cdot U_n = \frac{Q_n}{\omega_n} \cdot \frac{|U_n|^2}{\int_V \mu |H_n|^2 \, dV} \cdot I_B . \qquad (23)$$

This result can be written as

$$U = R \cdot I_B , \qquad (24)$$

where $R = Q_n \cdot \rho_n$ is the shunt impedance, Q_n is the unloaded quality factor of a cavity, and $\rho_n = R/Q_n$ is the characteristic impedance of a cavity. For ρ_n one can write

$$\rho_n = \frac{|U_n|^2}{\omega_n \int_V \mu |H_n|^2 \, dV} = \frac{|U_n|^2}{2\omega_n W_n} = \frac{|U|^2}{2\omega_n W} . \qquad (25)$$

Here W_n is the energy stored at $A_n = 1$ and W is the stored energy at the gap voltage U.

Shunt impedance can be calculated through the power dissipated in the walls of a cavity ($Q_n = \omega_n W/P$):

$$R = Q_n \cdot \rho_n = \frac{\omega_n W}{P} \cdot \frac{|U|^2}{2\omega_n W} = \frac{|U|^2}{2P} . \qquad (26)$$

In turn, power can be expressed through the shunt impedance

$$P = \frac{|U|^2}{2R} . \qquad (27)$$

If our assumption about the length of a gap is not valid, then the beam current at the fundamental frequency can be written as

$$I_B = I_m \cdot e^{-jk_e z} , \qquad (28)$$

where $k_e = \omega/v_e$ and v_e is the electron velocity.

The voltage across the gap is then

$$U = R \cdot I_m \cdot \alpha \,, \tag{29}$$

where α is the transit time factor,

$$\alpha = \frac{\int\limits_L \vec{E}_n \cdot e^{jk_e z} \cdot d\vec{z}}{\int\limits_L \vec{E}_n \cdot d\vec{z}} \tag{30}$$

In the simplest case $\vec{E}_n = \text{const}$ along the gap. Then

$$\alpha = \frac{\sin\theta/2}{\theta/2} \,, \tag{31}$$

where $\theta = k_e d$ is the transit angle and d is the length of a gap.

To put the expression for voltage into the form of Ohm's law, effective voltage $U_{eff} = U \cdot \alpha$ and effective shunt impedance $R_{eff} = R \cdot \alpha^2$ can be introduced. In these terms

$$U_{eff} = R_{eff} \cdot I_m \,. \tag{32}$$

Dissipated power also can be obtained in terms of effective values:

$$P = \frac{|U_{eff}|^2}{2R_{eff}} \,. \tag{33}$$

The characteristic impedance also should be multiplied by α^2,

$$\rho_{eff} = \rho \cdot \alpha^2 \,, \tag{34}$$

so that

$$R_{eff} = Q_n \cdot \rho_{eff} \,. \tag{35}$$

From here on we will use effective values of impedances and voltages without indexes.

If the frequency of the current harmonic is not equal to the cavity resonance frequency then the frequency multiplier appears

$$U = \frac{R}{1 + jQ_n \cdot x} \cdot I_m = Z_C \cdot I_m \,. \tag{36}$$

Note that such an impedance Z_C has a parallel resonant circuit. Therefore a cavity with a beam can be represented by a resonant circuit with a current source whose current is I_B (see Fig. 3). It is more convenient to use an admittance $Y_C = 1/Z_C$, $Y_C = G \cdot (1 + jQ_n \cdot x)$, $G = 1/R$ instead of an impedance. In Fig. 3 jB is the reactive part of the cavity admittance (susceptance): $B = G \cdot Q_n \cdot x$. The resonant circuit may be characterized by parameters Q_n, ω_n, and $\rho_n = R/Q_n$.

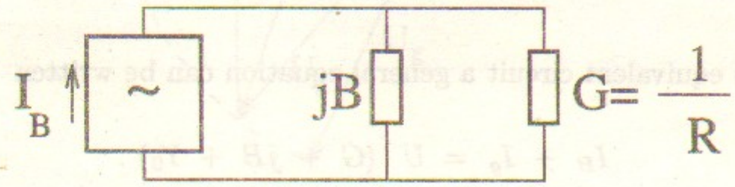

Figure 3: Equivalent circuit.

In reality a cavity is excited not only by a beam but also by a generator. Its action is described by the term b_n in Eq. (11). Since this term has the same dimension as the beam term a_n, the generator can also be represented as some equivalent current source I_g with its intrinsic admittance Y_0. If the generator is matched (for example, by a circulator) then Y_0 is a wave admittance of the coupling line transformed towards an accelerating gap. It can be easily calculated if the external quality factor of the cavity is known:

$$Y_0 = \frac{1}{\rho \cdot Q_{ext}} \,. \tag{37}$$

Keep in mind that the external quality factor is defined by the power radiated into a matched line coupled to a cavity (at free oscillations):

$$Q_{ext} = \frac{\omega_n W}{P_{rad}} \,. \tag{38}$$

An important value is the coupling factor,

$$\beta = \frac{P_{rad}}{P_{wall}} = \frac{Q_n}{Q_{ext}} = \frac{Y_0}{G} \,. \tag{39}$$

Thus a cavity with a beam and a generator may be represented by the equivalent circuit with two current sources (see Fig. 4).

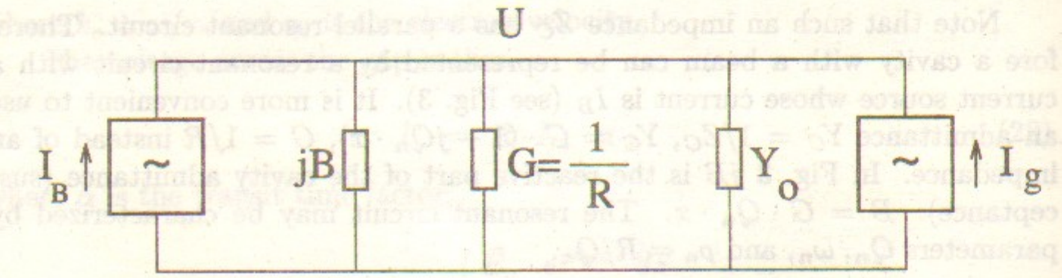

Figure 4: Equivalent circuit.

For this equivalent circuit a general equation can be written

$$I_B + I_g = U \cdot (G + jB + Y_0) . \tag{40}$$

3 Condition of an Equilibrium

It should be noted that I_B and I_g are not fully independent sources. They are connected by the condition that, during crossing a gap the energy eV be imparted to each particle, i.e. in the moment of crossing the voltage V be at the gap. This means that certain phase and amplitude relations exist between these currents.

The best way to illustrate these relations is a vector diagram where complex amplitudes of voltages and currents are depicted by some vectors.

The vector diagram in Fig. 5 is valid for energy above transition, but it can be easily modified for the case of energy below transition.

The vector I_B represents the beam current; it is taken real for convenience. Vector U_B represents the beam induced voltage. It lags in phase the beam current because the cavity usually is somewhat detuned in the direction of lower frequency (for energy above transition); its susceptance is capacitive.

Vector U_g represents voltage created by the generator. Its phase is determined by the condition that a projection of the sum vector $U = U_B + U_g$ on the direction of beam current should be equal to $-V$; V being accelerating voltage per turn. The minus sign indicates the transfer of the energy from the cavity to the beam. The problem of finding the sum voltage has two solutions, as shown in the diagram, if the vector U_g is large enough. Only solution U_1 is stable.

The amplitudes of the sum voltage U_1 through the gap and of the acceleration voltage per turn V are usually specified on the basis of the condition of an accelerator or storage ring operation. This determines the phase lag φ_s

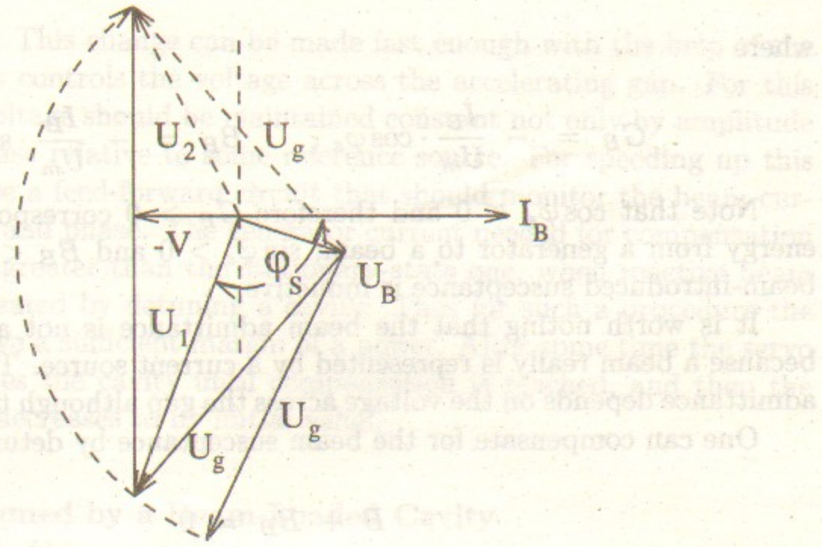

Figure 5: Vector diagram. I_B – beam current vector; U_B – beam induced voltage; U_g – generator voltage; U_1, U_2 – two solutions for cavity voltage; V – acceleration voltage per turn; φ_s – phase lag of U_1 relative to I_B.

of the gap voltage U_1 relative to the beam current I_B ($\pi/2 < \varphi_s < \pi$); φ_s is often called the equilibrium phase.

Let us return to the basic equation of the equivalent circuit

$$I_B + I_g = U \cdot (G + jB + Y_0) . \tag{41}$$

From this equation the input admittance seen by the generator can be found:

$$Y = \frac{I_g}{U} - Y_0 = G + jB - \frac{I_B}{U} . \tag{42}$$

Here an admittance introduced by the beam – "beam admittance" – is

$$Y_B = - \frac{I_B}{U} . \tag{43}$$

If the beam current amplitude is real, as assumed above, then the gap voltage can be represented as $U_m \cdot \exp(-j\varphi_s)$, where U_m is also real and positive.

The beam admittance is then

$$Y_B = - \frac{I_B}{U_m} e^{j\varphi_s} = - \frac{I_B}{U_m} (\cos\varphi_s + j \cdot \sin\varphi_s) = G_B + jB_B , \tag{44}$$

where

$$G_B = -\frac{I_B}{U_m}\cdot\cos\varphi_s\,, \qquad B_B = -\frac{I_B}{U_m}\cdot\sin\varphi_s\,. \tag{45}$$

Note that $\cos\varphi_s < 0$ and therefore $G_B > 0$ corresponds to transfer of energy from a generator to a beam; $\sin\varphi_s > 0$ and $B_B < 0$ means that the beam-introduced susceptance is inductive.

It is worth noting that the beam admittance is not a true admittance, because a beam really is represented by a current source. Therefore the beam admittance depends on the voltage across the gap although the circuit is linear.

One can compensate for the beam susceptance by detuning the cavity to

$$B + B_B = 0 \tag{46}$$

or

$$B = -B_B = \frac{I_B}{U_m}\cdot\sin\varphi_s\,. \tag{47}$$

As required for compensation, $B > 0$ (i.e. capacitive) detuning should be done in the lower frequency direction. Note that in the same direction the cavity should be detuned to avoid phase instability (Robinson instability).

As seen from the above equation, after compensation is reached, the input admittance of the beam-loaded cavity becomes real. Therefore such a process can be easily monitored by a phasemeter of the tuning servo system which can provide the tuning hold-up, necessary for compensation, automatically.

An important question is how to maintain the condition of equilibrium during variation of the beam current. One should differentiate between slow and fast variations.

Slow variation can be compensated by proper detuning of the cavity by means of a tuning servo loop. Simultaneously the power of a generator must be changed in accordance with the power put into the beam.

But this method is too slow for compensating fast variation of the beam current (for example, at injection). The only method in this case is to change the generator current to support an equality

$$I_B + I_g = U\cdot(G + jB + Y_0) = \text{const.} \tag{48}$$

In other words, for current increments the condition

$$\Delta I_g = -\Delta I_B \tag{49}$$

should be fulfilled. This change can be made fast enough with the help of the feedback loop that controls the voltage across the accelerating gap. For this purpose the gap voltage should be maintained constant not only by amplitude but also by its phase relative to some reference source. For speeding up this process one can use a feed-forward circuit that should monitor the beam current by amplitude and phase. The generator current needed for compensation can be noticeably greater than the stationary-state one, when reactive beam current is compensated by detuning a cavity. Thus for such a procedure the generator must have a sufficient margin of a power. After some time the servo tuning system tunes the cavity until compensation is reached, and then the generator current decreases to its initial value.

4 Power Consumed by a Beam-Loaded Cavity from a Generator

Let us calculate the power consumed from a generator by a cavity connected to the generator through a circulator, so that a reflected wave comes to a special load and is absorbed there. In this case the consumed power is equal to the power of the incident wave. This power consists of the power imparted to beam, the power dissipated in cavity walls, and the power reflected and absorbed in the circulator load.

The reflection coefficient can be calculated assuming the wave admittance of the coupling line to be Y_0:

$$\Gamma = \frac{Y_0 - Y}{Y_0 + Y}\,. \tag{50}$$

Here Y is the input admittance of the cavity loaded by the beam

$$Y = \frac{I_g}{U} - Y_0 = G + jB + Y_B\,. \tag{51}$$

The total voltage on a cavity can be expressed through the incident wave voltage U_{inc}

$$U = U_{inc}\cdot(1+\Gamma) = U_{inc}\cdot\frac{2Y_0}{Y_0+Y}\,. \tag{52}$$

From this

$$U_{inc} = \frac{U}{1+\Gamma} = \frac{U}{2\cdot Y_0}(Y_0 + Y)\,. \tag{53}$$

the power of the incident wave (the same as the power consumed from the generator) is

$$P = \frac{1}{2}|U_{inc}|^2 \cdot Y_0 = \frac{|U|^2}{8Y_0} \cdot |Y_0 + Y|^2 = \frac{U_m^2}{8Y_0}|Y_0 + Y|^2 . \quad (54)$$

Here

$$|Y_0 + Y|^2 = \left|Y_0 + G + jB - \frac{I_B}{U_m}e^{j\varphi_s}\right|^2 . \quad (55)$$

Now we express values that cannot be measured directly through values that can be measured:

$$\frac{Y_0}{G} = \beta , \qquad Y_0 = \beta \cdot G = \frac{\beta}{R} , \quad (56)$$

where β is the coupling factor of the cavity, and R is the shunt impedance.

Substitution into Eq. (54) gives

$$P = \frac{1}{4\beta}\left[(1+\beta)^2 \cdot \frac{U_m^2}{2R} + 2(1+\beta) \cdot V \cdot I_0 + \right.$$
$$\left. 2I_0^2 \cdot R + \frac{U_m^2}{2R} \cdot (BR)^2 - 2U_m \cdot I_0 \cdot BR \cdot \sin\varphi_s\right] \quad (57)$$

where $-U_m \cos\varphi_s$ is changed by V, the accelerating voltage per turn. For short bunches one can assume that I_0, the average current in the accelerator equals $I_B/2$.

At an empty cavity resonance ($B = 0$) the power consumed from a generator considerably exceeds the useful power spent on the beam and on the losses to the cavity walls due to high reflection.

Consumption can be minimized by tuning the cavity and by adjusting the coupling. Differentiating P with respect to B and equating the derivative to zero shows that the optimal value of B is

$$B = \frac{2I_0}{U_m}\sin\varphi_s = \frac{I_B}{U_m}\sin\varphi_s = -B_B . \quad (58)$$

This corresponds to compensation of the reactive beam current by the cavity susceptance, the beam-cavity system being tuned to a resonance. The power taken from the generator is now

$$P = \frac{1}{4\beta}\left[(1+\beta)^2\frac{U_m^2}{2R} + 2(1+\beta) \cdot V \cdot I_0 + 2I_0^2 \cdot R \cdot \cos^2\varphi_s\right] . \quad (59)$$

This power can be minimized with respect to the coupling factor β. It is clear that consumed power would be minimal if there were no reflection from the beam-cavity system. As the susceptance of the beam-cavity system is assumed to be zero ($B + B_B = 0$) full matching takes place if the following condition is satisfied:

$$G + G_B = Y_0 \quad (60)$$

or

$$\frac{Y_0}{G} = 1 + \frac{G_B}{G} . \quad (61)$$

But

$$\frac{Y_0}{G} = \beta , \quad G_B = -\frac{I_B}{U_m} \cdot \cos\varphi_s = -\frac{2I_0}{U_m} \cdot \cos\varphi_s , \quad \frac{1}{G} = R . \quad (62)$$

Thus the optimal coupling factor is

$$\beta_{opt} = 1 - R \cdot \frac{2I_0}{U_m} \cdot \cos\varphi_s > 1 \quad (63)$$

(as $\cos\varphi_s < 0$). Substitution into Eq. (59) yields, as expected,

$$P = \frac{U_m^2}{2R} + V \cdot I_0 \quad (64)$$

because reflection is absent.

Unfortunately, the coupling factor cannot be adjusted operationally in accordance with the beam current. Therefore it should be established in the best way beforehand. The most preferable is to design the coupling factor for the maximal intended beam current. Then if the current should be less, the voltage in the line never exceeds the limiting value.

An important case is a superconducting cavity. For such cavities losses in walls can be neglected. Therefore the general formula for power calculation can be used for a superconducting cavity if one goes to the limit with $R \to \infty$, $\beta \to \infty$, $R/\beta \to 1/Y_0 = Z_0 = \text{const}$.

Passage to the limit yields

$$P = \frac{1}{4}\left[\frac{U_m^2}{2Z_0} + 2VI_0 + 2I_0^2 Z_0 + \frac{U_m^2}{2Z_0}(BZ_0)^2 - 2U_m I_0 BZ_0 \sin\varphi_s\right]. \quad (65)$$

Here $Z_0 = 1/Y_0$ is the wave impedance of the feeding line as transformed towards the accelerating gap. This impedance depends on the coupling with the line and can be expressed via external cavity quality factor and characteristic cavity impedance (R/Q):

$$Z_0 = Q_{ext} \cdot \rho\,. \quad (66)$$

At the optimal tuning $(B + B_B = 0)$, the above formula transforms to

$$P = \frac{1}{4}\left[\frac{U_m^2}{2Z_0} + 2 \cdot V \cdot I_0 + 2I_0^2 \cdot Z_0 \cdot \cos^2\varphi_s\right]. \quad (67)$$

This power would be minimal if

$$Z_0 = -\frac{U_m}{2I_0 \cdot \cos\varphi_s} \quad (68)$$

and this minimal power is equal simply to

$$P = V \cdot I_0 \quad (69)$$

as one would expect.

Up to now we considered the case of a generator matched by a circulator. But sometimes the generator is not matched. As an example, consider a tube amplifier mounted directly on a cavity. This can be approximated by a current source in an equivalent circuit without shunting of wave admittance. All power supplied by a generator in this case is spent by a beam and wall dissipation. But an additional reactive current consumed by a beam-loaded cavity leads to an increase of power dissipation on the tube anode. Therefore in this case some margin of allowable cathode current and anode power dissipation of the tube is required.

In conclusion I list some related topics that were beyond the scope of this lecture: (1) beam loading at a partially filled ring; (2) beam loading with several cavities in a ring; (3) beam loading with two counterrotating beams in a storage ring; (4) feedback loop and feed-forward circuit operation.

Bibliography

1. J.C. Slater, Microwave Electronics, Van Nostrand, New York 1957.
2. M.M. Karliner, G.N. Ostreiko, I.A. Shekhtman, *Soviet Phys. – Tech. Phys.* 14, 327 (1969).
3. D. Boussard, Operational Experience with the LEP2 SC Cavity System, CERN-SL-96-16, 18 June 1996.
4. A. Gamp, in *CAS – RF Eng. for Part. Acc. Proc.*, 3-10 April 1991, CERN 92-03, vol. II, 396 (1992).
5. D. Boussard, in Ibid., p. 474.
6. S. Ninomiya, A Technique for Beam–Loading Cancellation, *KEK Report* 96-9, July, 1996.

STANDING-WAVE STRUCTURES

E.V. KOZYREV
Budker Institute of Nuclear Physics
630090 Novosibirsk, Russia

The purpose of this lecture is to review the definitions of the main parameters that describe accelerating structures in general and standing-wave structures in particular. The lecture also containes some deductions from the classical standing-wave structure theory. Specific examples of structures developed at various accelerator centers illustrate the widespread feasibility of their application in accelerator physics.

1 Introduction

Basically all charged particles increase or decrease in kinetic energy when they travel in the direction of an electric field; a magnetic field may be used for deflection only. The acceleration can be along a straight path or along a closed orbit. For the first, linear accelerators are used, with single-pass acceleration; for the second, cyclic accelerators, with many-pass acceleration.

The simplest accelerators with constant electric field are used for low energy acceleration (a few tens MeV); these are Van de Graaff generators. In these, a high voltage is shared between a set of electrodes, creating an electric accelerating field between them, and the maximum energy of the particles is limited by the discharge effects of the high-voltage source.

Much higher energies may be reached by accumulative processes, but in this case the particle beam must be chopped into bunches. The beam will then arrive at accelerating electrodes in a sequence of bunches with gaps of comparable length between them. The gaps allow the polarity of the accelerating voltages to be switched periodically while the bunches are screened by a metallic pipe (drift tube) or similar device, so that the voltages applied to the beam particles, will be multiplied by the number of beam passages. In principle any periodic electric fields could be used, but because of the technology derived from radio communications, sinusoidal radio-frequency fields are used. The layout of this accelerator type (known as Wideröe-type [1]) is shown in Fig. 1.

The drift tube length L must satisfy the synchronism condition

$$L = \frac{\beta\lambda}{2}, \qquad (1)$$

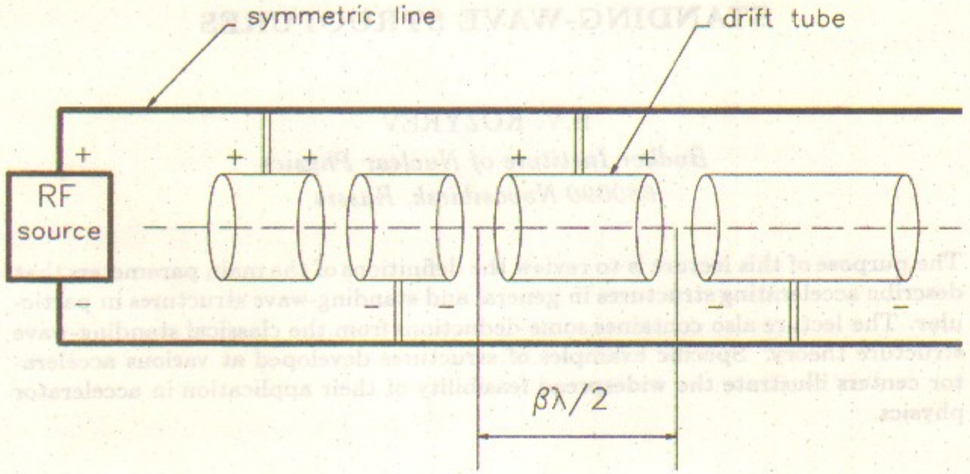

Figure 1: Wideröe-type accelerator.

where $\beta = v/c$, v is particle velocity, λ is free-space wavelength of the RF field, and c is the velocity of light.

Clearly the length of drift tubes for nonrelativistic particles will soon become prohibitive at higher energies unless the input RF frequency is increased. Higher-frequency generators became available only after World War II, as a consequence of radar developments.

At high frequency it is convenient to enclose the accelerating gap between drift tubes in a cavity and to make the resonant frequency of the cavity equal to that of the accelerating field. Figure 2 illustrates the simplest standing-wave accelerating structure.

The accelerator can consist of a series of such cavities fed individually with power sources. Also, several cavities can be coupled in single chain, forming a structure with many accelerating gaps fed by a common RF power source. As can be readily established, in this case for N cavities the full wall losses will be N times less than for one cavity if the energy gain is equal for the two cases, because the losses are proportional to the square of the accelerating electric field strength. The main advantages of coupled structures are:

* the use of larger power supplies
* a reduced number of power feeds
* a reduced number of tuners, if the cells are coupled strongly
* a possible saving of precious space in the beam line of the machine.

All such systems are characterized by a set of fundamental parameters, which may be introduced for a single right cylindrical cavity.

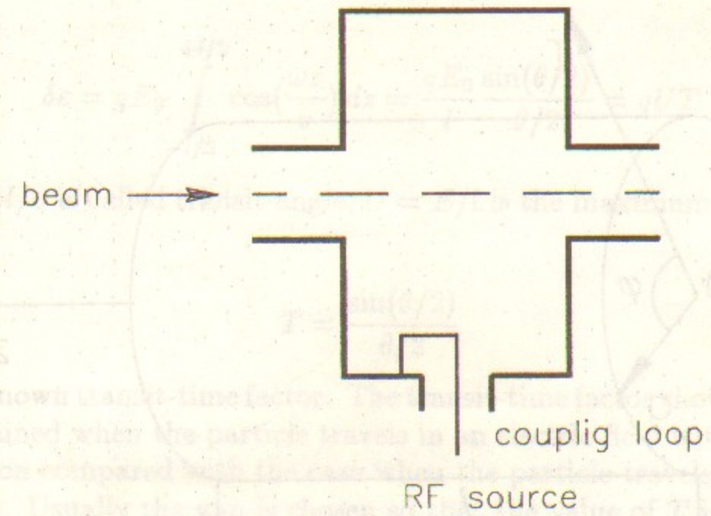

Figure 2: Standing-wave single-gap accelerating structure.

2 Basic Parameters of Accelerating Structures

2.1 Pill-box Cavity

Pill-box cavities are conventional for the accelerating structures in most cases (Fig. 3). For acceleration usually the TM_{010} mode is used. The field components of TM_{mnq} modes are given by

$$E_z = \frac{\nu_{mn}^2}{a^2} J_m(\frac{\nu_{mn}}{a} r) \cos(\frac{\pi q z}{l}) \cos(m\varphi) ,$$

$$E_r = -\frac{a}{\nu_{mn}} J'_m(\frac{\nu_{mn}}{a} r) \sin(\frac{\pi q z}{l}) \cos(m\varphi) ,$$

$$E_\varphi = \frac{a^2}{\nu_{mn}^2} \frac{\pi qm}{lr} J_m(\frac{\nu_{mn}}{a} r) \sin(\frac{\pi q z}{l}) \sin(m\varphi) ,$$

$$H_z = 0 ,$$

$$H_r = -j \frac{a^2}{\nu_{mn}^2} \frac{mk}{Z_o r} J_m(\frac{\nu_{mn}}{a} r) \sin(\frac{\pi q z}{l}) \sin(m\varphi) ,$$

$$H_\varphi = -j \frac{a}{\nu_{mn}} \frac{k}{Z_o} J'_m(\frac{\nu_{mn}}{a} r) \cos(\frac{\pi q z}{l}) \cos(m\varphi) ,$$

$$k = \frac{4\pi^2}{\lambda^2} = \sqrt{(\frac{\pi q}{l})^2 + (\frac{\nu_{mn}}{a})^2} . \qquad (2)$$

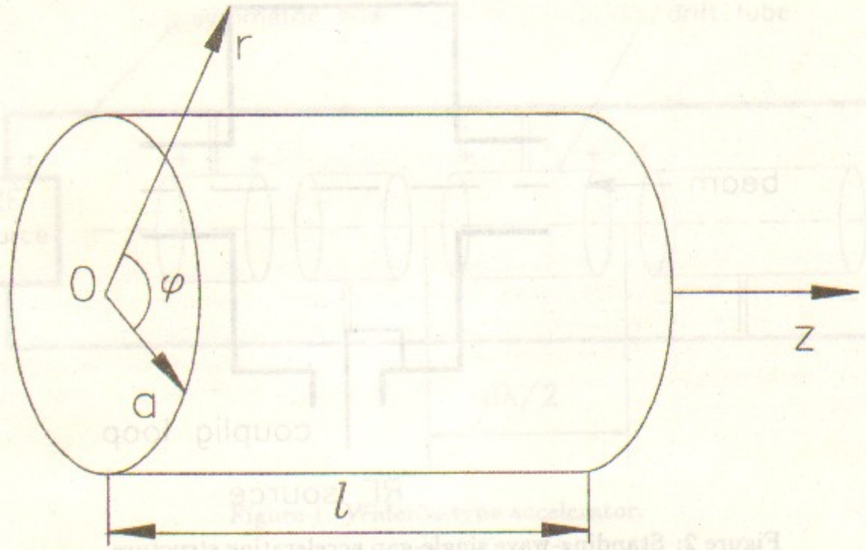

Figure 3: Cylindrical cavity.

Here ν_{mn} is the nth root of $J_m(x) = 0$ and λ is the free-space wavelength.

The TM_{010} mode has only two components:

$$E_z = \frac{\nu_{mn}^2}{a^2} J_0(\frac{\nu_{mn}}{a} r) ,$$

$$H_\varphi = -j \frac{1}{Z_o} J_1(\frac{\nu_{mn}}{a} r) ,$$

$$J_0'(x) = -J_1(x) . \tag{3}$$

Thus we can see that for this mode the electric field does not depend on the longitudinal coordinate z. The resonant frequency is given by $\nu_{mn} = 2.4$:

$$\omega = c \frac{2.4}{a} , \quad \lambda = \frac{2\pi a}{2.4} . \tag{4}$$

2.2 *Transit Time Factor*

Consider an accelerating gap and assume that the particle passes along the axis. In this case for a pill-box cavity the electric field of the TM_{010} mode is $E_z = E_0 \cos \omega t$.

If the particle passes through the center of the gap at $t = 0$ with a velocity v its coordinate is $z = vt$. We assume that the velocity of the particle does not change during the transit. Then the total energy gain is

$$\delta\varepsilon = qE_0 \int_{-l/2}^{+l/2} \cos(\frac{\omega z}{v}) \, dz = \frac{qE_0}{l} \frac{\sin(\theta/2)}{\theta/2} = qUT \tag{5}$$

where $\theta = \omega l/v$ is called transit angle, $U = E/l$ is the maximum voltage in the gap, and

$$T = \frac{\sin(\theta/2)}{\theta/2} \tag{6}$$

is the well-known transit-time factor. The transit-time factor shows the amount of energy gained when the particle travels in an electric field with a sinusoidal time variation compared with the case when the particle travels in a constant electric field. Usually the gap is chosen so that the value of T is about 0.8 to 0.9. In the more general case where the electric field is not homogeneous in the gap, the transit-time factor is given by

$$T = \mathrm{Re} \left| \frac{\int E_z(z) \exp(j\omega t) \, dz}{\int E_z(z) \, dz} \right| . \tag{7}$$

2.3 *Quality Factor*

The most important characteristic of a cavity is its quality factor Q, which is defined as

$$Q = 2\pi \frac{\text{stored energy}}{\text{energy dissipated per cycle}} = 2\pi \frac{W_s}{T_o P_d} = \frac{\omega W_s}{P_d} , \tag{8}$$

where T_o is the period of oscillation, P_d is the average power loss in the cavity walls, and ω is the resonant frequency. If the cavity is coupled with external systems, the loaded quality factor Q_L is used with the same definition ,but P_d is the power lost in the cavity and external systems.

The stored energy W_s in the resonant cavity is given by

$$W_s = \frac{\mu}{2} \int_V |H|^2 \, dv = \frac{\varepsilon}{2} \int_V |E|^2 \, dv . \tag{9}$$

Note that the magnetic field induces a surface current in the walls with a density $\vec{k} = \vec{H} \times \vec{n}$. Then for the power loss we obtain

$$P_d = \frac{1}{2} \int_S R_s |H|^2 \, ds , \tag{10}$$

where R_s is the surface resistance, $R_s = \sqrt{\mu\omega/2\sigma}$, where σ is the material conductivity and μ is the magnetic permeability. Then

$$Q = \omega \cdot \frac{\mu/2 \int_V |H|^2 \, dv}{1/2 \int_S R_s |H|^2 \, ds} = \frac{2}{\delta} \cdot \frac{\int_V |H|^2 \, dv}{\int_S |H|^2 \, ds} , \tag{11}$$

where $\delta = \sqrt{2/\mu\sigma\omega}$ is the skin depth.

It is also common to use the stored energy per unit length dW_s/dz. Then

$$Q = \omega \frac{dW_s/dz}{dP_d/dz} , \tag{12}$$

where dP_d/dz is the fraction of the power lost per unit length in the walls.

Considering the TM_{010} mode in a pill-box cavity one gets

$$Q = \frac{l}{\delta} \frac{a}{a+l} . \tag{13}$$

2.4 Shunt Impedance

An important quantity characterizing the efficiency of a cavity is its shunt impedance, as defined by

$$R = \frac{U^2}{2P_d} . \tag{14}$$

The shunt impedance R is a figure of merit which relates the accelerating voltage U to the power loss P_d in the cavity walls. The factor 2 in the denominator is applied to keep the analogy to Ohm's law $U_{eff}^2 = RP_d$, with $U_{eff} = U/\sqrt{2}$.

Very often the shunt impedance is defined as a quantity per unit length, and a more general definition is

$$R_L = \frac{E_z^2}{2P_d'} = \frac{R}{L} , \tag{15}$$

where L is the cavity length, E_z is the amplitude of the accelerating field and $P_d' = P_d/L$ is the power dissipated per unit length. Sometimes an incorrect shunt impedance Z is used where U is the integral of the field envelope along the gap. Then, to take care of the transit time factor T, the true shunt impedance becomes

$$R = ZT^2 . \tag{16}$$

Also often used is the ratio of shunt impedance to quality factor,

$$\frac{R}{Q} = \frac{U^2}{\omega W_S} . \tag{17}$$

Since $W_s \sim U^2$ this expression depends only on the cavity geometry and allows comparison of the effectiveness of different cavities and structures. For a pill-box cavity one can get

$$\frac{R}{Q} = \frac{ZT^2}{Q} \cong 184.5 \cdot T^2 \left(\frac{l}{a}\right) . \tag{18}$$

3 Examples of Standing-Wave Accelerating Structures

Single-gap pill-box cavities with TM_{010} mode of oscillation could be placed adjacent to each other (Fig. 4). The coupling between cavities is obtained in this case via drift tubes. Instead of capacitive coupling through the central passage, one can use "inductive" coupling slots. To reduce the capacitive coupling and increase the transit-time factor the small drift-tube nose is introduced. Thus a simple periodic cavity chain is formed.

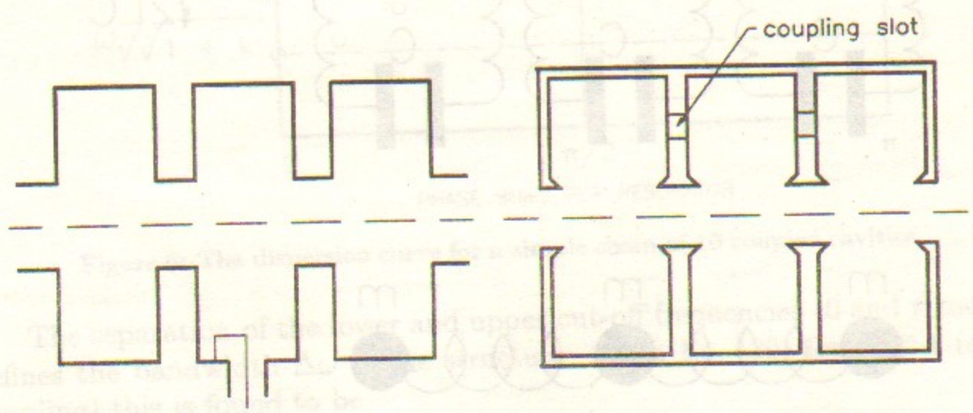

Figure 4: Simple cavity chain.

An analogy may be drown between a chain of coupled cavities and chain of masses supported by springs. The excitation of this system may be described in terms of normal modes of oscillation. When we speak of cavity-chain modes, we refer to these normal modes, not to individual-cavity electromagnetic modes such as the TM_{010} mode. Each of these individual-cavity electromagnetic modes has its own set of normal modes of oscillation. For a chain of $N+1$ cavities, there are $N+1$ normal modes, one for each combination of phase shifts down the chain yielding $n\pi$ total phase shift, where $n = 0, 1, \ldots, N-1$.

It is convenient to introduce here a mathematical model of the cavity chain used by Nagle[2]. As a starting point it takes the lowest frequency mode of an isolated cavity, and treats a tank as a chain of one-dimensional harmonic oscillators coupled with strength k. Figure 5 shows schematically the model considered.

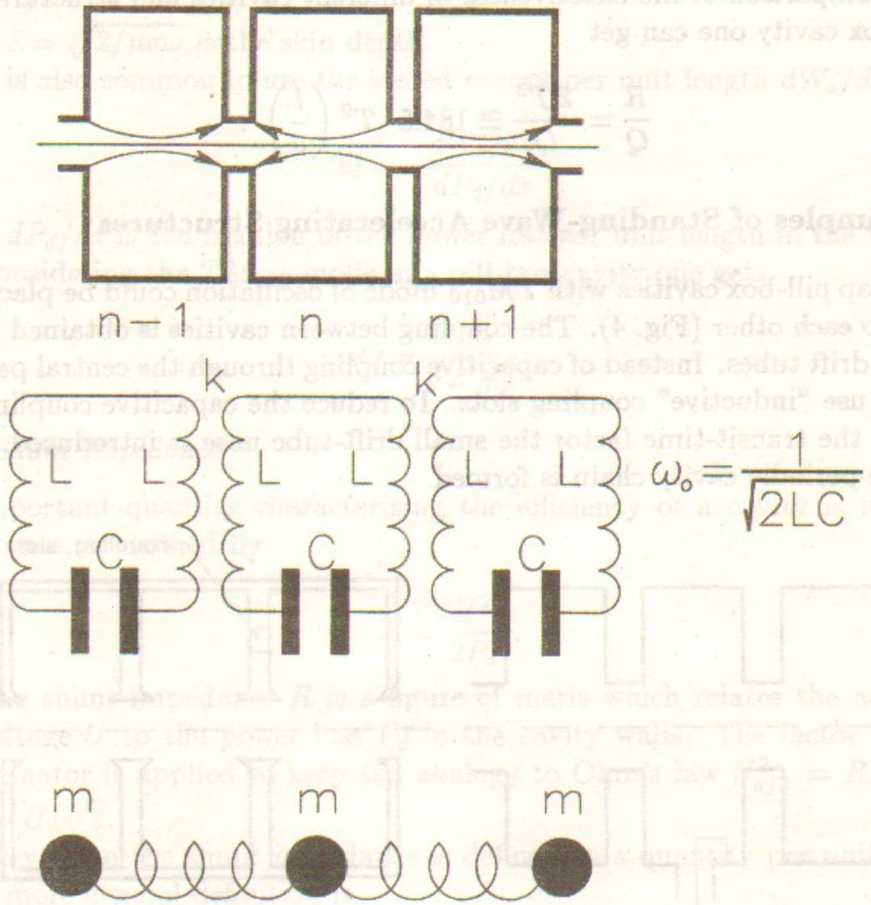

Figure 5: Coupled resonator model for a chain of coupled cavities, a chain of coupled lumped circuit constant resonators, or a chain of coupled masses.

The dispersion relation and amplitude of oscillation in cell n for a linear array (in the lossless case) are

$$X_n^{(q)} = \text{const} \cdot \cos(\frac{\pi q n}{N}) \exp(j\omega_q t) \ , \quad n = 0, 1, \ldots, N-1 \tag{19}$$

$$\omega_q = \frac{\omega_0}{\sqrt{1 + k\cos(\pi q/N)}} \ , \quad q = 0, 1, \ldots, N-1 \tag{20}$$

where q is the number of the mode with resonant frequency ω_q, and ω_0 is the resonant frequency of the individual circuits. It is clear from Eq. (19) that in the lossless case the phase shift between fields in adjacent cavities is restricted to 0 or π for any mode. The dispersion curve for a simple chain of $N+1$ coupled cavities, which also describes the behaviour of a series of coupled lumped circuits, is plotted in Fig. 6.

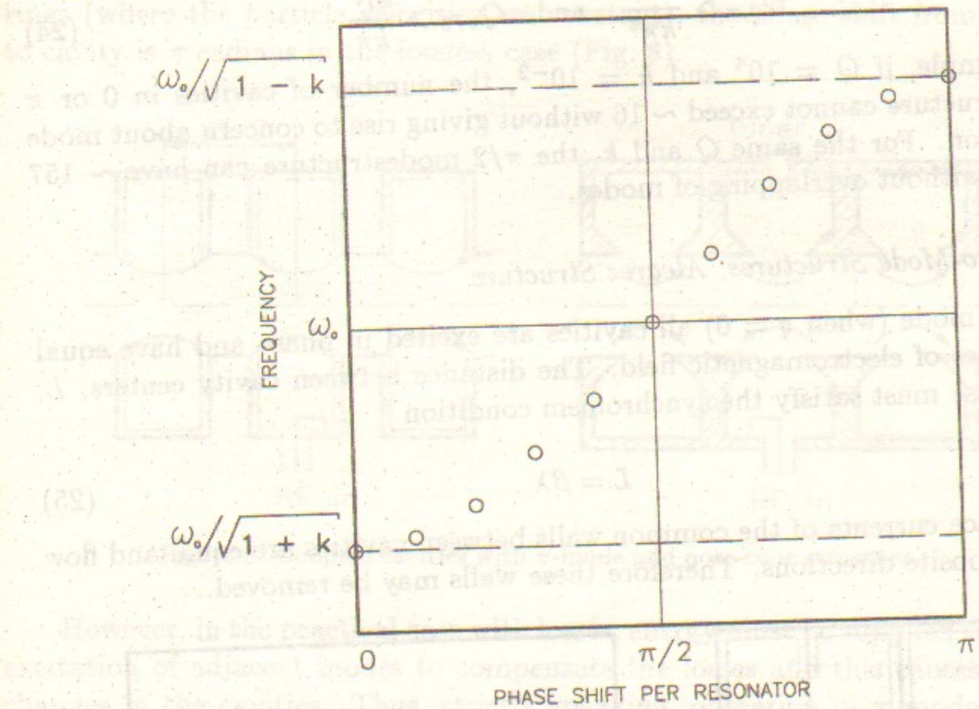

Figure 6: The dispersion curve for a simple chain of 10 coupled cavities.

The separation of the lower and upper cut-off frequencies (0 and π modes) defines the bandwidth $\Delta\omega$ of the structure. From Eq. (20) for $k \ll 1$ (small coupling) this is found to be

$$\Delta\omega \cong k\ \omega_0 \ . \tag{21}$$

The separation of the zero and π modes from the ones nearest them is

$$\Delta\omega \cong k\ \omega_0 \frac{\pi^2}{4N^2} \tag{22}$$

whereas the separation of the $\pi/2$ mode from its nearest neighbors is

$$\Delta\omega \cong k\ \omega_0 \frac{\pi}{2N} \ . \tag{23}$$

Thus, for a given structure, the separation of modes near the $\pi/2$ mode is $2N/\pi$ times as great as the separation near zero and π modes. Operation at a particular mode without excitation of its neighboring modes requires that the Q of the structure be sufficiently high to prevent overlapping of the mode resonances. From Eqs. (22) and (23) it is clear that

$$Q_{0,\pi} > \frac{4N^2}{k\pi^2} \quad \text{and} \quad Q_{\pi/2} > \frac{2N}{k\pi} \; . \tag{24}$$

For example, if $Q = 10^4$ and $k = 10^{-2}$, the number of cavities in 0 or π mode structure cannot exceed ~ 16 without giving rise to concern about mode interaction. For the same Q and k, the $\pi/2$ modestructure can have ~ 157 cavities without overlapping of modes.

3.1 Zero-Mode Structures, Alvarez Structure

For zero mode (when $q = 0$) all cavities are excited in phase and have equal amplitudes of electromagnetic field. The distance between cavity centers, L, in this case must satisfy the synchronism condition

$$L = \beta\lambda \; . \tag{25}$$

The surface currents of the common walls between cavities are equal and flow in the opposite directions. Therefore these walls may be removed.

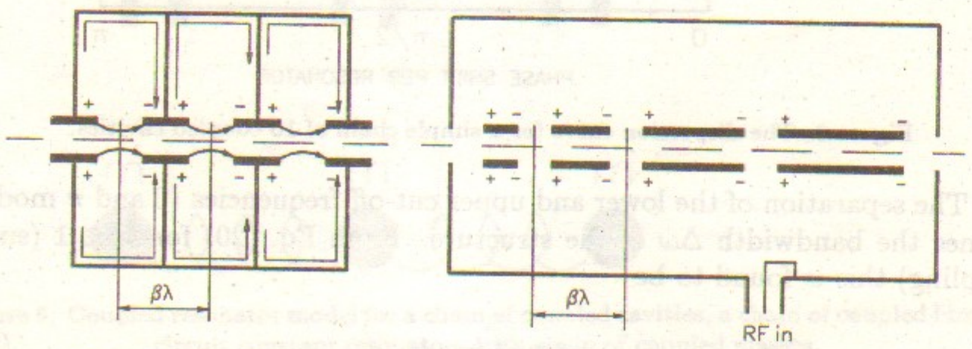

Figure 7: Coupled cavities with zero mode and Alvarez-type structure.

Since the TM_{010} mode is consequently independent of the longitudinal cavity size, the distance from one accelerating gap to the next is determinated only by the particle velocities. A variant of zero-mode structure without the common walls between cavities is shown in Fig. 7. This scheme consists of placing the drift tubes in a single resonant tank such that the field has the same phase in all gaps. Such a resonant accelerating structure was invented by

Alvarez [3] and was followed by the construction of a 32-MeV proton drift-tube linac powered by a 200-MHz source.

3.2 π-mode Structures

In the π-mode structures used for a wide range of synchrotrons and storage rings (where the particle velocities are constant), the phase shift from cavity to cavity is π radians in the lossless case (Fig. 8).

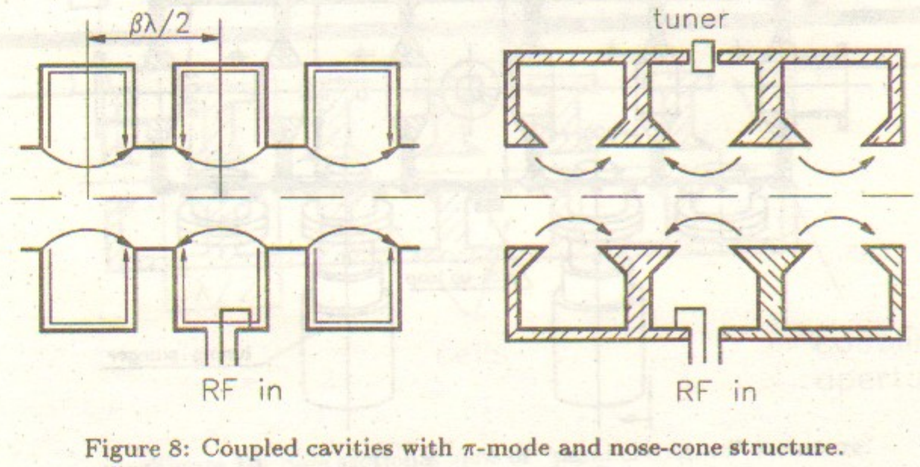

Figure 8: Coupled cavities with π-mode and nose-cone structure.

However, in the practical case with losses, energy must be supplied through excitation of adjacent modes to compensate the losses and this causes phase changes in the cavities. Thus, strictly speaking, operation in π mode is not possible. The phase deviation from π radians per cavity was given by Nagle [2], Knapp [4], and Smith [5] as

$$\Delta\varphi_{n,n-1} = \frac{2(1-k)^{1/2}}{Qk}(N - n + \frac{1}{2}) \; . \tag{26}$$

Thus, the phase shift over the entire length of the structure is

$$\Delta\varphi_{0,\pi} = \frac{(1-k)^{1/2}}{Qk}N^2 \; . \tag{27}$$

For example, if Q and k are the same as in the previous case and the number of cells is $N = 16$, the net phase shift is ≈ 2.5 radians, which is obviously excessive. To reduce the phase shift to a tolerable level, the coupling coefficient k of the structure would have to be increased; if this cannot be done, the number of cells must be decreased. Since it is technically impossible

to increase the coupling coefficient k to a value higher than a few percent, π-mode structures usually contain only a few cavities.

Figure 9 shows examples of five-cell structures operating with π mode (CERN, DESY).

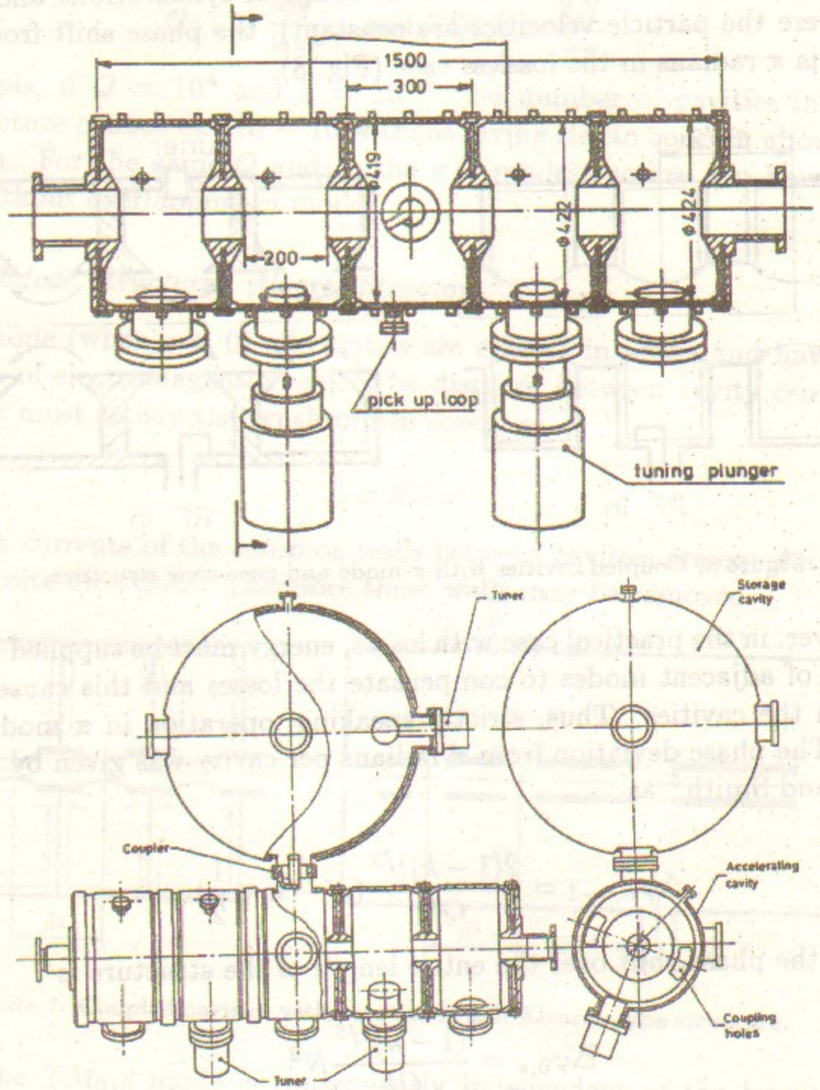

Figure 9: PETRA(DESY) and LEP(CERN) π-mode accelerating structures.

The low coupling coefficient, rather high quality factor, and proximity of neighboring modes cause the π-mode structure to be sensitive to beam-loading variations, and to heating and dimensional errors. To overcome these

disadvantages, various technical solutions are used; an example is the "parallel coupled" structure (Fig. 10).

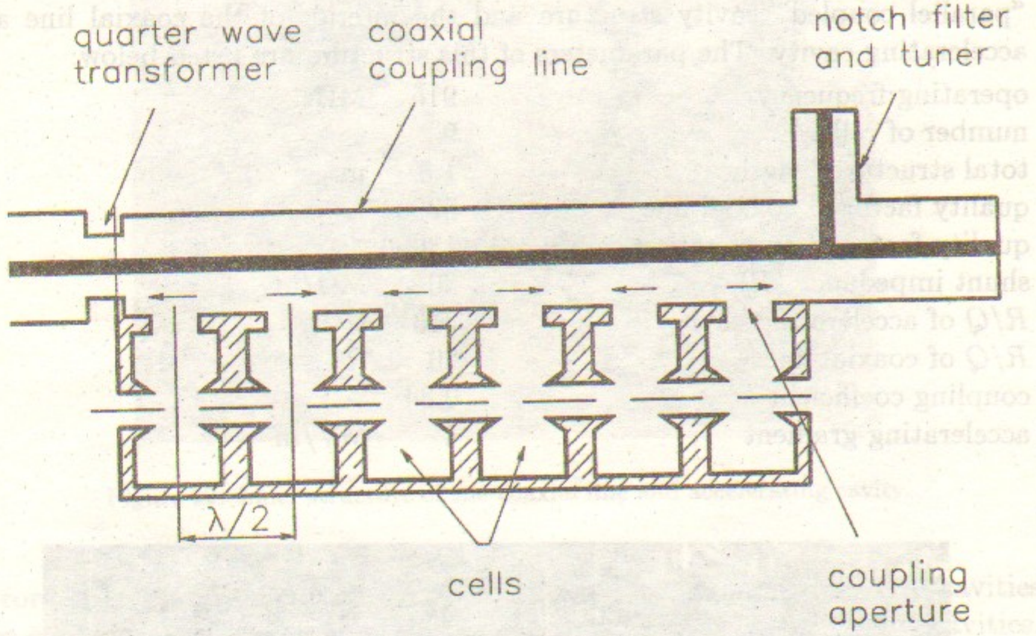

Figure 10: Side sectional view of "parallel coupled" structure.

In the coaxial coupling line the TEM standing wave becomes established. The coupling apertures with accelerating cavities are placed at points where the coaxial line wall current is maximum (the distance between them is $\lambda/2$). Thus all of the accelerating cavities are excited by the same current amplitudes with opposite phases.

The principal properties of this structure are as follow. The shunt impedance is maximized by using optimized cell shapes. Only one feed point is used for all cells. Overlap of the modes in the passband, a common problem when many cells are incorporated in one π-mode cavity, is eliminated because there is only one mode in the passband. A single mode occurs because the power does not propagate serially through the cells in the usual fashion. Other modes do occur in the coupling line, but their frequencies are sufficiently removed from the cell resonant frequency that a negligible fraction of the energy appears in the cells. The notch filter closely approximates a short circuit at operating frequency. The tuning angle of the structure can be adjusted to compensate for variations in the beam loading by moving the tip of the center conductor of the notch filter parallel to the beam direction. This avoids the need for mechanical tuners in each cell.

Similar structures were made at Cornell University (USA, CESR) for use in an e^+e^- storage ring and at Budker Institute of Nuclear Physics (BINP Russia) for a racetrack microtron. Figures 11 and 12 show the 9-cell BINP "parallel coupled" cavity structure and the interior of the coaxial line and accelerating cavity. The parameters of this structure are listed below:

operating frequency	915	MHz
number of cells	9	
total structure length	1.5	m
quality factor of coaxial line	5000	
quality factor of accelerating cavity	18000	
shunt impedance (R)	30	MΩ/m
R/Q of accelerating cavity	213	Ω
R/Q of coaxial line	20	Ω
coupling coefficient k	0.84	%
accelerating gradient	4	MV/m

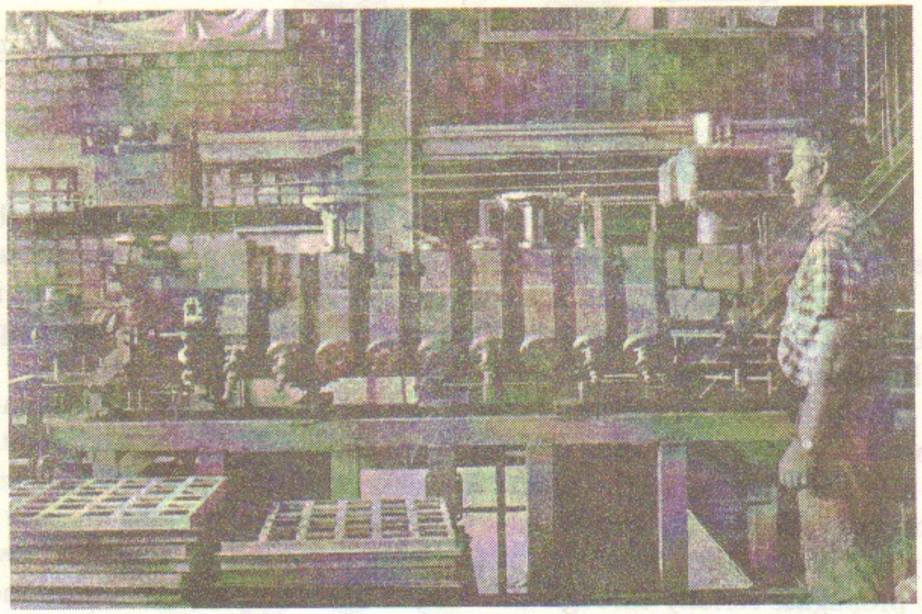

Figure 11: General view of BINP "parallel coupled" structure.

3.3 $\pi/2$-mode Structures

The advantages of these structures were shown by Knapp[4] and Giordano[6]. The $\pi/2$ mode is much less sensitive to beam loading variations and to dimensional

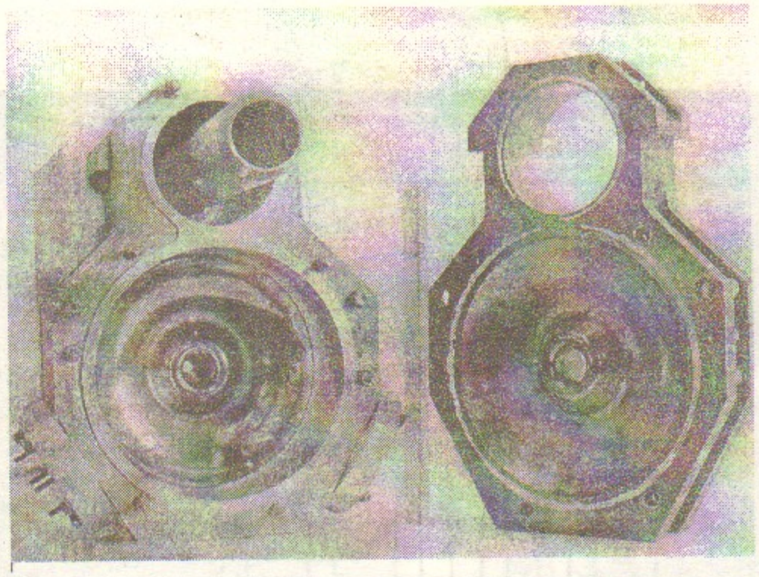

Figure 12: Inner structure of the coaxial line and accelerating cavity.

errors. For the $\pi/2$ mode even cavities have the same amplitudes, odd cavities are empty, and there is a π-radian phase shift between adjacent even cavities. This is shown in Fig. 13(a). This geometry would be suitable for accelerator applications if the synchronous condition were satisfied:

$$L = \frac{\beta\lambda}{2} , \tag{28}$$

where β is particle synchronous velocity in units of light velocity.

If this geometry were used directly, the efficiency of the system for particle acceleration would be extremely poor, because half of the accelerator provides no energy transfer to the beam. However, the model developed here has no restriction on the geometrical shape of the adjacent cavities. In fact, the chain may look biperiodic (alternating-periodic structure – APS), as shown in Fig. 13(b), and if the cavities are all tuned to the same uncoupled resonant frequency, the $\pi/2$-mode characteristics will remain identical to that for the periodic system. This observation allows consideration of a multitude of possible cavity configurations, all with the same mode characteristics. One possible configuration, which has a high shunt impedance (up to 40 MΩ/m), is the "side-coupled" structure (SCS), shown in Fig. 13(c).

This scheme has substantional advantages over many of the others considered, namely:

a) Maximum length along the beam line is available for accelerating field,

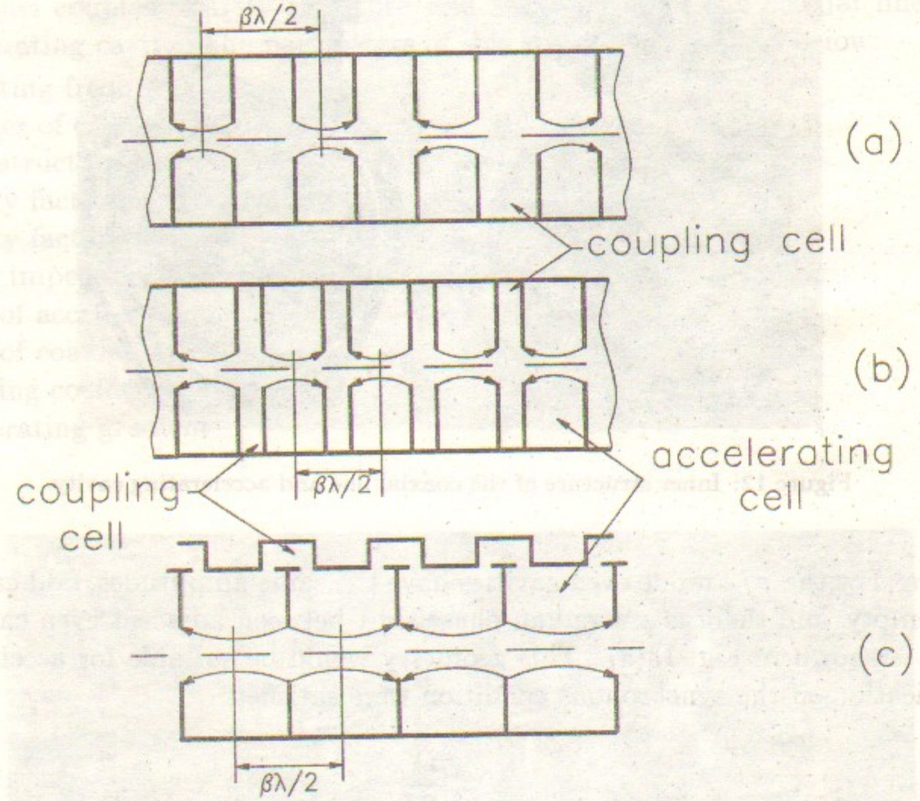

Figure 13: $\pi/2$-mode operation of a cavity chain: (a) periodic cavity chain; (b) biperiodic cavity chain; (c) side-coupled chain.

which leads to optimum shunt impedance.

b) Only small slots at the outer wall are required for coupling, allowing almost complete freedom to design the on-line cavity for maximum shunt impedance. For example, introducing capacitive loading near the beam line by putting "nose cones" in the cavities increases the transit time factor T and also the average axial electric field for a given stored energy. Curving the outer walls also gives minimum power loss for a given stored energy.

c) The offset cavity stores very little energy even in a typically lossy case and thus little attention need be paid to its Q factor or geometry.

An example of a biperiodic structure is shown in Fig. 14. This structure was developed at BINP (Russia) and used in an electron linear accelerator, the

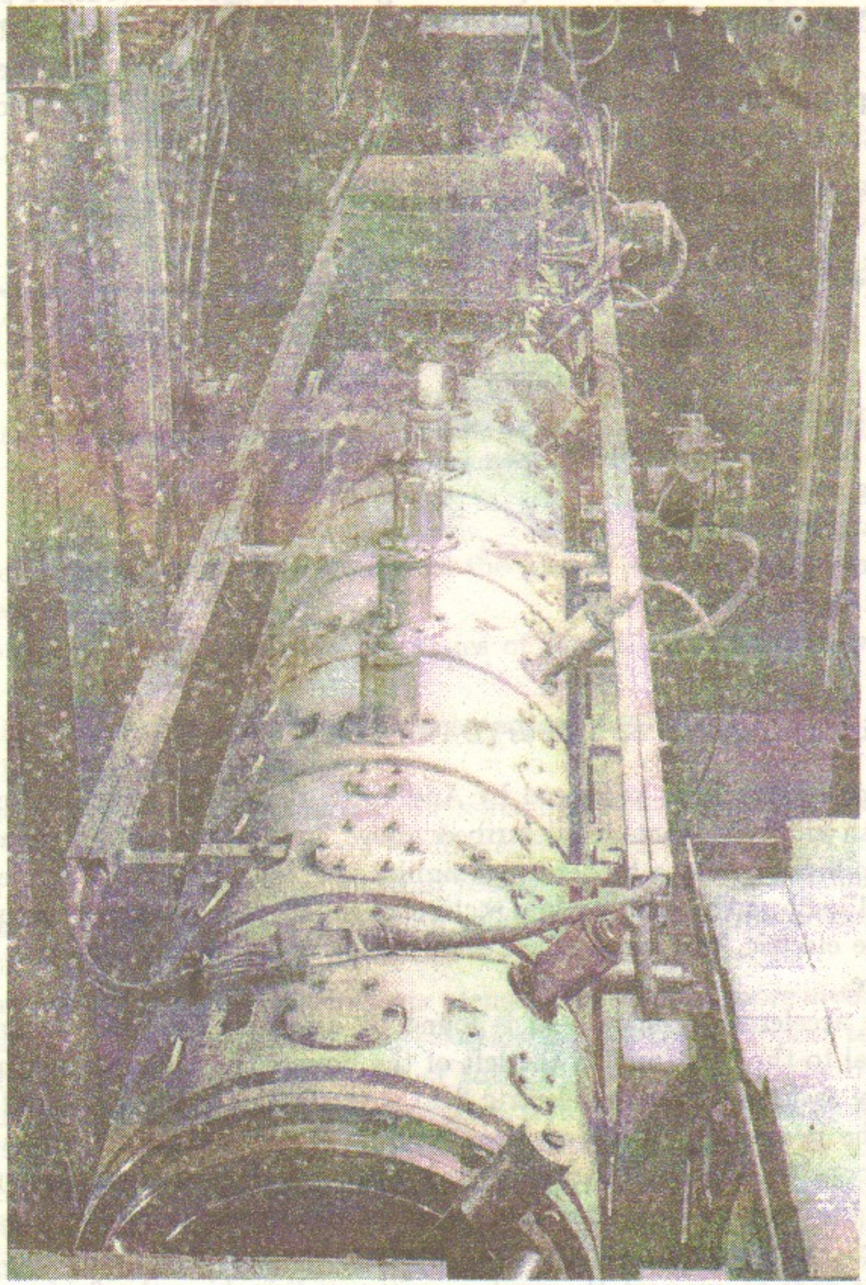

Figure 14: BINP biperiodic structure for injector of VEPP-4.

injector of the VEPP-4 storage ring. The accelerator consists of two identical sections fed by the high power pulse RF generator gyrocon (output power of 65 MW at pulse duration of 10 μs). This accelerator operates in a high stored energy mode and its filling time is rather short compared with the power source pulse length. Therefore the value of the structure shunt impedance is not critical. The main accelerator parameters are listed below:

operating frequency	430	MHz
mode	$\pi/2$	
number of structures	2	
number of structure cells	19 (10+9)	
quality factor of structure	20000	
quality factor of accelerating cavity	22000	
shunt impedance (R)	12	MΩ/m
R/Q of accelerating cavity	200	Ω
coupling coefficient k	10.6	%
accelerating gradient	8	MV/m
full energy gain	55	MeV
electron beam pulse current	33	A

3.4 Disk and Washer Structures (DAW)

This type of structure, proposed by Andreev [7], represents a biperiodic structure with all the advantages described above, but, instead of a fundamental TM_{010} pill-box mode, a higher mode similar to TM_{020} is used for acceleration. Figure 15 shows the longitudinal section of a disk and washer structure and gives the electric field maps of the accelerating and coupling modes in such a structure.

The accelerating mode field is found by assuming that the electric field is normal to the right and to the left of the boundary. The coupling mode is found by assuming that the electric field is tangential to the right and to the left of the boundary. Both boundary conditions give the same frequency and we can consider the DAW structure as a variation of the biperiodic structure.

For the accelerating mode there is a distance from the cavity axis where the longitudinal field E_z vanishes and where it is possible to insert metallic or dielectric rods to support the washers without disturbing the field appreciably. The full-circumference slot between the washers and the outer cylinder produces a strong coupling between cells of about 40%. The theoretical shunt impedance in this case is higher because of the lower current density on the tank walls. However, in actual operation in many cases the supporting rods

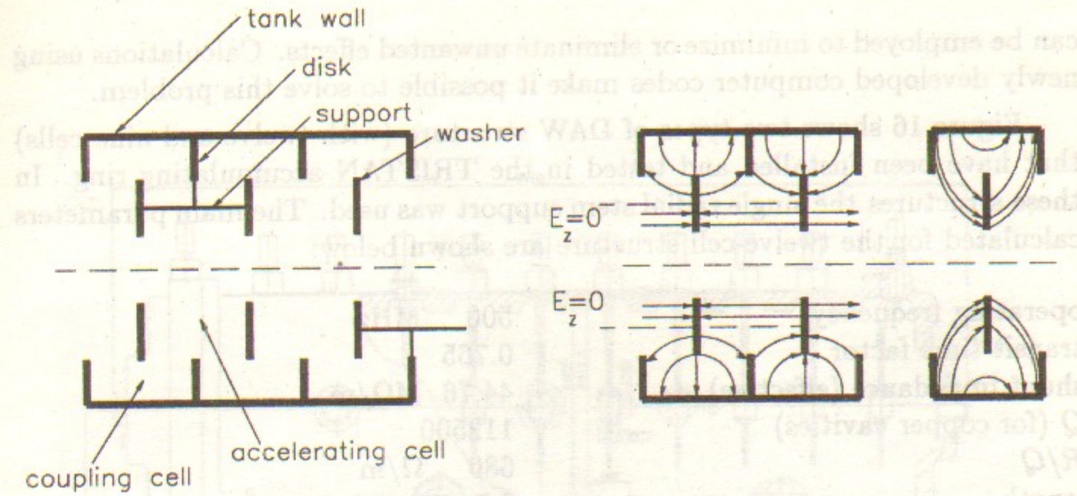

Figure 15: Disk and washer structure and electric field of the accelerating mode (left) and that of the coupling mode (right).

produce such high losses that nearly all the gain in shunt impedance is compensated.

Two of the most attractive properties of the disk and washer structures are:

* the high degree of coupling between adjacent RF cavities,
* the high shunt impedance.

The first property is important for reducing the structure's sensitivity to tuning and assembly errors, beam loading effects, and transients. The second is important for possible savings from reduced RF power and reduced heat removal or higher average accelerating gradients for the same investment in RF sources.

Two aspects of the DAW geometry identified as needing more investigation were higher-order-mode studies and selection of a suitable support technique for the washers that dissipate most of the RF heat. Because the operating passband encompasses the frequency region from the TM_{010}-like mode to the TM_{020}-like mode (a consequence of the DAW's main asset – its high coupling coefficient), it was obvious from published mode charts for right pill-box cavities that the TE_{111}-like, TM_{110}-like, TE_{211}-like and TM_{210}-like mode passbands would be in the vicinity of the $\pi/2$ operating mode over the practical range of the geometric dimensions. Therefore, for any structure, it is important to know the mode locations and their field distributions, mode RF characteristics as a function of geometric changes, and mode influence on beam transmission. With this information, geometries can be selected and methods

can be employed to minimize or eliminate unwanted effects. Calculations using newly developed computer codes make it possible to solve this problem.

Figure 16 shows two types of DAW structure (with twelve and nine cells) that have been installed and tested in the TRISTAN accumulating ring. In these structures the single radial stem support was used. The main parameters calculated for the twelve-cell structure are shown below:

operating frequency	500	MHz
transit time factor	0.765	
shunt impedance (effective)	44.76	MΩ/m
Q (for copper cavities)	112500	
R/Q	680	Ω/m
length	3.7	m
coupling coefficient	0.4	

The achieved shunt impedance was approximately 0.6 of the calculated one, apparently because of non-optimal length of the radial stem. This length must be close to $\lambda/4$ (quarter of free-space wave length). In this case the current distribution along the stem will be such that at the point where the stem is connected to the washer the current will be zero. The frequency of the operating mode also will be the same as without stems.

An example of such a solution is the DAW standing-wave structure linac-preinjector for the SIBERIA-2 SR complex (Russia) (Fig. 17). Each washer is supported by three radial stems, and the length of each is close to $\lambda/4$. The stems are dispersed homogeneously along the circle.

As a result of numerical and experimental studies the optimal geometry of the DAW structure provided a very high shunt impedance of 95 MΩ/m and the absence of high-order modes near the operating TM_{02} mode. The nearest non-operating TM_{11} mode has the 20 MHz higher frequency. The dispersion curves of this structure are shown in Fig. 18 and its main characteristics are presented below:

operating frequency	2797	MHz
shunt impedance (effective)	47.5	MΩ/m
Q (for copper cavities)	28000	
R/Q	1.7	kΩ/m
length	6	m
coupling coefficient	0.4	

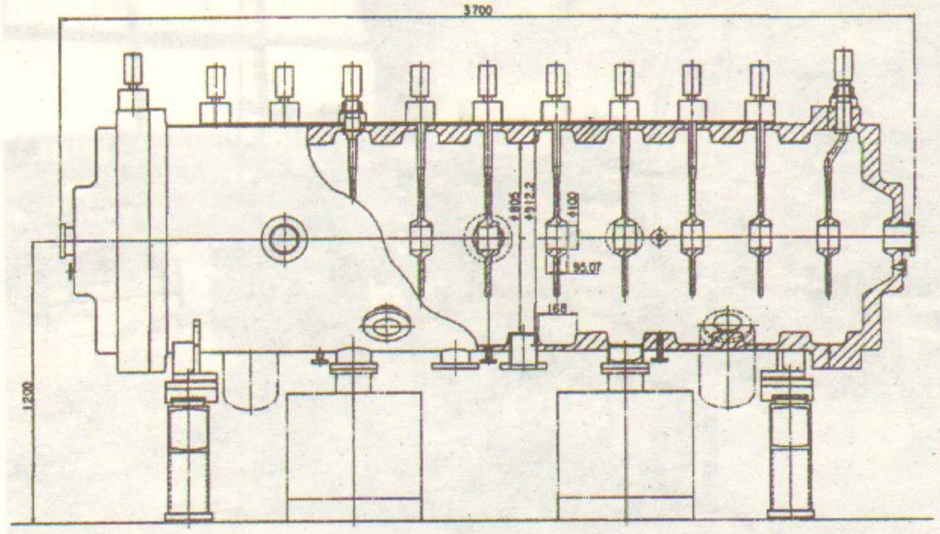

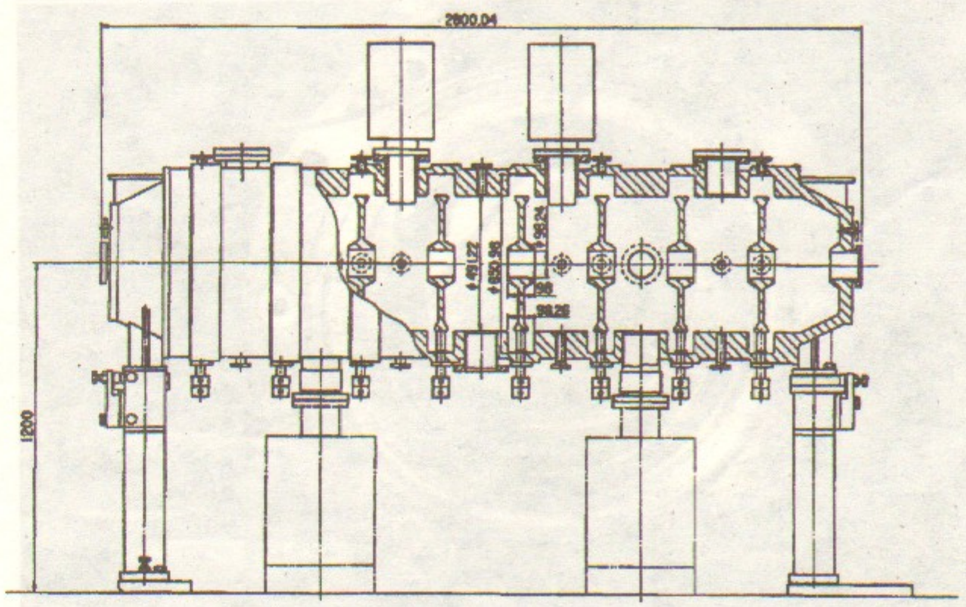

Figure 16: Two types of TRISTAN DAW structures.

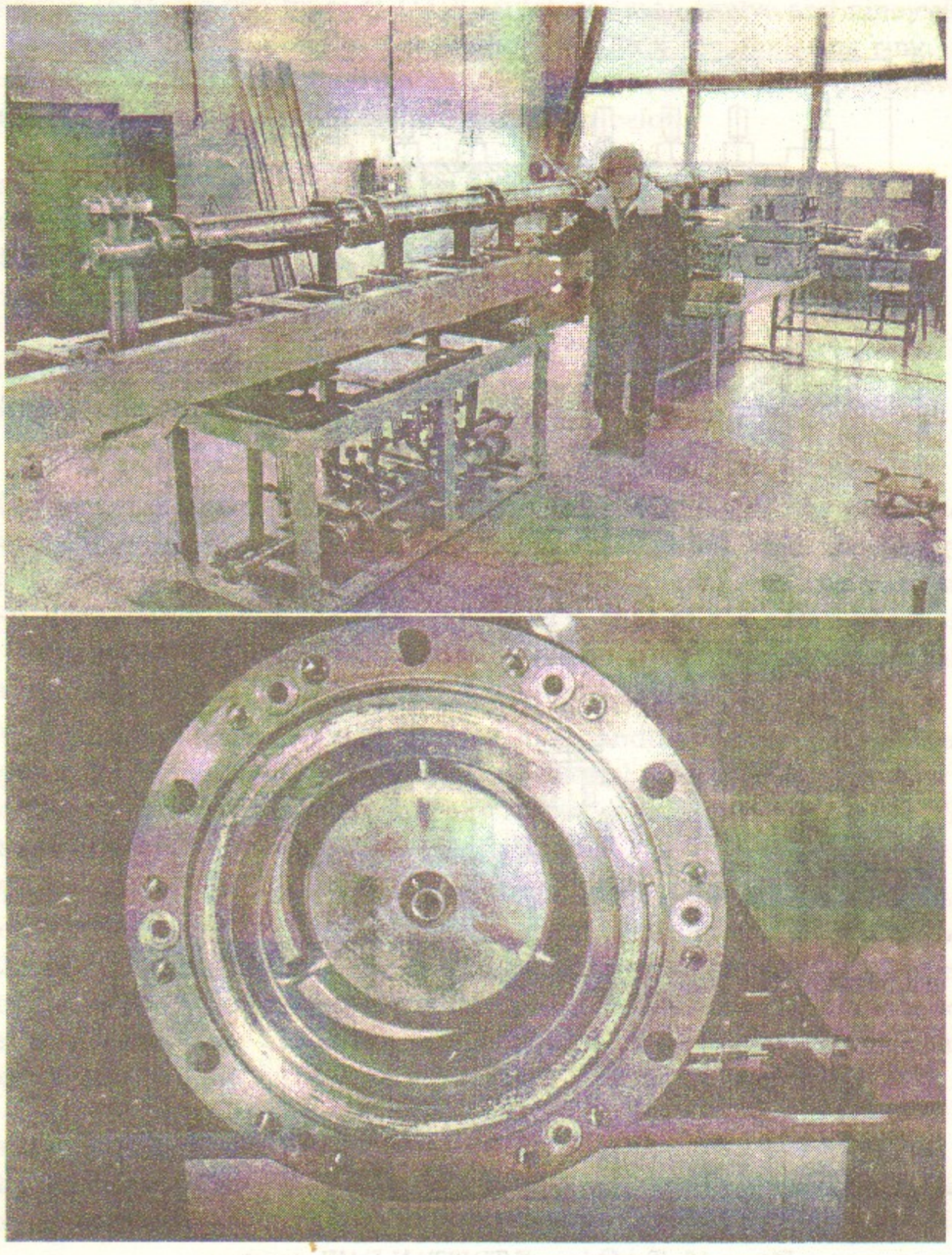

Figure 17: Layout of SIBERIA-2 linac-preinjector and interior of its DAW structure.

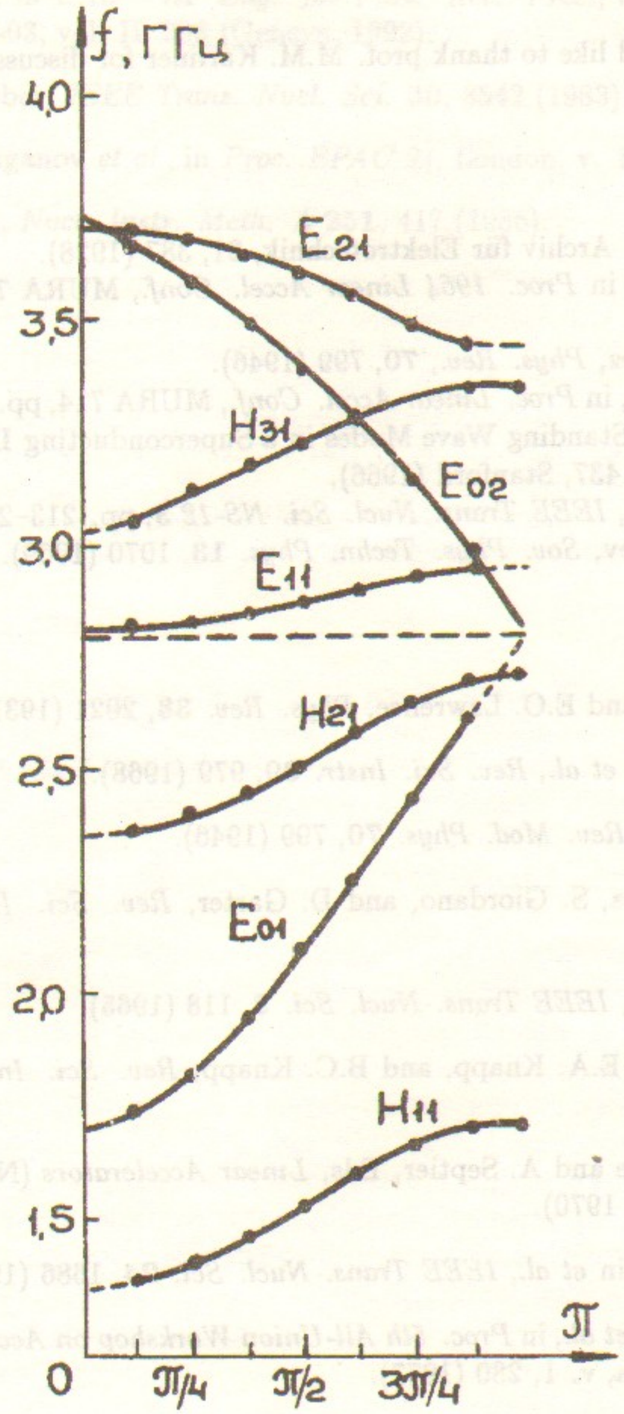

Figure 18: Dispersion curves of SIBERIA-2 DAW structure.

Acknowledgments

The author would like to thank prof. M.M. Karliner for discussions and valuable suggestions.

References

1. R. Wideröe, Archiv für Elektrotechnik, 21, 387 (1928).
2. D.E. Nagle, in *Proc. 1964 Linear Accel. Conf.*, MURA 714, pp. 21–30 (1964).
3. L.W. Alvarez, *Phys. Rev.*, **70**, 799 (1946).
4. E.A. Knapp, in *Proc. Linear Accel. Conf.*, MURA 714, pp. 31–59 (1964).
5. T.I. Smith, Standing Wave Modes in a Superconducting Linear Accelerator, HEPL 437, Stanford (1966).
6. S. Giordano, *IEEE Trans. Nucl. Sci. NS-12* **3**, pp. 213–216 (1965).
7. V.G. Andreev, *Sov. Phys. Techn. Phys.* **13**, 1070 (1969).

Bibliography

P.H. Sloan and E.O. Lawrence, *Phys. Rev.* **38**, 2021 (1931).

E.A. Knapp *et al.*, *Rev. Sci. Instr.* **39**, 979 (1968).

J.C. Slater, *Rev. Mod. Phys.* **70**, 799 (1946).

T. Nishikawa, S. Giordano, and D. Garter, *Rev. Sci. Instr.* **37**, 652 (1966).

E.A. Knapp, *IEEE Trans. Nucl. Sci.* **3**, 118 (1965).

D.E. Nagle, E.A. Knapp, and B.C. Knapp, *Rev. Sci. Instr.* **38**, 1583 (1967).

P. Lapostolle and A. Septier, Eds, *Linear Accelerators* (North Holland, Amsterdam, 1970).

R.M. Sundelin *et al.*, *IEEE Trans. Nucl. Sci.* **24**, 1686 (1977).

G.I. Budker *et al.*, in *Proc. 5th All-Union Workshop on Accel. of Charged Part.*, Dubna, v. 1, 280 (1977).

V. Akimov *et al.*, in *Proc. 11th All-Union Workshop on Accel. of Charged Part.*, Dubna, v. 1, 268 (1989).

A. Gamp, in *CAS – RF Eng. for Part. Acc. Proc.*, 3–10 April 1991, CERN 92-03, vol. II, 396 (Geneva, 1992).

S.O. Schriber, *IEEE Trans. Nucl. Sci.* **30**, 3542 (1983).

V. Korchuganov *et al.*, in *Proc. EPAC 94*, London, v. 1, 739 (1994).

S. Inagaki, *Nucl. Instr. Meth. A* **251**, 417 (1986).

OTHER RF POWER SOURCES

G.Ya. KURKIN
Budker Institute of Nuclear Physics
630090 Novosibirsk, Russia

The main subjects discussed in this paper are as follows. Triode tube; main characteristics of the equivalent schematic of the amplifying stage. Requirements for operation of a triode stage loaded with an accelerating cavity. Influence of parameters of the output stage and transmission line length on the output impedance of RF system for the beam. Typical design of the power output stage. Magnetron, travelling wave tube, principles of operation, main parameters. Magnetron loaded with the cavity of microtron, methods of coupling, requirements for stable operation. Magnicon - BHF generator with a circular deflection of the electron beam, principle of operation, results of development.

1 Triode tube

Klystrons have wide acceptance as an RF power source, but at frequencies lower than 300 MHz they are not used. Therefore frequencies below 300 MHz are in the domain of grid tubes - triodes and tetrodes. An RF system with lower frequency has some advantages: reduced interaction with material structures (elements of the vacuum chamber and cavity) because of larger bunch length, the possibility of having a high peak current in one bunch and effective injection because of a larger energy bucket.

The triode tube has an anode and a heated cathode (Fig.1). Electrons are emitted from the cathode and collected at the anode. The energy of the electrons is a function of the voltage between the anode and the cathode. The grid is usually a helix made of wire wound around the cathode. Since the grid is installed between cathode and anode, its influence on the electric field near the cathode is stronger. The voltage between grid and cathode determines the number of electrons collected at the anode, i.e. the electric current between the electrodes. Variation of anode potential also influences the current, but by much less. Negative voltage between grid and cathode holds up electrons coming out of the cathode surface; the space charge is increasing and the number of electrons going through the grid is decreasing.

If a positive voltage is applied between grid and cathode, some electrons get to the grid causing a grid current. A larger portion of the electrons go to the anode, so the cathode current Ik divides into two components, forming the anode current *Ia* and the grid current *Ig*:

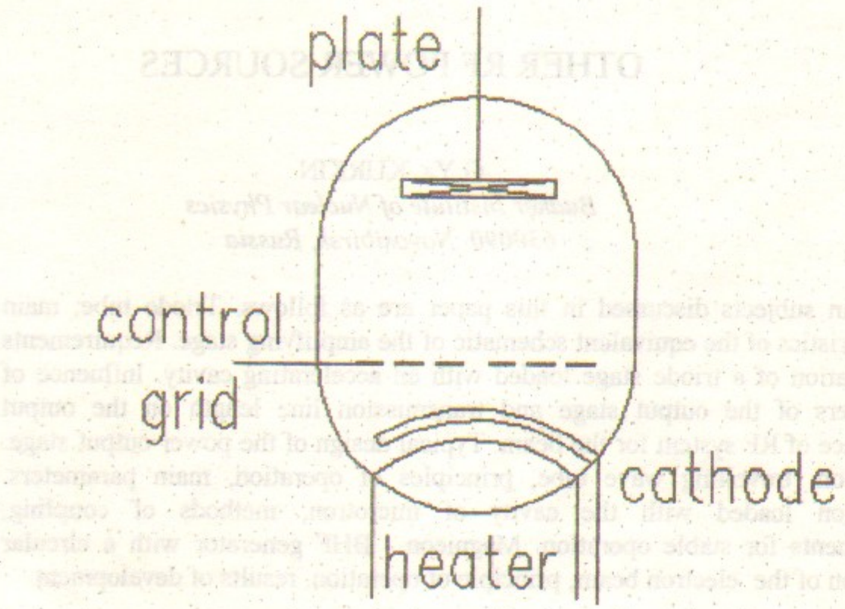

Figure 1: Triode tube.

$$I_k = I_g + I_a \qquad (1)$$

These current values depend on anode voltage *Va* and grid voltage *Vg*, and the triode behaviour can be described by 4 functions:

$$I_a = f(V_g) \qquad V_a = const, \qquad (2)$$
$$I_a = f'(V_g) \qquad V_g = const, \qquad (3)$$
$$I_g = \varphi\,(V_g) \qquad V_a = const, \qquad (4)$$
$$I_g = \varphi'(V_g) \qquad V_g = const. \qquad (5)$$

All these functions are usually obtained by direct measurement. For example, in order to get characteristic curve (2) one varies grid voltage and measures anode current with the anode voltage kept constant. These functions are called static characteristic curves. The typical triode characteristics (2) and (4) are shown in Fig. 2a and characteristics (3) and (5) in Fig. 2b.
Both families of characteristic curves may show some variation depending on the specific design or the area of application of the tubes, but the same tendencies are seen in the curves for any type of triode. Since either of the two families is a graphic representation of Eqs. (2) to (5), they are interdependant.

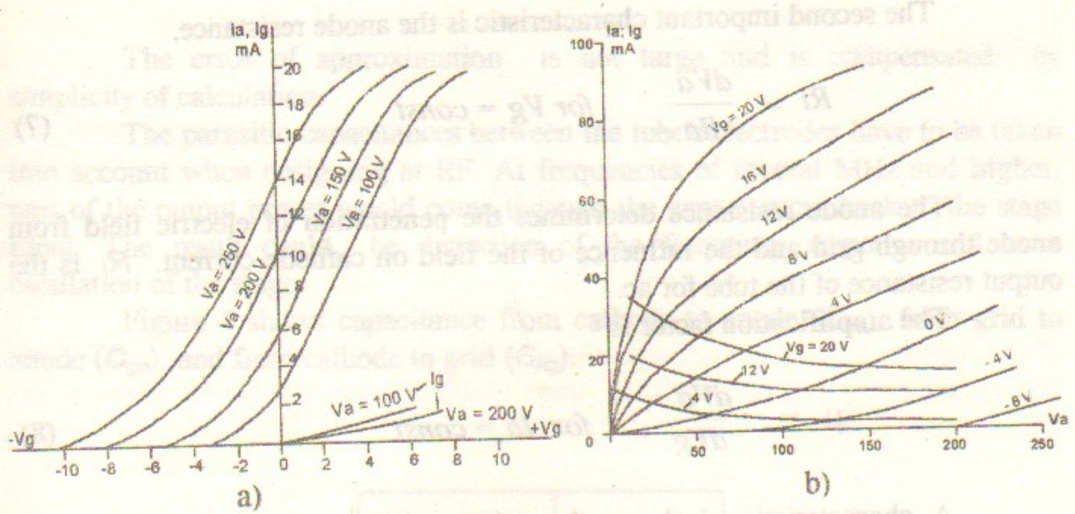

Figure 2: Two families of anode-grid characteristic curves.

One can to transform the family of Fig. 2a into that of Fig. 2b by using another coordinate system.

These two sets of characteristics provide complete information about a tube's parameters within the range shown. For quick estimation of the suitability of a tube for a specific application, to compare two tubes, the static characteristics are often used. For example, Fig. 2 shows the dependence of the anode current on the grid voltage is not uniform throughout the range of anode voltage. Usually static characteristics show the behaviour of the tube in the most usable range of parameters or at some given operational point.

One of the most important characteristics is the transconductance *S*. It shows the change in anode current per volt of grid voltage change:

$$S = \frac{dIa}{dVg} \qquad for\ Va = const \qquad (6)$$

Often the anode current is measured in mA, then the dimension for the transconductance is mA/V. Transconductanse is affected strongly by anode and grid voltage, but only one value that is given in the tube data sheet: the average value for the rising and sufficiently large and linear part of the anode and grid curve, the part used as operational for amplifiers and generators. The transconductance of power triode tubes is in the range 10 to150 mA/V.

The second important characteristic is the anode resistance,

$$Ri = \frac{dVa}{dIa} \qquad for\ Vg = const \tag{7}$$

The anode resistance determines the penetration of electric field from anode through grid and the influence of the field on cathode current. R_i is the output resistance of the tube for ac.

The amplification factor is

$$\mu = - \frac{dVa}{dVg} \qquad for\ Ia = const \tag{8}$$

A characteristic μ shows the relative influence of anode and grid potentials on the anode current. The value of μ is dimentionless and is in the range 10 to 100.

Usually for practical calculations the curves in Fig. 2a,b are approximated by lines (Fig. 3 a,b):

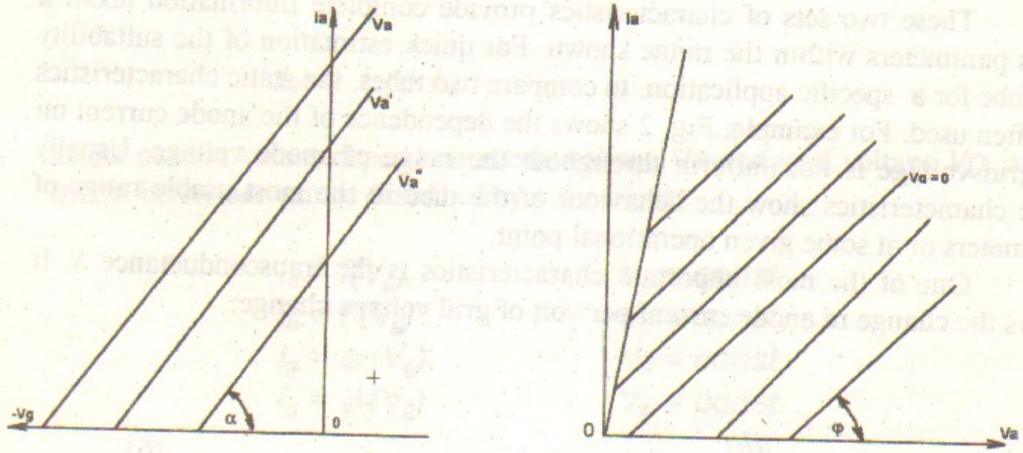

Figure 3: Approximation of anode-grid characteristic curves.

$$tg\ a = S = \frac{\Delta Ia}{\Delta Vg}; \qquad tg\ \varphi = \frac{1}{Ri} = \frac{\Delta Ia}{\Delta Va} \tag{9}$$

for V_a = const for V_g = const

The error of approximation is not large and is compensated by simplicity of calculation.

The parasitic capacitances between the tube's electrodes have to be taken into account when designing at RF. At frequencies of several MHz and higher, part of the output power would come through the capacitances back to the stage input. The result could be distortion of the frequency response and even oscillation of the stage.

Figure 4 shows capacitance from cathode to anode (C_{ka}), from grid to anode (C_{ga}), and from cathode to grid (C_{kg}).

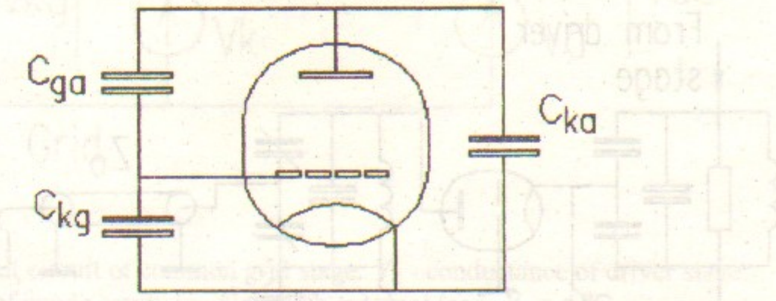

Figure 4: Capacitances of triode.

At lower frequency the common cathode configuration is often used. The equivalent schematic of the stage is shown in Fig. 5.

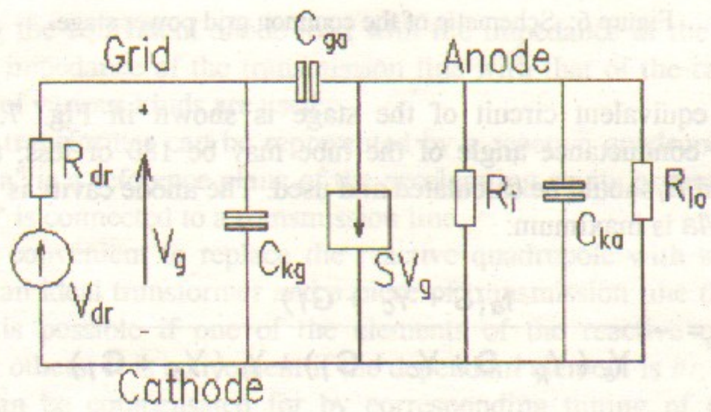

Figure 5: Equivalent circuit of a common cathode stage *Rdr* - output impedance of the driver stage, *Vdr* - driver voltage., *Rlo* - load impedance.

Usually on power stages of RF generators the triode is in the grounded grid configuration. This offers larger power gain because of smaller feedback through the parasitic capacitance C_{ka}:

$$C_{ka} << C_{ga} \qquad (10)$$

If the frequency band in not large, the resonance circuits are used as anode load. An example of the power triode stage coupled with the cavity through the transmission line is shown in Fig. 6.

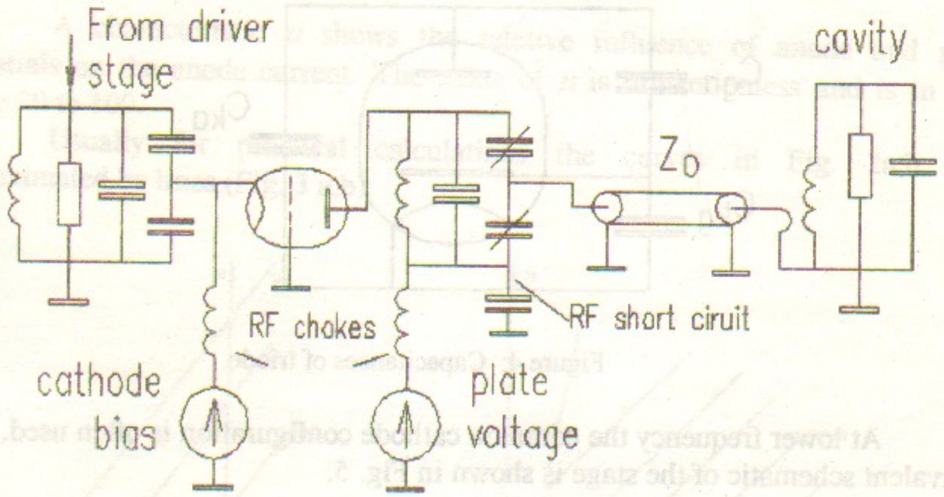

Figure 6: Schematic of the common grid power stage.

The equivalent circuit of the stage is shown in Fig. 7. For higher efficiency the conductance angle of the tube may be 180 or less; therefore the effective S and R_i should be calculated and used. The anode cavity is tuned so that the ratio Vaa/Ia is maximum:

$$V_{aa} = -\frac{I_a(S + Y_c + G_i)}{Y_a\,(Y_k + S + Y_c + G_i) + Y_k\,(Y_c + G_i)} \qquad (11)$$

If the denominator of this Eq. (11) is 0, the stage will lose its stability. This may be used as the condition for the stage oscillation. To increase the stage stability, additional resistive loading of anode and/or cathode circuits is used.

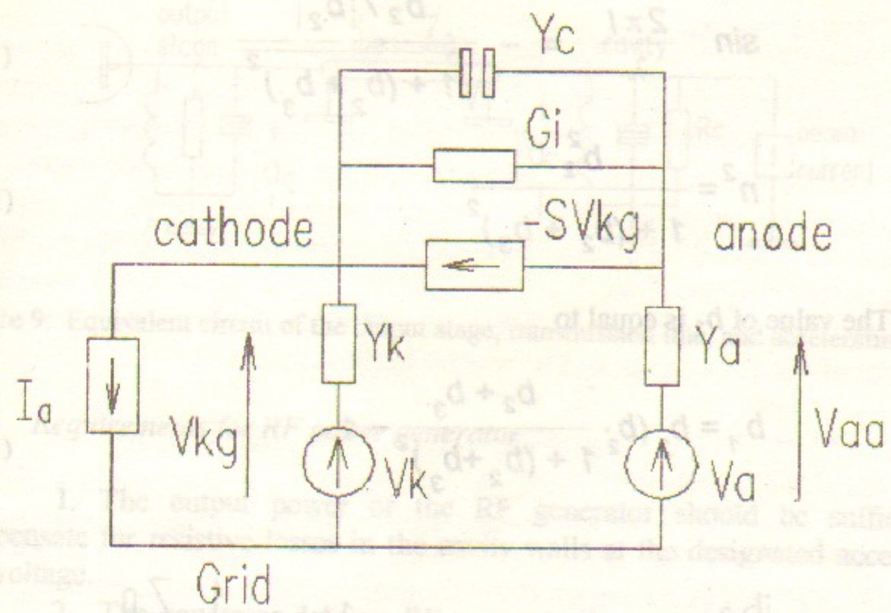

Figure 7: Equivalent circuit of common grid stage. Y_k - conductance of driver stage; Ya - conductance of anode cavity together with external load; $Y_c = 1/jC_{ka}$; G_i - effective anode conductance; S - effective tube transconductance; V_k - DC cathode bias; V_a - DC anode power supply; I_a- equivalent driver current.

1.2 Equivalent Circuit of the Output Stage

For matching the equivalent anode load with the impedance of the transmission line, and the impedance of the transmission line with that of the cavity coupler. transformers of various kinds are used.

The transformer can be represented by a reactive quadrupole (Fig. 8a). The section "a" is a reference plane of the accelerating cavity or generator output stage, and "b" is connected to a transmission line.

It is convenient to replace the reactive quadrupole with some uniform network, i.e. an ideal transformer and a piece of transmission line (Fig. 8b). The replacement is possible if one of the elements of the reactive quadrupole is dependent on others. It is convenient if the dependant element is b_1, because then its change can be compensated for by corresponding tuning of the anode or accelerating cavity connected to section "a." The length of transmission line piece l and the transformation factor n are determined by b_2 and b_3, which are normalised to the line impedance:

$$\sin \frac{2\pi l}{\lambda} = - \frac{b_2 / |b_2|}{\sqrt{1 + (b_2 + b_3)^2}} \qquad (12)$$

$$n^2 = \frac{b_2^2}{1 + (b_2 + b_3)^2} \qquad (13)$$

The value of b_1 is equal to

$$b_1 = b_2 \left(b_2 \frac{b_2 + b_3}{1 + (b_2 + b_3)^2} - 1\right). \qquad (14)$$

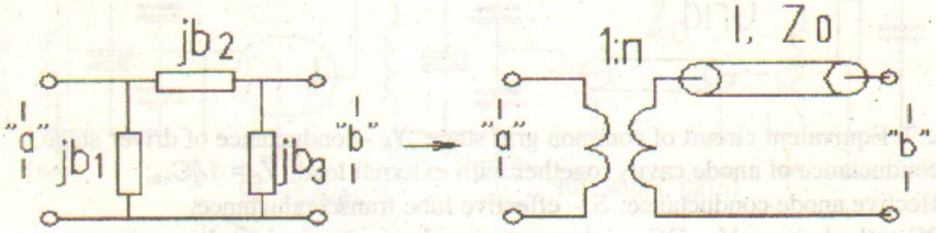

a) b)

Figure 8: Equivalent representation of reactive quadrupole.

These equations show that the coupling of the cavity with the output stage can be adjusted by variation of 3 parameters:

a) *n1* - the transformation factor from anode to transmission line,
b) *n2* - the transformation factor from cavity to transmission line,
c) L_e - the equivalent length of transmission line.

The parameters of the whole network will not be changed if both transformers are excluded and the parameters of the anode and accelerating cavity are replaced with ones that are normalised to the transmission line. Sections "a_g" and "a_c" (Fig. 9) are the reference planes of the generator and cavity respectively, and L_e is the equivalent length of transmission line between sections.

This representation provides a simple model that describes the interaction of beam with the RF system.

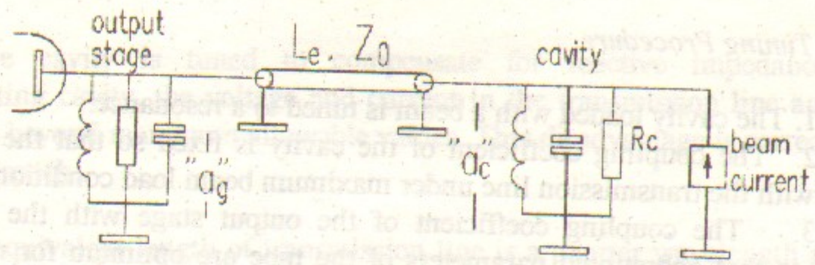

Figure 9: Equivalent circuit of the output stage, transmission line, and accelerating cavity.

1.3 Requirements for RF power generator

1. The output power of the RF generator should be sufficient to compensate for resistive losses in the cavity walls at the designated accelerating gap voltage.

2. The generator delivers RF power to the cavity, which is transferred through the electric field to the charged particles to accelerate them or to compensate their energy losses due to synchrotron radiation and other causes.

3. The reactive beam current through the cavity can be compensated for by corresponding tuning of the cavity, but it changes quickly after injection. In order to maintain the designated gap voltage until the tuner reacts, this reactive current must be compensated for by additional current from the output stage. In some machines this additional current may be as large as the stationary one or even larger. Therefore the output tube should have reserves of anode current and anode dissipation power.

4. The output impedance of the RF system transferred to the cavity gap must satisfy certain requirements. Since the output stage and the power transmission line are coupled to the cavity, the RF output impedance depends on these elements, and this must be taken into account during RF system design.

5. The amplitude and phase modulations of the RF generator output signal cause phase oscillation of bunches and growth of their length. This growth should be much smaller than the normal bunch length defined by quantum fluctuations of synchrotron radiation.

6. The output stage of the RF generator may be coupled with the cavity through a long transmission line. In that case the impedance of the anode cavity has resonances near the generator frequency. The shunt impedance of those resonances may be much higher than that of a working one. In this situation the stable gain of the output stage will be smaller and special measures have to be taken against oscillation.

1.4 The Tuning Procedure.

1. The cavity loaded with a beam is tuned to a resonance.
2. The coupling coefficient of the cavity is fixed so that the cavity is matched with the transmission line under maximum beam load condition.
3. The coupling coefficient of the output stage with the cavity is arranged so that operational parameters of the tube are optimum for maximum power in the transmission line.
4. The anode cavity is tuned to resonance, because the equivalent impedance of anode cavity should be real for optimal operation.

1.5 Methods of RF System Design.

Two methods of RF system design are possible.

I. The equivalent length of the transmission line is half wavelength multiplied by an integer:

$$L_e = n\,\frac{\lambda}{2} \qquad n = 0, 1, 2, \ldots . \qquad (15)$$

The ratio of cavity gap voltage to anode RF voltage does not depend on beam current and energy for this design. When the cavity load is growing, the driver power is increased by the action of a feedback loop in order to keep the cavity voltage constant. The efficiency of the output stage does not change. This method of coupling provides optimum operational parameters of the output stage when the real conductance of the load varies over wide range. Tuning of the anode cavity and correction of coupling are not required during operation. The RF system needs only one on-line tuner for the accelerating cavity.

The impedance of the RF system for the beam is like that of one resonance LC circuit, formed by summing the anode and accelerating cavity conductances. Therefore, the tuning of the cavity down the frequency for reactive beam current compensation provides for desirable frequency response and results in damping of synchrotron oscillation. If the accelerating cavity is detuned, the output stage is working on short circuit, and all power consumed from the DC anode supply will be dissipated at the anode. Therefore the current in the cavity coupling loop is limited by maximum ratings for anode dissipation.

The drawback of such a design is the possibility of sparking or overload in the transmission line and cavity coupler when tuning of the cavity is wrong.

If anode cavity is tuned to compensate for reactive impedance of the accelerating cavity, the voltage and current in the transmission line and coupler may rise beyond maximum allowable values. This disadvantage is corrected in the next approach.

II. The equivalent length of transmission line is a quarter wavelength multiplied by an odd number:

$$L_e = (2n+1)\cdot\frac{\lambda}{4} \qquad n = 0, 1, 2, \ldots . \qquad (16)$$

For this design the ratio of cavity gap voltage to anode current is constant and does not depend on the beam load. An increase of cavity load under constant gap voltage conditions results in an increase of anode ac voltage. The anode current practically does not change. Power dissipation at anode drops and the efficiency of the output stage grows. Thus the range of load variation is limited by the maximum rating for output tube plate dissipation. The maximum current of the coupling loop of the detuned cavity is equal to that of the matched transmission line under maximum output power conditions. The amplitude of the current:

$$I_a = V_{amax} / Z_0, \qquad (17)$$

where V_{amax} is the ac voltage amplitude at anode reference plane for critical mode of tube operation. For any tuner position of the anode or accelerating cavities, the voltage in the transmission line can not exceed V_{amax} and the current in the line and coupler will not exceed V_{amax} / Z_0. Thus an emergency situation is impossible in this RF system.

1.6 Example of RF triode power stage (Fig. 10)

Triode characteristics:		Capacintances pF:
Amplifiction factor	u = 40	Ckg = 170
Transconductance	S = 50 mA/V	Cga = 47
Anode resistance	Ri = 800 Ohm	Cka = 2.8

Operational parameters (design):

Frequency	181 MHz	Anode DC voltage	5 kV
Input power	6 kW	Cathode DC bias	200 V
Output power	39 kW	Anode RF amplitude	3.6 kV
Anode dissipation	37 kW	Cathode RF amplitude	500 V
Anode current	14 A		

Test results:

Anode DC voltage	5 kV	Output power	45 kW
Cathode DC bias	200 V	Input power	8 kW
Efficiency	50 %		

2 Magnetron

2.1 Magnetron operation principles

A magnetron is a cylindrical high-vacuum diode with a cavity resonator system imbedded in the anode. In the presence of suitable crossed electric and magnetic fields the magnetron can be used for generation of continuous-wave and pulsed signal in the higher frequency band. A schematic drawing of the magnetron is shown in Fig. 11.

The magnetic field in the magnetron is applied in parallel to the device axis. The anode DC or pulsed voltage source is connected between anode and cathode, so that magnetic and electric fields are crossed in the interaction zone. The energy available within the zone is coupled out and launched in a coaxial line or waveguide by means of the output probe or antenna.

The magnetron has no separate parts to bunch electrons, a drift space and catcher cavity, as a klystron has. All processes take place in the interaction zone. (See Fig. 12).

The anode DC power supply creates an electric field *Ea* which, except for a small areas near the cavity slits, is homogeneous. The magnetic field *B* is perpendicular to the plane of the drawing. The cathode is heated and electrons are emitted from it into the interaction zone.

Suppose, that the magnetron does not oscillate and therefore an RF field is zero. The emitted electron will be accelerated by the electric field *Ea* and start

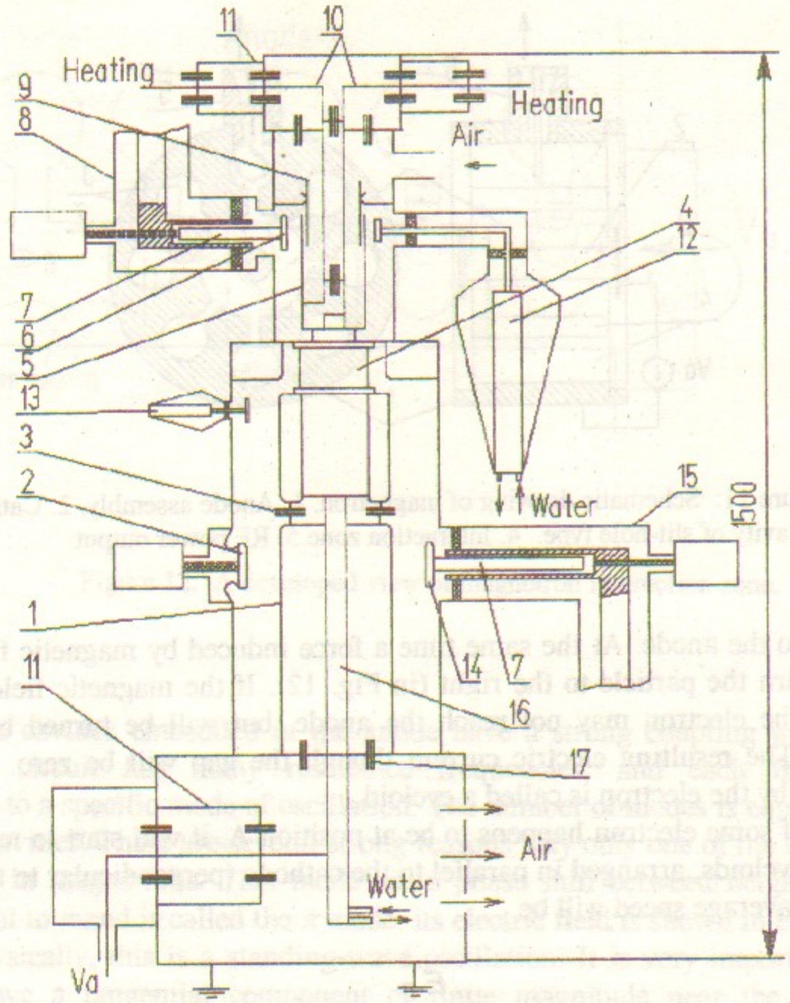

Figure 10: Schematic drawing of rf power stage.

1. Anode cavity
2. Anode cavity tuner
3. Bypass capacitor
4. Triode tube GI-50 (Russia)
5. Cathode cavity.
6. Input coupling capacitor electrode
7. Cylinder capacitance
8. Input transmission line
9. Variable capacitor of cathode cavity tuner
10. RF chokes
11. Low-pass filters
12. Cathode cavity resistive load
13. Resistive load for damping higher-order modes
14. Output coupling capacitance electrode
15. Output transmission line
16. RF choke
17. Blocking capacitor

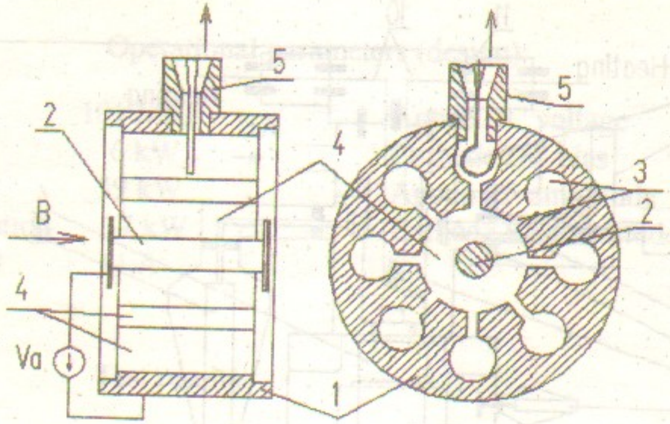

Figure 11: Schematic drawing of magnetron. 1. Anode assembly. 2. Cathode. 3. Cavity of slit-hole type. 4. Interaction zone.5. RF power output.

to move to the anode. At the same time a force induced by magnetic field B will start to turn the particle to the right (in Fig. 12). If the magnetic field is strong enough, the electron may not reach the anode, but will be turned back to the cathode. The resulting electric current though the gap will be zero. The curve described by the electron is called a cycloid.

If some electron happens to be at position A, it will start to move by the chain of cycloids, arranged in parallel to the cathode (perpendicular to the electric field). Its average speed will be

$$V_{aver} = \frac{E_a}{B}. \qquad (18)$$

The oscillation frequency is a cyclotron frequency ω_c

$$\omega_c = \frac{eB}{m}, \qquad (19)$$

where m is the mass of electron, e is the charge of the electron and the vertical amplitude of oscillation is

$$A_v = \frac{2mE_a}{eB^2}. \qquad (20)$$

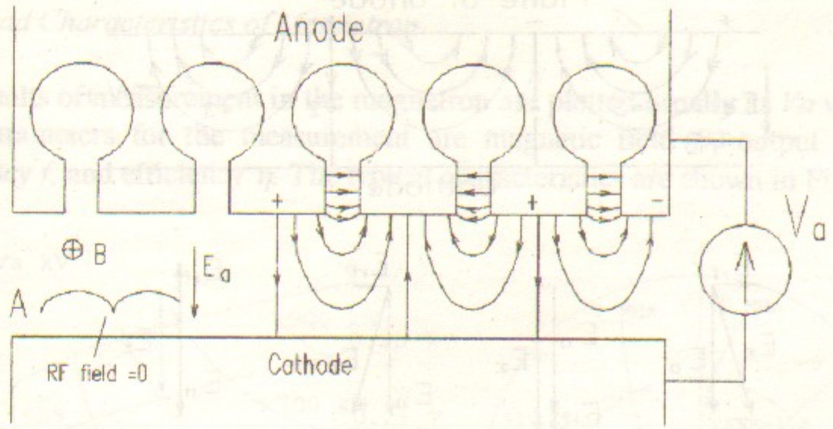

Figure 12: A developed view of magnetron interaction zone.

The cavities embedded in the anode have a strong coupling with each other. The circuit has many resonance frequencies, and each frequency corresponds to a specific mode of oscillation. The number of modes is equal to the number of cavities. There are several strong reasons why only one of the modes is widely used in magnetrons. That mode has a phase shift between neighbouring cavities equal to π and is called the π mode; its electric field is shown in Fig. 12.

Physically, this is a standing-wave oscillation. It is very important that the field have a tangential component of finite magnitude near the cathode surface.

The standing wave can be presented as a sum of 2 waves travelling in opposite directions. The electric field of one, travelling to the right, is shown in Fig. 13.

A magnetron can be designed so that the average speed of an electron is close to the speed of that travelling wave, *Vph*:

$$V_{ph} = V_{aver}. \qquad (21)$$

If an electron is moving in a phase of wave where the electric force is opposite to the direction of electron speed, then for a considerable span of time the electron will transfer its energy to the field's wave.

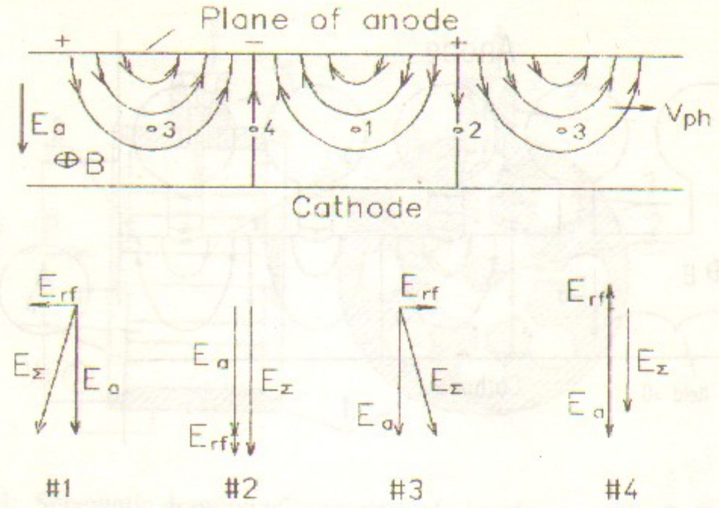

Figure 13: Electric field of the travelling wave in the interaction zone of the magnetron.

That is electron #3 in Fig. 13. The electric field of the wave will be nearly constant for this electron, and the total field that affects the electron's movement can be found as a sum of *Ea* and the wave field. The corresponding vector diagram for electron #3 is shown in Fig. 13. As mentioned above, the chain of cycloids is arranged perpendicular to the electric field, so the electron will go up the slope, until it hits the anode. The electric current start to flow though the magnetron. The energy of the hitting electron is much lower than that of the electron accelerated by total V_a in the absence of magnetic field. This difference in energy goes to the electric field of the wave and determines the efficiency of magnetron. Part of this energy is lost in cavity walls, but the major part goes to the magnetron load. For electron #1 the slope will go down, so that the emitted electron will return to the cathode. The direction of the electric field for the particles #2 and #4 will not change, but its value will be different . Therefore, in accordance with the formula for V_{aver}, both electrons will approach electron #3 and eventually will go to the anode. This focusing mechanism increases the current of the magnetron and the output power.

In spite of progress in the design of other types of microwave generators, magnetrons still maintain one of the leading positions for efficiency. It is in the range of 60-70% at a wavelength of 10 cm and 20-30% at 1 cm. Maximum output power is in the 10's of MW in pulse mode.

2.2 *Load Characteristics of Magnetron.*

The results of measurement in the magnetron are plotted usually as *Va* vs. *f (Ia)*. The parameters for the measurement are magnetic field *B*, output power *P*, frequency *f*, and efficiency η. The typical characteristics are shown in Fig. 14a.

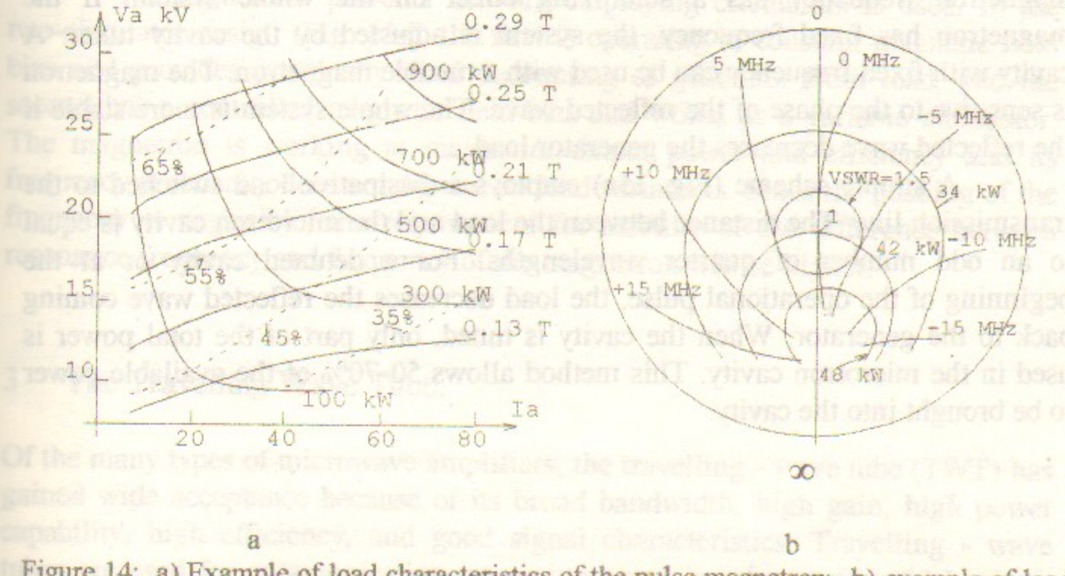

a b

Figure 14: a) Example of load characteristics of the pulse magnetron; b) example of load diagram of the pulse magnetron. λ =3 cm, B = 0.55 T, I_a=10 A. The zero frequency pushing curve corresponds to 9375 MHz.

For a constant magnetic field, the anode current grow rapidly with rising anode voltage and eventually is limited by the emission of the cathode. Thus small variations in applied voltage can cause appreciable changes in operating current.

The constant output power characteristics are like hyperbolas, but the curves are lifted at lower anode voltage and higher current, because of the decrease of the magnetron efficiency.

The load diagram of the magnetron is similar to that of other microwave generators with an output resonance circuit, e.g. a reflex klystron. The data-sheet value of the magnetic field and the anode current are used as fixed parameters for the load diagram. The reference plane for the load diagram is usually the output flange of the tube. A typical load diagram is shown in Fig. 14 b.

One of the important parameters for the magnetron is the pushing of frequency as a result of variation of load. Usually it is given for VSWR=1.5.

Magnetrons are often used as RF power sources for microtrons. As a rule, they are pulse tubes with an output power of several megawatts. They are coupled with the microtron cavity through a ferrite isolator or use a dissipative load. Pushing of the magnetron frequency has a stabilizing effect on the whole system. If the magnetron has fixed frequency, the system is adjusted by the cavity tuner. A cavity with fixed frequency can be used with a tunable magnetron. The magnetron is sensitive to the phase of the reflected wave. The whole system is more stable if the reflected wave decreases the generator load.

A simple scheme (Fig. 15a) employs a dissipative load switched to the transmission line. The distance between the load and the microtron cavity is equal to an odd number of quarter wavelengths. For a detuned cavity or at the beginning of the operational pulse, the load decreases the reflected wave coming back to the generator. When the cavity is tuned, only part of the total power is used in the microtron cavity. This method allows 50-70% of the available power to be brought into the cavity.

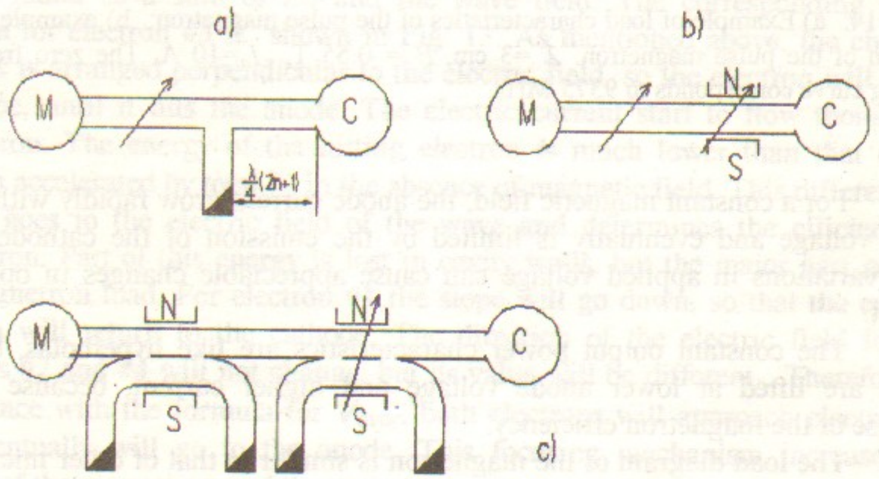

Figure 15: Methods of coupling between magnetron and microtron cavity. C - microtron cavity, M - magnetron.

The coupling with the cavity is simple if a ferrite isolator or circulator is used. Isolators are used for small machines and allow use of nearly 90% of the output power (Fig. 15b). The isolator does not provide ideal decoupling of generator from cavity, and the reflected wave still comes to the generator. If a phase of the reflected wave unloads the magnetron, a pushing of frequency, however small, has sufficient stabilizing effect upon the system.

For higher RF power a network employing circulators is used. In the two-circulator design (Fig. 15c), the first is operating at constant magnetic field bias and provides practically ideal decoupling of generator from load, and the second has a controlled magnetic field bias and works as a variable attenuator. The magnetron is working at maximum output power and efficiency and its frequency practically does not depend on load variations. Since the pushing of the frequency is negligible, the requirement for stability of the difference between resonance frequency and frequency of the magnetron will be higher.

3 The Travelling Wave Tube.

Of the many types of microwave amplifiers, the travelling - wave tube (TWT) has gained wide acceptance because of its broad bandwidth, high gain, high power capability, high efficiency, and good signal characteristics. Travelling - wave tubes are used for communication transmitters and in many types of laboratory equipment. The TWT consists of four major elements, shown in Fig. 16.

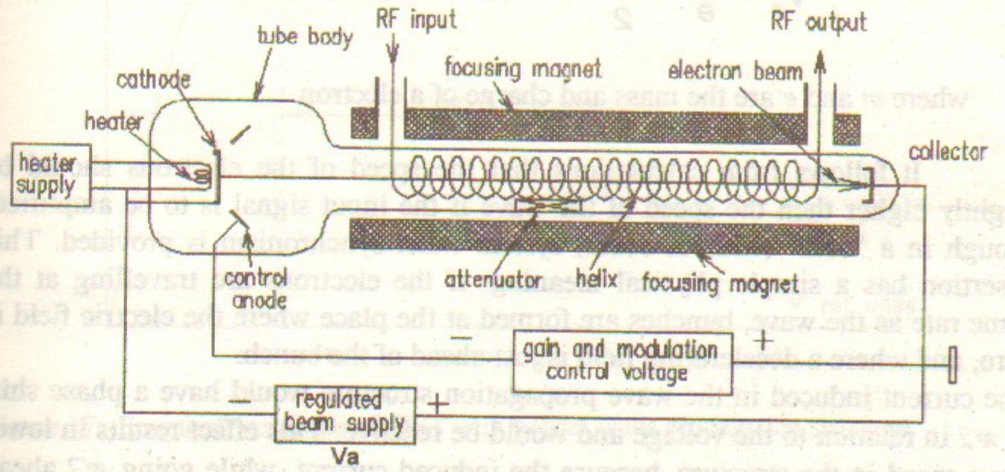

Figure 16: Schematic drawing of the travelling - wave tube.

They are an electron gun, a microwave interaction structure where the electron beam and the microwave signal interact, a magnetic focusing structure that confines the electron beam so that it moves through the interaction structure, and a collector that dissipates the energy in the electrons which originates at a heated cathode and is shaped by the electrostatic and magnetic focusing fields.
A stream of electrons is emitted by the cathode of the electron gun and accelerated by a voltage *Va* of the regulated beam supply. A focusing magnet forms a thin beam moving along the axis of the structure. Suppose the structure has the form of a helix. The input RF signal creates a wave that moves along the helix turns with a speed close to the speed of light. This wave produces a travelling electric field at the helix axis.

The speed of this field *Vph* is much lower than the speed of light *c* (usually around *c/10*) and is

$$V_{ph} = c \cdot \frac{S}{\sqrt{(2\pi a)^2 + S^2}} \,. \qquad (22)$$

Where *S* is the helix pitch, and *a* is the helix radius.

The accelerating voltage *Va* is chosen so that the speed of the electrons is close to *Vph*. The condition for that is

$$V_a = \frac{m}{e} \cdot \frac{V_{ph}^2}{2} \,. \quad \text{(non-relativistic case)} \qquad (23)$$

where *m* and *e* are the mass and charge of a electron.

It follows from calculations that the speed of the electrons should be slightly higher then the speed of the wave if the input signal is to be amplified, though in a "cold" (without beam) system exact synchronism is provided. This assertion has a simple physical meaning: if the electrons are travelling at the same rate as the wave, bunches are formed at the place where the electric field is zero, and where a decelerating field is just ahead of the bunch.
The current induced in the wave propagation structure would have a phase shift of $\pi/2$ in relation to the voltage and would be reactive. This effect results in lower wave speed in the structure, because the induced current, while going $\pi/2$ ahead the field voltage, creates a capacitance load of the structure. The speed of the bunch will be a little higher than the speed of the wave and all electrons will be

moving ahead in relation to a wave with a small speed equal to the difference. As a result, the bunch center will come into a decelerating area of the wave and start to transfer its kinetic energy to the electromagnetic field of the wave. The wave amplitude will grow exponentially.

The gain is proportional to the tube length, but in reality it is limited. One of the reasons is that the microwave signal at the tube output can be reflected back by a mismatch on the output line. This can cause regenerative gain variation or even oscillation. To avoid this condition most TWTs use an attenuator near the center of the circuit length. The attenuator can include physical severence of the circuit into two or more sections or only carbon attenuation to absorb any reflected power. Usually the attenuation factor for a "cold" system is 10 - 20dB higher then the total gain of the tube. The real gain of the TWT is in the range 30-50dB.

One of the important advantages of the TWT is that of great bandwidth, which is 20-50% of central frequency and more. A typical frequency response of a TWT with helix wave propagation structure versus relative frequency is shown in Fig. 17.

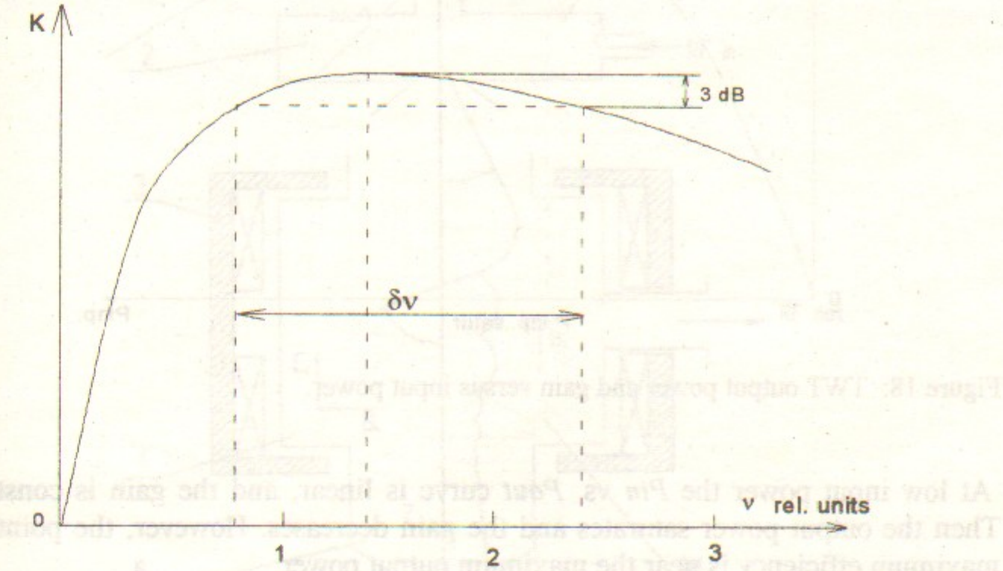

Figure 17: Frequency response of TWT with helical wave propagation structure.

It follows from experience that the frequency bandwidth is actually limited by technical circumstances. Matching of input and output of the tube in a wide frequency range is a difficult problem.

While electrons advance in a decelerating field, their speed drops and becomes even smaller than the speed of the wave. Thus the condition for amplification of the travelling wave is violated. Electrons get back into the accelerating field and start to take back the energy from the wave. Therefore the efficiency and tube gain drop. Real efficiency of a power TWT would not exceed 30 -40%. It is possible to increase the efficiency by using wave propagation structures that vary the wave speed along the circuit. This method and some others allow to increasing the efficiency up to 50% and higher.

The noise factor is very important for amplification of low level signals. Special types of TWT were developed that use various mechanical and electric configurations and technology. The noise factor of these tubes may be 3dB and less.

Amplitude characteristic curves showing the dependence of output power and gain on input power are plotted in Fig. 18.

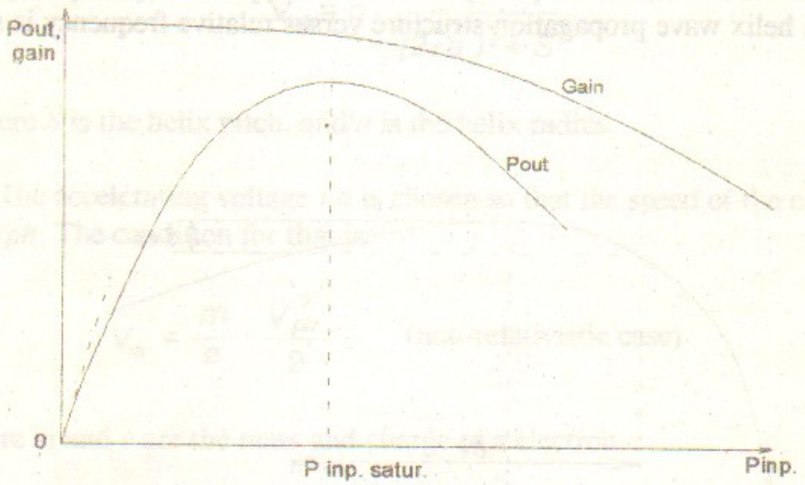

Figure 18: TWT output power and gain versus input power.

At low input power the *Pin* vs. *Pout* curve is linear, and the gain is constant. Then the output power saturates and the gain decreases. However, the point for maximum efficiency is near the maximum output power.

The phase difference between input and output signals of the TWT depends on the input power. It may be explained by a greater drop of the bunch's speed for a higher input signal. This results in slowdown of the structure wave and an increase of output signal delay. The data sheet gives this dependence as AM to PM conversion. Typically it is 2-4° for 1dB of input power.

4 Magnicon: Microwave Generator with Circular Deflection of Electron Beam.

The magnicon design is shown schematically in Fig. 19. A continuous electron beam from the electron source 1 reaches the circular deflection cavity 2, where it is deflected at an angle by an RF magnetic field rotating with a deflection frequency . The field distribution in the cavity is shown in Fig. 20. In the drift space, the electron trajectories separate from device axis, and then enter the stationary magnetic field B_z of the solenoid 3. While entering the magnetic field, the longitudinal velocity of the electrons is transformed into rotational transverse velocity (Larmor motion), and the degree of the transformation is characterised by the pitch angle α. Further on, travelling along helical trajectories and steadily changing their entry point into the output

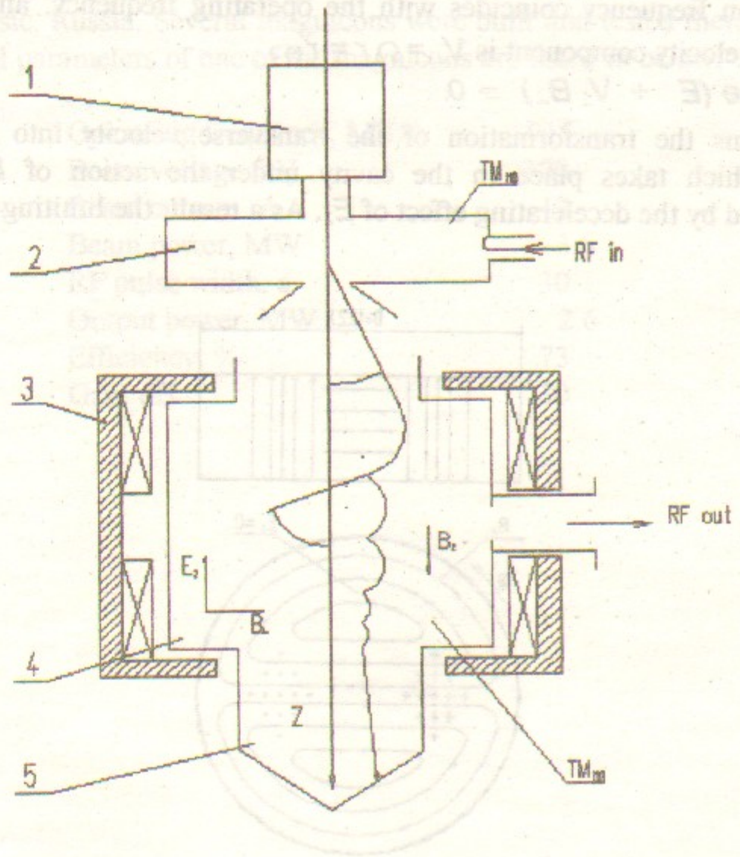

Figure 19: Schematic of the magnicon: 1) source of electrons; 2) circular deflection cavity; 3) solenoid; 4) output cavity; 5) collector.

cavity 4, the electrons excite an RF wave in the cavity that rotates in synchronism with the entry point of the electrons (TM_{110} oscillation mode, Fig. 20) and transfer their energy to this wave. If the cyclotron frequency Ω is close to the operating frequency ω (i.e. to the circular deflection frequency, to which the cavity is also tuned), and the direction of the cyclotron rotation coincides with that of the deflection device, then the interaction can remain effective during many periods of RF oscillation.

The particles' energy is transferred to the electromagnetic field on the magnicon output cavity because their transverse velocity decreases, wile their axial velocity remains almost constant. This can be easily explained by using as an example the deceleration of a nonrelativistic electron rotating in a homogeneous static magnetic field around the cavity axis. The fields in the cavity are known to have the following relations: $E_z = \omega r B_\perp$ (r is the radius). When the cyclotron frequency coincides with the operating frequency, and hence the transverse velocity component is $V_\perp = \Omega r = r\omega$,

then $F_z = e(E + V_\perp B_\perp) \equiv 0$.

Thus the transformation of the transverse velocity into longitudinal velocity, which takes place in the cavity under the action of B , is fully compensated by the decelerating effect of E_z. As a result, the limiting electron

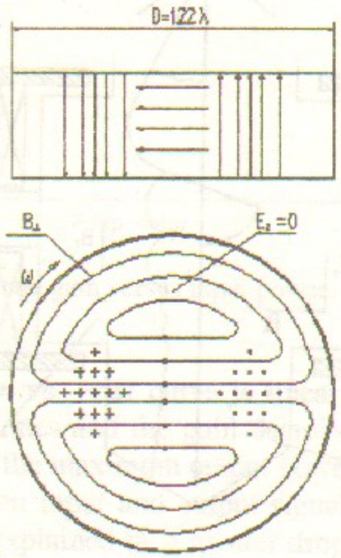

Figure 20: Distribution of electromagnetic field in output and deflection cavities. (TM_{110} mode)

efficiency is determined by the efficiency of the election energy transfer into rotational motion at the entrance into the magnetic field (i.e. by the pitch angle α) and is equal to $\eta_e \approx \sin^2 \alpha$.

In a magnicon, the electrons are not rotating around the cavity axis, and the longitudinal force is equal to zero "on average" for the period of the RF oscillations. This nevertheless does not change the character and efficiency of the interaction.

A long interaction and the resulting length of the output cavity lead to an essential decrease in RF field strength, in ohmic losses and in specific heat release. In addition, the large hole made for the beam in the center of the cavity end walls combined with the "magnetic accompaniment" essentially eliminates the problem of current interception. Thus, the magnicon can efficiently produce high power in the short wavelength range.

This type of microwave generator was invented at the Budker Institute of Nuclear Physic, Russia. Several magnicons were built and tested there. The main experimental parameters of one of the magnicons are listed in below.

Operating frequency, MHz	915
Beam voltage, kV	300
Beam current, A	12
Beam power, MW	3.6
RF pulse width, s	30
Output power, MW	2.6
Efficiency, %	73
Gain dB	30

Bibliography

1. L. Altman, Microwave Circuits, Van Nostrand, New York, (1964).
2. A.H.W. Beck, Thermoionic valves, Cambridge (1953).
3. . Oleg A. Nezhevenko, Gyrocons and Magnicons, IEEE Trans. Plasma Sci. 22, p.756 - 772, (1994).
4. Care & feeding of Power Grid Tubes, Varian Eimac (1967).
5. K.Spangenburg, Vacuum Tubes, McGraw-Hill (1948).
6. V.G.Veshcherevich et al, RF System of VEPP-3 Storage Ring for Energy of 3 GeV, Proc. 4th All-Union Conf. On Charged Particle Accelerators, Moscow, Nov. 1974, V.2, 337-340 (in Russian).
7. S.P. Kapitsa, V.N.Melekhin, Microtron, Moscow, NAUKA (in Russian) 1969.
8. V.N. Dulin, Electron and Ion Tubes, Moscow, Gosenergiozdat (in Russian) (1963).
9. V.M Berezin, V.S. Buriack et al., Microwave Electron Elements., Moscow, Vysshaay Shkola (in Russian) (1985).
10. I.V.Lebedev, Technique and Elements of Microwave Circuits, V.1, V.2, Moscow, Vysshaia Shkola (in Russian) 1972.

RF PULSE COMPRESSION FOR THE FUTURE LINEAR COLLIDER

I.V.SYRACHEV
Branch INP, Protvino, 142284, Moscow reg., Russia.

RF pulse compression is a method of exchanging the long low-power RF pulse by a short pulse of higher peak power. This is essential for the Future Linear Collider, where the required peak power of about 100 MW per meter of accelerator can not be produced with conventional RF sources. The most advanced methods of RF pulse compression are described. Theories are briefly presented, with their special features. Various schemes are illustrated with their specific designs and compared for particular collider configurations.

1 Introduction

The Future e^+e^- Linear Collider is intended to be one of the most powerful tools for detailed investigations in the field of elementary particle physics. Several projects for such a machine with a center-of-mass energy of 500 GeV to 1 TeV are under intensive development in different national accelerator laboratories: NLC (SLAC, USA), JLC (KEK, Japan), VLEPP (BINP, Russia), TESLA and SBLC (DESY, Germany), and CLIC (CERN, Switzerland). Considering the costs of fabrication and operation of the Future Linear Collider and the need to keep its total length to a reasonable value, much of the international acceleration physics community has decided to aim for an accelerating gradient of 50-100 MeV/m. To reduce the amount of pulsed RF power required to reach these gradients, in most of the projects mentioned (except TESLA and SBLC) it was decided to leave the S-band frequencies that had been developed with linacs and to open up a centimeter-range X-band. This has resulted in much R&D toward a suitable X-band RF power source, which can produce pulsed RF power in the range 100 to 200 MW per meter of accelerator.

Many exotic RF power source concepts for the X-band linear collider have been proposed during the last decade. However they were not likely to produce practical, reliable devices on a reasonable time scale. Thus now the most advanced approach is to:

1. Develop conventional klystron tubes at X- band frequency capable of producing 50 to 100- MW pulses lasting several times as long as the structure filling time.

2. Use an RF pulse-compression scheme to exchange longer pulse length for higher peak power.

Modern experience indicates that the problem of an X-band klystron has practically been solved. Such a device has already been manufactured at SLAC and has demonstrated the $1.1\mu sec \times 75 - MW$ RF pulse[1]. In other laboratories (KEK and BINP) R&D work in this field has also been quite successful.

The history of the application of RF pulse compression to linear accelerators covers more than 20 years. The basic idea of the method was discovered in 1973 at SLAC by Z.D. Farkas and P.B. Wilson. They received a 1991 IEEE Particle Prize for their invention. The advantages of RF pulse compression are many. The demand on the klystrons for peak power is reduced. Consequently, the tube can operate at lower voltage and at lower perveance, possibly allowing increased efficiency. Pulse compression devices are passive microwave networks without a beam, and hence are not sensitive to peak power problems as are RF power amplifiers based on beam-RF interaction. Thus they naturally have lower capital, maintenance and replacement costs then the tube. Also, the use of longer-duration pulses in klystrons reduces the effects due to rise- and fall-times in the pulse modulators and in other components of the RF system.

This lecture reviews the present status of RF pulse compression in relation to the design of the Future Linear Collider.

2 RF Pulse Compression Concepts

At present a few RF pulse compression schemes (RPC) are under development. Their common principle of operation is as follows: delivered RF energy builds up in some RF storage element during the major part of the klystron pulse duration and then is largely extracted during the last fraction of the pulse. RPC can be separated into two groups according to the means of RF energy storage: high-Q resonators, or delay lines with low RF energy consumption. The transformation in the RPC from RF energy build-up to RF energy utilization also can be done in several ways:

(1) changing the coupling of the storage element,
(2) reversing the RF phase of the feeding pulse,
(3) combining these two methods.

2.1 RPC with Interference Switch (SPC)

Figure 1 is a schematic illustration of the basic idea[2]. A high-Q storage cavity is coupled to an H-plane T that acts as the interference switch. In the storage state (Fig. 1a), a standing wave is produced by reflection off a short in one arm of the T. In this storage state, the cavity is filled with energy from the RF source, and ideally no power is fed to the load. In the dumped state (Fig. 1b), a fast RF switch moves the short position by $\lambda_g/4$ toward the resonator. This couples the microwaves directly to the load. Note that the output pulse is phase-locked to the drive.

If τ_d is the decay time of the energy stored in the cavity in a dumped state and τ_s is the storage time, then in the ideal case the power gain is $P_g = \tau_s/\tau_d$. Nevertheless, despite the simplicity of the idea, the real application of this method for high gradient linacs meets some problems:

- The need to use an RF-switch that must operate at a high level of RF power (about 100 MW) requires that a very special device be designed. This might turn out more complicated and expensive than the whole RPC system.

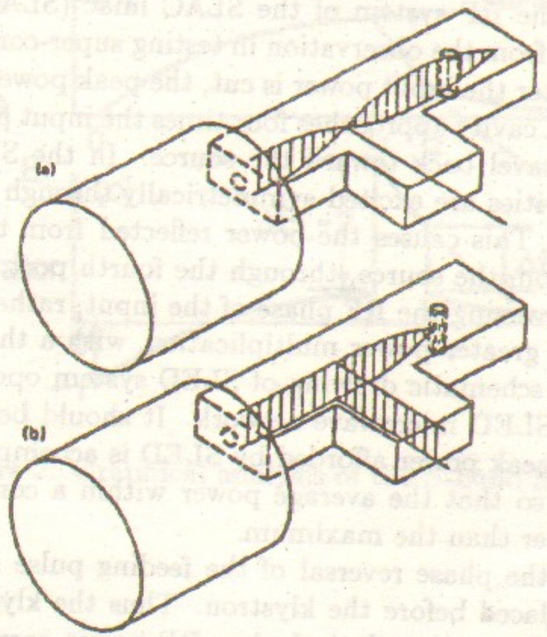

Figure 1: Scheme of microwave cavity and H- plane T showing the electric envelope in (a) the storage state, and (b) the dumped state.

- In the storage state, the switch is in a resonant circuit of the RPC. This imposes very severe requirements for the stability of its parameters and reduces the reliability of the system tuning and operation.

- The advantages of this scheme become evident if the pulse compression ratio reaches 10^2 for cavities with normal conductivity, or 10^5 for superconducting cavities[3]. This is the principal feature of the method, because of the weak coupling of the high-Q cavity to the RF source during the energy storage period, and it limits its applicability for the future X-band linear collider, where the compression ratio is less than 10 because of the RF source peculiarity.

The compression efficiency in the method reaches 10 to 20%.

Therefore SPC is not considered now as a possible candidate for the RPC for the Future Linear Collider. Below, other methods that seem more attractive for our purposes will be discussed.

2.2 SLED-type Pulse Compressors

Historically, the S-band SLAC Energy Doubler (SLED) was the first RPC scheme applied to the RF system of the SLAC linac (SLAC, USA)[4]. The SLED idea emerged from the observation in testing super-conducting cavities that immediately after the input power is cut, the peak power emitted from a heavily over-coupled cavity approaches four times the input power. Normally, this power would travel back toward the source. In the SLED network, a pair of resonant cavities are excited symmetrically through a four-port 3-db directional coupler. This causes the power reflected from the resonators to be directed away from the source, through the fourth port. Furthermore, it was realized that reversing the RF phase of the input, rather than switching it off, gave an even greater power multiplication, with a theoretical limit of nine. Figure 2 is a schematic drawing of SLED system operation. Figure 3 shows the S-Band SLED microwave network. It should be noted, however, that the increased peak power afforded by SLED is accompanied by a sharp exponential decay, so that the average power within a compressed pulse is generally much lower than the maximum.

In this scheme the phase reversal of the feeding pulse is organized with the phase shifter placed before the klystron. Thus the klystron's pulse manipulation can be done at a relatively low RF power corresponding to the level of the drive klystron's power – less than 1 kW. This advantage of the SLED over the above method simplifies the RPC operation significantly and makes it very reliable.

In order to understand the theory of SLED, it is helpful to consider the

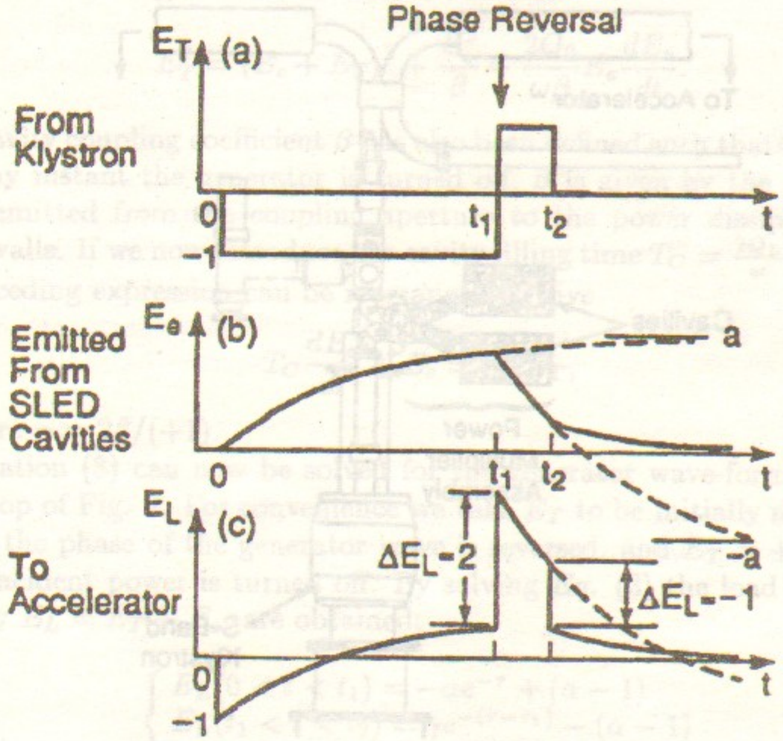

Figure 2: Graphical analysis of the S-band SLED.

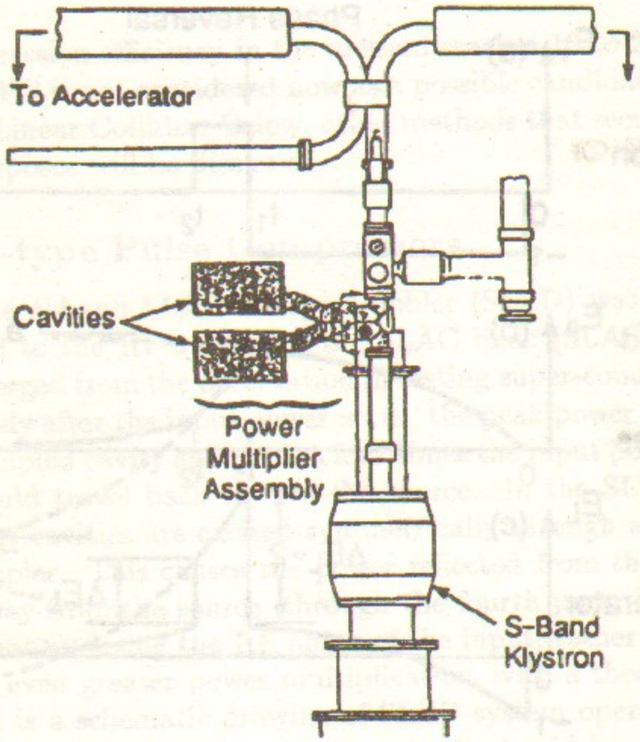

Figure 3: View of a SLAC S-band klystron plus SLED pulse compressor.

transient behavior of the reflected and stored fields in a single resonant cavity. By conservation of power[4]:

$$P_T = P_L + P_C + \frac{dW_C}{dt}, \tag{1}$$

where P_T is the incident power, P_L is the net reflected power, P_C is the power dissipated in the cavity, and W_C is the energy stored in the cavity at time t. Using $P_C = \omega W_C/Q_0$, together with the fact that power is proportional to the square of the field ($P = kE^2$), and denoting the amplitude of the emitted wave as E_e, the above relation becomes

$$E_T^2 = (E_e + E_T)^2 + \frac{E_e^2}{\beta} + \frac{2Q_0}{\omega\beta} E_e \frac{dE_e}{dt}. \tag{2}$$

A cavity coupling coefficient β has also been defined such that $kE_e^2 = \beta P_C$. If at any instant the generator is turned off, β is given by the ratio of the power emitted from the coupling aperture to the power dissipated in the cavity walls. If we now introduce the cavity filling time $T_C = \frac{2Q_L}{\omega} = \frac{2Q_0}{[\omega(\beta+1)]}$, the preceding expression can be rearranged to give

$$T_C \frac{dE_e}{dt} + E_e = -\alpha E_T, \tag{3}$$

where $\alpha = 2\beta/(+1)$.

Equation (3) can now be solved for the generator wave-form E_T shown at the top of Fig. 2. For convenience we take E_T to be initially negative. At time t_1 the phase of the generator wave is reversed, and $E_T = +1$. At time t_2 the incident power is turned off. By solving $Eq.$ (3) the load waveforms, given by $E_L = E_T + E_e$, are obtained:

$$\begin{cases} E_L(0 < t < t_1) = -\alpha e^{-\tau} + (\alpha - 1) \\ E_L(t_1 < t < t_2) = \gamma e^{-(\tau - \tau_1)} - (\alpha - 1) \\ E_L(t > t_2) = (\gamma e^{(\tau_2 - \tau_1)} - \alpha) e^{-(\tau - \tau_2)} \end{cases} \tag{4}$$

where $\gamma = \alpha(2 - e^{-t_1/\tau})$ and $\tau = t/T_c$. These equations for the field describe the time plots of Fig. 2, where the lowest part shows the output waveform.

As our interest is limited to RPC operation, we will not discuss the benefit of SLED in terms of charged particle acceleration. Therefore we will define the most important parameters of the RPC systems as follows: energy compression efficiency is $\eta_{rpc} = \int_{t_1}^{t_2} E_L(t)^2 dt / t_2 E_T^2$ and power gain is $P_g = \eta_{rpc} C_r$, with $C_r = t_2/(t_2 - t_1)$ being the ratio of the output to input pulse durations.

A SLED microwave network, attached to each klystron, has been in use on the SLAC linac since 1979, boosting the linac energy by about 60%. It utilizes cylindrical resonant cavities oscillating at 2.856 GHz in the TE_{015} mode, with a Q_0 of 10^5. Each is coupled to a 3-*db* hybrid in a rectangular waveguide through a circular aperture such that $\beta = 5$. Operating with a $3.5\mu s$ input pulse for compression ratio $C_r = 4.27$, SLED provides a compression efficiency $\eta \approx 70\%$. Implementation of SLED was a major step in achieving the goal of 50 GeV per beam in the Stanford Linear Collider.

A similar system known as LIPS (LEP Injector Power Saver) serves the injector linac of the Large Electron-Positron Collider (CERN). LIPS uses double side-wall irises, rather than a single end-wall iris , to allow greater peak power. In KEK (Japan) in a similar model with double side-wall irises a power flow of 380 MW without an RF break-down was achieved[5].

During RPC operation it is desirable to provide both efficiency and power gain as high as possible. Following Eq. (4), the loaded Q- factor, i.e. the coupling coefficient β must be optimized. In any given case this optimization must be done individually. But for general purposes the following consideration can be used as a good approximation. For a given storage period t_1 , the maximum RF energy will be stored in the cavity with unloaded quality factor Q_0 if the coupling coefficient β satisfies the condition

$$\beta = \frac{1.26Q_0}{\pi f t_1} - 1 \tag{5}$$

where c is a compression factor and f is the operating frequency. If we then define new dimensionless variables as

$$x = \frac{Q_0}{\pi f t_2}, y = \frac{t}{t_2}, \tag{6}$$

then the amplitude of the output signal (see Eq. 4) in the time interval $t_1 < t < t_2$ can be rearranged to give

$$E_L(y) = 2(1 - \frac{1}{x}\frac{c-1}{1.26c})[6e^{-y\frac{1.26c}{c}} - 1] + 1, \frac{c-1}{c} < y < 1. \tag{7}$$

By integrating this equation in accordance with the definitions of η_{rpc} and P_g, we get families of curves for these parameters (see Fig. 4). For practical reasons, it is better to use other curves (see Fig. 5), that define x and c parameters for the given values of rpc or Pg.

Figure 5 indicates clear limits for the design parameters of SLED-type compressors. For example, if we try to obtain a power gain > 3.5 with

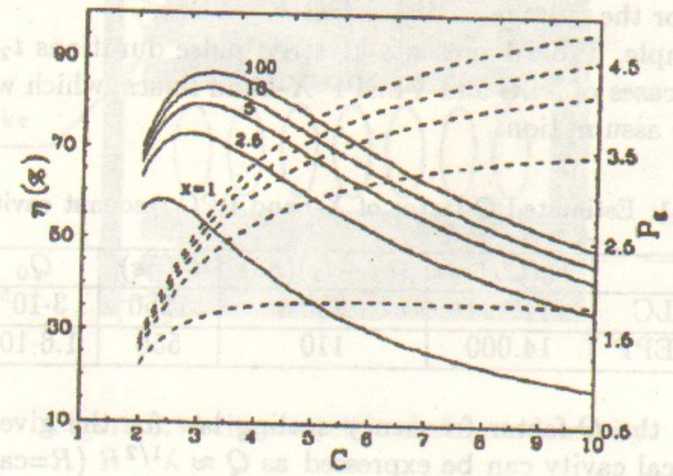

Figure 4: Efficiency (solid line) and power gain (dotted line) *vs*, compression ratio c for different values of parameter x.

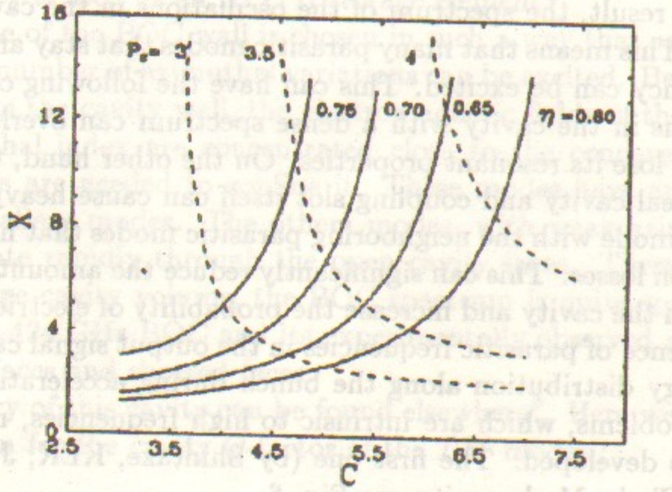

Figure 5: Efficiency (solid line) and power gain (dotted line) level lines in $c - x$ coordinates

efficiency > 0.7, the parameter x should be > 6.7 and the compression ratio stays within the limits $4.5 < c < 5.5$ with the optimum at $c \approx 5$. Adapting this example to the design parameters of the accelerator, we can get the requirements for the storage cavity Q-factor.

As an example, Table 1 presents klystron pulse durations t_2 and the Q-factors for the cases of NLC and VLEPP X-band linacs, which we calculated with the above assumption.

Table 1: Estimated Q-factor of X-band RPC resonant cavity.

	$F_0(GHz)$	$(t_2 - t_1)(ns)$	$t_2(ns)$	Q_0
NLC	11.424	250	1250	$3{\cdot}10^5$
VLEPP	14.000	110	550	$1.6{\cdot}10^5$

In general, the Q-factor frequency scaling law for the given oscillation in the cylindrical cavity can be expressed as $Q \approx \lambda^{1/2} R$ (R=cavity radius). Thus if in the X- band cylindrical cavity we want to provide a higher Q- factor than was used in the original S-Band SLED, then we need to use a cavity whose dimension-to-wavelength ratio is large. For example for the VLEPP case (Table 1), the excess of this ratio compared to the S-band SLED will be about 5. As a result, the spectrum of the oscillations in the cavity becomes rather dense. This means that many parasitic modes that stay around the operation frequency can be excited. This can have the following consequences. The oscillations in the cavity with a dense spectrum can overlap, and thus the cavity will lose its resonant properties. On the other hand, the non-ideal shape of the real cavity and coupling slot itself can cause heavy coupling of the operation mode with the neighboring parasitic modes that have small external radiation losses. This can significantly reduce the amount of RF power extracted from the cavity and increase the probability of electrical discharge. Also, the presence of parasitic frequencies in the output signal can distort the designed energy distribution along the bunch during acceleration. To overcome these problems, which are intrinsic to high frequencies, new technical solutions were developed. The first one (by Shintake, KEK, Japan[6]) used the so-called Choke-Mode cavity, see Fig. 6.

In this configuration of the cylindrical cavity all the modes that have longitudinal currents are damped. But the operating mode H_{01n} is trapped because of the special choke design, which is like a kind of quarter-lambda radial waveguide mode filter. This renders the spectrum much sparser, but it avoids dealing with the many H_{0mn} modes that would be predominant parasitic modes in the axi-symmetric cavity.

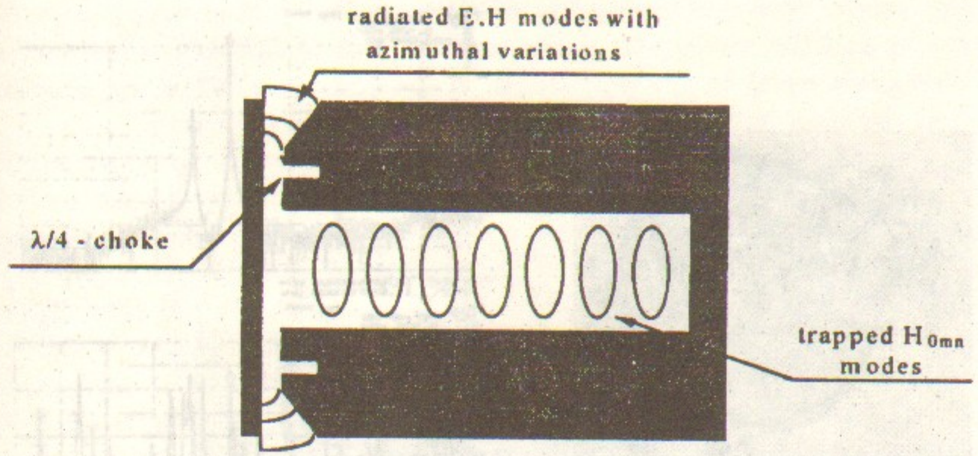

Figure 6: Axi-symmetric choke-mode cavity.

The VLEPP Power Multiplier (VPM), proposed in 1990 by Balakin and Syrachev (BINP, Russia)[7-8], is another attempt to create an effective X-band SLED-type compressor. In this device the so-called Barrel-shape Open Cavity (BOC) is used as an RPC rf storage element.

The shape of the BOC wall is chosen in such a way that only oscillations with a large number of azimuthal variations can be excited. Being repeatedly reflected from the cavity wall, the electromagnetic fields of the mode with a large azimuthal index are concentrated close to the concave wall, so that no end plates are needed to confine it. These modes have an exotic name, whispering-gallery modes. The others modes, with weak azimuthal dependencies radiate rapidly through the open cavity faces. Therefore despite a relatively large cavity volume, the BOC spectrum is quite sparse. Figure 7 shows the 11.424 GHz BOC and its experimentally observed spectra for the open cavity faces and shorted faces.

The theory of this cavity can be found elsewhere[9]. Here we will give only the expression for the cavity Q-factor of the TM modes :

$$Q_{TM} = \frac{a}{\sigma} \tag{8}$$

where a is the cavity radius and σ is the penetration depth for the cavity surface. It is easy to see that for the copper cavity the quality factor will be > 100000, provided the ratio $2a/\lambda$ is more than 5. A few samples of the 11.424- and 14-GHz BOC were manufactured. Their parameters are

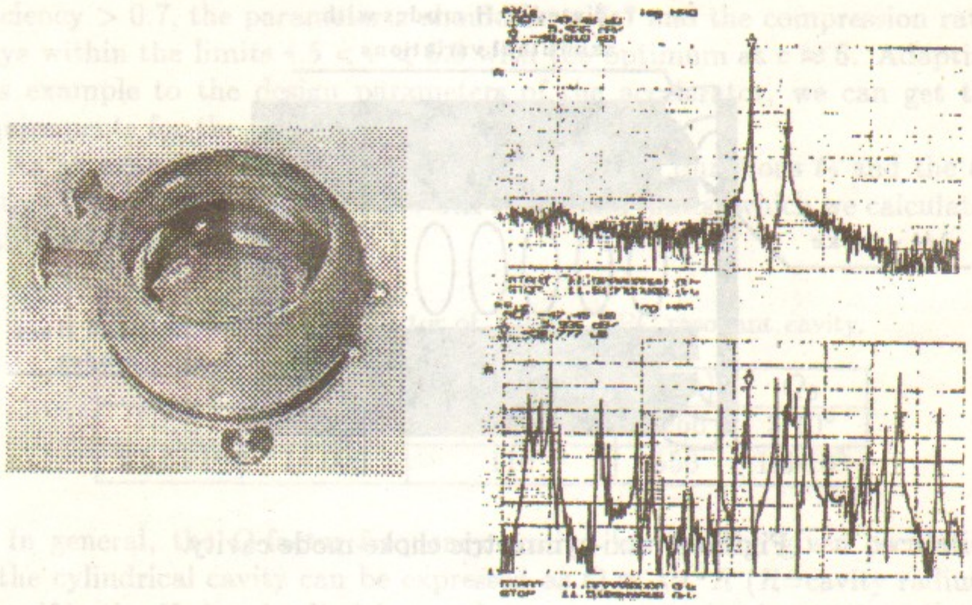

Figure 7: General view of the 11.424 GHz Barrel-shape Open Cavity and its measured spectra for open (upper) and shorted (lower) faces.

presented in Table 2.

A large number of azimuthal variations of the whispering- gallery mode make it possible to use the traveling-wave regime of operation. In this regime, the electro-magnetic field rotates in the cavity along the cavity surface. This is accomplished by feeding the cavity through many coupling slots that are placed in the common wall of the cavity and waveguide. The feeding waveguide lies around the cavity on its median plane. The VPM assembly is shown in Fig. 8.

Table 2:Parameters for the three types of the Barrel-shape Open Cavity.

Mode	Diameter (cm)	Frequency (GHz)	$Q_0/10^5$ measured	$Q_0/10^5$ calculated
$TM_{51,1,1}$	40	14	3.1	3.3
$TM_{31,1,1}$	26	14	2.0	2.1
$TM_{26,1,1}$	26	11.424	1.8	1.9

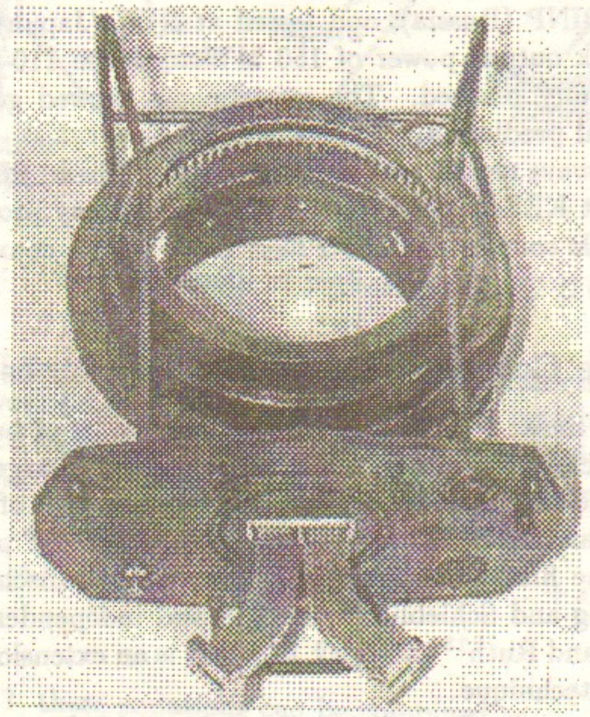

Figure 8: General view of the 11.424-GHz VPM. This is a version of the device for the RF high power tests.

The proper choice of waveguide width provides equal phase velocities in the cavity and the waveguide. This, together with a slot-to-slot distance in the waveguide equal to 1/4 wavelength at the operating frequency, provides the best coupling and matching of the cavity and the waveguide.

The travelling-wave regime of the VPM operation has advantages over the original SLED scheme. Because only one storage cavity is used, no 3-*db* hybrids are necessary. Also, having a large number of coupling slots (more than 100) solves the problem of the single-slot electrical strength at high level RF power operation. The 11.424-GHz version of the VPM (Fig. 8) was manufactured at BINP (Russia), and tested at KEK (Japan) at a high RF power[10]. The peak output power of 150 MW with the 110-*ns* compressed pulse was successfully reached. The experiments showed good agreement with the theoretical prediction.

The travelling-wave regime was also used in the *S*-band SLED-type compressor designed at KEK(Japan) for the KEK B- factory project[11]. In this project the two-hole coupler and the TE_{620} mode with a coaxial cylinder as a cavity were used.

2.3 RF Pulse Compressors with Delay Lines

A next-generation linear collider will require long trains of bunches per RF fill to achieve sufficient luminosity while keeping space-charge effects down. This, along with the very tight energy stability requirements of the final focus system, makes a standard SLED scheme unusable. A flat RF pulse is needed.

SLED II is the first approach of this type we will discuss. Originally conceived by Fiebig and Schieblich[12] in 1988 and independently developed by Farkas, Wilson and Ruth[13] at SLAC, SLED II is an extension of the SLED pulse compression technique.

In SLED II, the resonant cavities are replaced by long resonant delay lines. These can be lengths of low-loss waveguide, shorted at one end and iris-coupled to adjacent ports of a 3-*db* coupler at the other. The SLED II high- power system is shown in Fig. 9.

The length of the delay lines is determined by the desired width of the compressed pulse and must be an integer number of the guide half-wavelengths. As the wave emitted from the lines changes at discrete time intervals, given by the round-trip travel time, a flat output pulse can be produced. This makes SLED II useful for accelerating long trains of bunches. It also increases the intrinsic efficiency and reduces the peak-to-average field ratio in the compressed pulse.

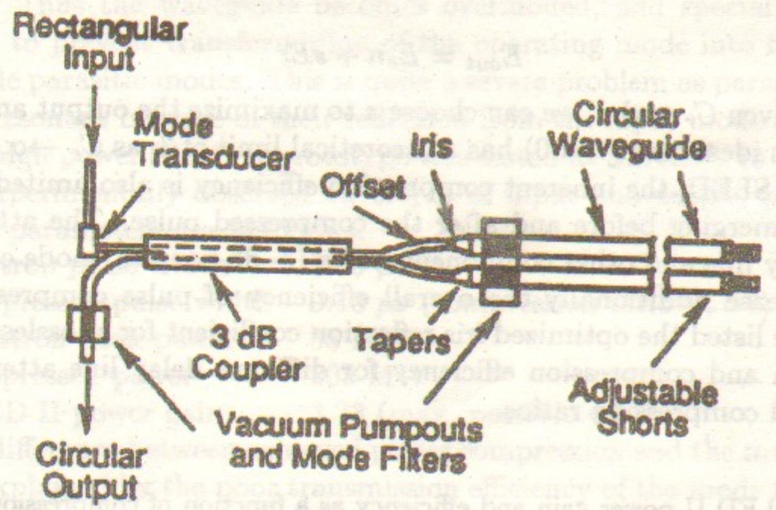

Figure 9: Schematic layout of high-power SLED II system.

Next, SLED II theory is briefly given. Let s be the reflection coefficient of the coupling network when the line is terminated in a matched load, and let τ be its attenuation in nepers. After turning on an incident field of amplitude E_i , the emitted field after n round-trip passes in units of lines is given by[13]

$$E_e(0), E_e(n) = E_i(1-s^2)e^{-2\tau} \times [1 + se^{-2\tau} + s^2e^{-4\tau} + ... + s^{(n-1)}e^{-(n-1)2\tau}], \quad n = 1, 2, 3, ... \tag{9}$$

Since $se^{-2\tau} < 1$, these equations can be combined as

$$E_e(n) = E_i \frac{(1-s^2)e^{-2\tau}}{1-se^{-2\tau}}[1 - s^n e^{-n2\tau}], n = 0, 1, 2, 3, ... \tag{10}$$

Define an integer compression ratio C_r as the ratio of the input pulse length to the delay time $t_d = 2L/vg$, where L is the line length and vg is the group velocity in the line. Superposition of the emitted field with the iris reflection yields the output

$$E_{out} = E_e(n) - sE_i, n = 0, 1, ..., C_r - 2. \tag{11}$$

At time $t = (C_r - 1)t_d$, the phase of the input pulse is shifted by π, so that the waves add together, and we get a compressed output pulse of duration t_d with amplitude

$$E_{out} = E_e n + sE_i \tag{12}$$

For a given C_r and τ, we can choose s to maximize the output amplitude, which in an ideal case ($\tau = 0$) has a theoretical limit of 3, as $C_r \to \infty$ and $s \to 1$. As with SLED, the inherent compression efficiency is also limited because of power emerging before and after the compressed pulse. The attenuation in the delay line and other component losses (3- db coupler, mode converter, etc.) decrease additionally the overall efficiency of pulse compression. In Table 3 are listed the optimized iris reflection coefficient for a lossless system, power gain and compression efficiency for different delay line attenuations, and several compression ratios.

Table 3: SLED II power gain and efficiency as a function of compression factors and delay line attenuation.

C_r	s	$\tau = 0.0$		$\tau = 0.015$		$\tau = 0.05$		
		P_g	$\eta(\%)$	P_g	$\eta(\%)$	P_g	$\eta(\%)$	
3	0.549	2.66	89	2.52	84	2.23	74	
4	0.610	3.44	86	3.21	80	2.77	69	
5	0.651	4.02	80	3.72	74	3.12	62	
6	0.685	4.49	75	4.08	68	3.36	56	
8	0.733	5.14	64	4.60	58	3.64	46	
10	0.767	5.62	56	4.90	49	3.78	38	
12	0.790	6.00	50	5.1	43	3.90	32	

To obtain the required attenuation in the delay line (say $\tau < 0.015$), a circular waveguide with H_{01} mode is used as a delay line of the X-band SLED II. For the guided-wave transmission lines with normal conductivity, this mode has the lowest ohmic losses. For the given delay time $T_d = t_d/2$, the H_01 attenuation and the length of the copper circular waveguide with diameter D are

$$\tau = \frac{\lambda_0^{3/2}}{29.5D^3} cT_d, \qquad L = \nu_g T_d = \sqrt{1} - (\lambda_0/082D)^2 cT_d \tag{13}$$

Adjusting the desired attenuation of the delay line for the 11.424-GHz NLCTA parameters ($T_d = 125\ ns$) we get that the guide diameter must be

$> 7cm$. Thus the waveguide becomes overmoded, and special care must be taken to prevent transformation of the operating mode into neighboring waveguide parasitic modes. This is quite a severe problem as parasitic modes become resonant because of their reflection from the input mode transducer.

The high power SLED II prototype was tested at SLAC[14]. In Fig. 10 are shown experimentally observed envelopes of input and output pulses. The obtained parameters are as follows:

klystron pulse width	1.05 μs
compressed pulse width	0.15 μs (compression ratio C_r=7)
klystron peak power	55 MW
compressed power	205 MW
SLED II power gain	3.73 (max. possible 4.84).

The difference between achieved power compression and the maximal possible is explained by the poor transmission efficiency of the mode transducer, which decreased the component efficiency from 0.9 (estimated) to 0.77 (obtained).

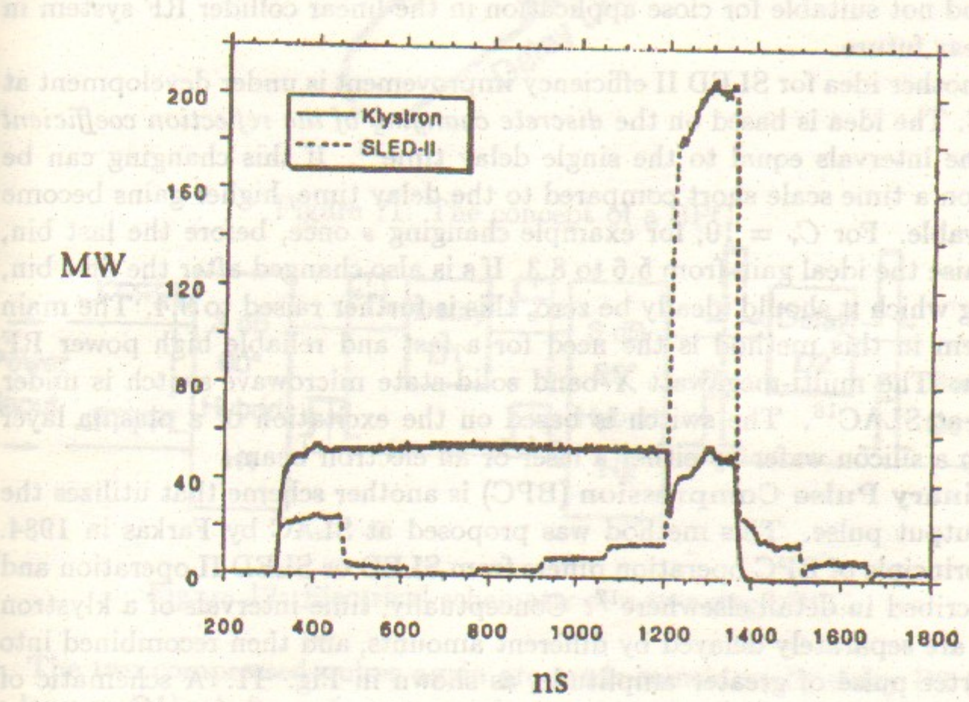

Figure 10: High power klystron and SLED II outputs.

The flat output pulse of the SLED II makes it possible to upgrade the system in order to increase inherent efficiency or to provide higher power gain.

One way is to organize *the cascading of the individual SLED II stages*, which gives a peak power gain > 10 with a reasonable compression efficiency. A cascaded system requires special phase modulation of the input signal[11]. The compression factor in this case is the product of ratios at each stage ($n_1 n_0$), and does not depend on the relative values of n_1 and n_0 . The power gain and compression efficiency also depend only on the product $n_1 n_0$. Therefore if $n_1 \neq n_0$, then we should choose $n_1 > n_0$ if we wish to minimize line length, and $n_1 < n_0$ if we wish to minimize switching transition.

As an example, let us examine a two-stage system using the data from Table 3. Let the first stage have n_1=4 and attenuation τ_1=0.05, and the second $n_0 = 3, \tau_0 = 0.015$. Then the power gain will be P_g=7 and the compression efficiency η=0.59, whereas in the single-stage SLED II, for compression factor $C_r = n_1 n_0 = 12$ and $= 0.05$, we have P_g=3.9 and $\eta = 0.32$. However, the large overall compression factor and the relatively low efficiency make this method not suitable for close application in the linear collider RF system in the near future.

Another idea for SLED II efficiency improvement is under development at SLAC. The idea is based on the *discrete changing of the reflection coefficient* at time intervals equal to the single delay time[15]. If this changing can be done on a time scale short compared to the delay time, higher gains become achievable. For $C_r = 10$, for example changing s once, before the last bin, can raise the ideal gain from 5.6 to 8.3. If s is also changed after the first bin, during which it should ideally be zero, this is further raised to 9.4. The main problem in this method is the need for a fast and reliable high power RF switch. The multi-megawatt X-band solid state microwave switch is under R&D at SLAC[16]. The switch is based on the excitation of a plasma layer within a silicon wafer by either a laser or an electron beam.

Binary Pulse Compression (BPC) is another scheme that utilizes the flat output pulse. This method was proposed at SLAC by Farkas in 1984. The principle of BPC operation differs from SLED or SLED II operation and is described in detail elsewhere[17]. Conceptually, time-intervals of a klystron pulse are separately delayed by different amounts, and then recombined into a shorter pulse of greater amplitude, as shown in Fig. 11. A schematic of a two-stage BPC is shown in Fig. 12. It works as follows: Two RF inputs are phase-coded into four time-bins with phases 0 or π, denoted by "+" or "-", respectively. A 3-dB coupler or "hybrid", labeled H1 in Fig. 12, acts as the "switch" in Fig. 11. The hybrid combines the two inputs and directs the

combined power to either output port, depending on the relative phase of the two inputs. In this way, the hybrid can produce output pulses with half the pulse-length and twice the peak power of the input pulses (in the "ideal" lossless case), properly phase-coded for the next stage.

The compressed pulses are sequential, not coincident. They are made coincident at hybrid H2 by delay D1. In the second stage, H2 again doubles the peak power and halves the pulse length.

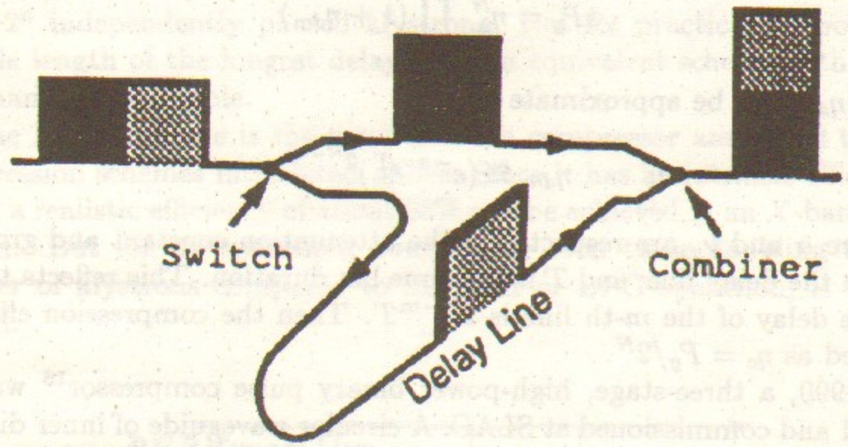

Figure 11: The concept of a BPC

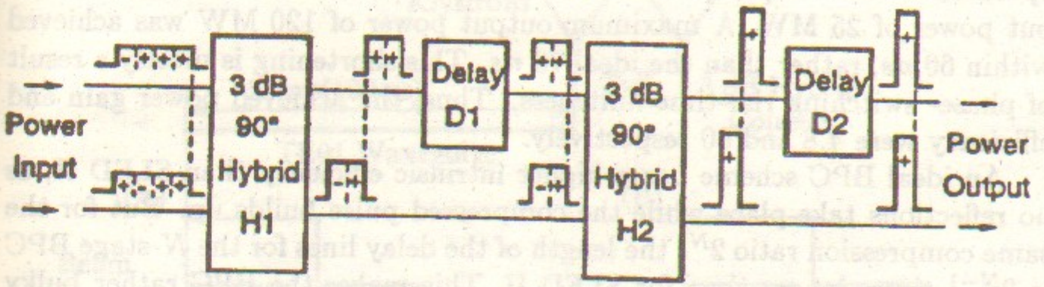

Figure 12: Electrical schematic of a two-stage BPC.

The two compressed pulses again are made coincident by delay D2 (half as long as D1). A "more"-stage requires more hybrids and delay lines, and more complicated phase-coding. Thus, for the ideal case the power gain of an N-stage BPC will be equal to 2^N. The two output pulses from any number of stages may be used separately to energize a linac, or may be combined (by

an additional hybrid) into a single high-power pulse.

In the real system, the same as for SLED II, the chief causes of inefficiency are ohmic losses in individual components, reflections, and mode conversion, where possible. Denote the average power-combining efficiency of a coupler, or hybrid, and short connecting line as η_h. Let one minus the additional loss to a pulse traveling through delay line m be called η_{dm} . We then write the following expression for the expected power gain of an N-stage BPC:

$$P_g = \eta_h^N \prod_{m=1}^{M} (1 + \eta_{dm}) \tag{14}$$

and η_{dm} can be approximate by

$$\eta_{dm} \cong (e^{-\alpha v_g T})^{2^{N-m}} \tag{15}$$

where α and v_g are respectively the attenuation constant and group velocity in the delay line, and T is the time bin duration. This reflects the fact that the delay of the m-th line is $2^{N-m}T$. Then the compression efficiency is defined as $\eta_c = P_g/2^N$.

In 1990, a three-stage, high-power binary pulse compressor[18] was constructed and commissioned at SLAC. A circular waveguide of inner diameter 7.1 cm was chosen for the delay line. With H_{01} mode this has a theoretical loss of $1.08dD/\mu s$ (or $4.\times 10^{-3}$ dD/m). In this configuration, the BPC was operated with an input pulse of 500-ns duration and with a maximum input power of 25 MW. A maximum output power of 120 MW was achieved within 60 ns, rather than the ideal 70 ns. This shortening is mostly a result of phase- switching rise-time finiteness. Thus, the achieved power gain and efficiency were 4.8 and 60 respectively.

An ideal BPC scheme has a higher intrinsic efficiency than SLED II, as no reflections take place while the compressed pulse builds up. But for the same compression ratio 2^N, the length of the delay lines for the N-stage BPC is 2^{N-1} times longer than for SLED II. This makes the BPC rather bulky compared to SLED II. That is why BPC is best suited to high frequencies, where accelerator section fill times are short. The physical length and losses of delay lines become reasonable in such cases. BPC might not be appropriate at X-band, but merits consideration at the higher frequencies of some Future Linear Collider.

Delay Line Distribution System (DLDS) is the last scheme from the series of original methods to be introduced in this chapter. This method was proposed by Mizuno (KEK, Japan) in 1994[19]. Formally DLDS is a part of a

single-stage BPC. The idea is to combine RF power from two klystrons with a 3-dB coupler and use phase reversal in one klystron to direct the leading half of the combined pulse into the H_{01} mode delay line and the trailing half straight to the accelerator. The novelty here is that rather than folding the delay line back on itself, it is used to power a distant upstream section of the linac. The delay time required is equal to half the sum of the section filling time and the bunch train length. In Figure 13 the layout of the method is shown.

An equivalent system with a compression factor 2^n can be constructed using 2^n independently phased klystrons. But for practical purposes (reasonable length of the longest delay line) an equivalent scheme with a factor less than 4 is preferable.

The DLDS scheme is the most effective compressor among all the pulse compression schemes introduced above. Since it has an intrinsic efficiency of 100%, a realistic efficiency of about 98% can be achieved in an X-band DLDS system. But for its operation, doubling or even twice doubling the total number of klystrons compared to SLED II or BPC operation, is certainly needed.

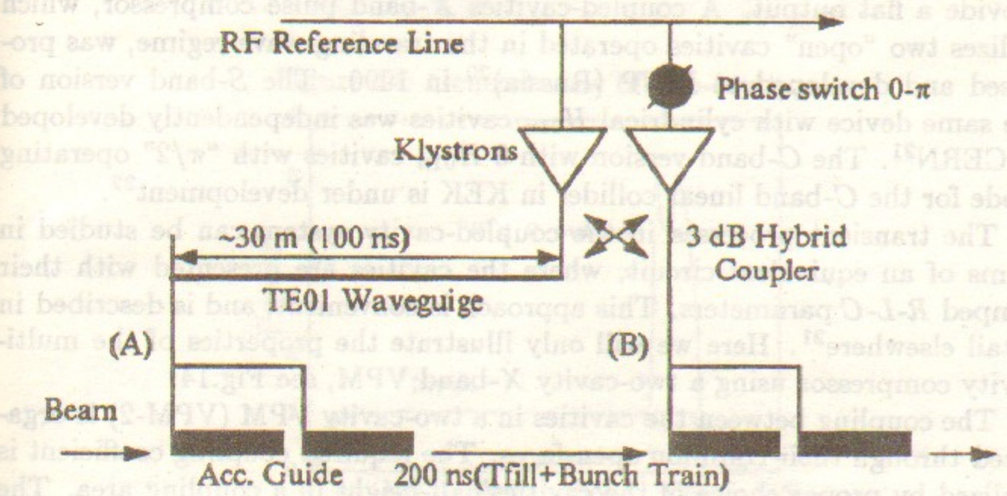

Figure 13: A schematic diagram of the delay line distribution system.

3 Other Approaches

The desire to operate with compact and effective pulse compressors (rather than with delay-line compressors), capable of producing an output pulse suitable for the future collider, is reflected in much of the R&D on some new approaches that use a SLED-type compressor as a base element. With this approach, RF pulse compression can be pursued in two ways:

"Passive", supposing improvement of the SLED storage element.

"Active", externally modulating the klystron drive signal in some way, to compensate for the exponential decay of the standard SLED output pulse. These two ways also can be combined.

In this chapter, the most advanced methods for SLED improvement will be briefly introducted. The main goal of these methods is to correct the shape of the SLED output pulse; they are called Pulse Shape Correction (PSC) techniques.

3.1 Passive PSC Methods

A chain of coupled cavities is well known in radio- engineering as an analogue of the delay line. Thus it can be used in RF pulse compression to provide a flat output. A coupled-cavities X-band pulse compressor, which utilizes two "open" cavities operated in the traveling-wave regime, was proposed and developed at BINP (Russia)[20] in 1990. The S-band version of the same device with cylindrical H_{01n} cavities was independently developed at CERN[21]. The C-band version with 3 H_{01n} cavities with "$\pi/2$" operating mode for the C-band linear collider in KEK is under development[22].

The transient processes in the coupled-cavity system can be studied in terms of an equivalent circuit, where the cavities are presented with their lumped R-L-C parameters. This approach is convenient, and is described in detail elsewhere[21]. Here we will only illustrate the properties of the multi-cavity compressor using a two-cavity X-band VPM, see Fig.14.

The coupling between the cavities in a two-cavity VPM (VPM-2) is organized through their common open faces. The required coupling coefficient is realized by proper choice of the cavities'half-height in a coupling area. The specific feature employed in the VPM-2 is that the cavities'natural frequencies are slightly different. This makes possible the individual tuning of the coupled- oscillation loaded Q-factors of the system, and thus provides an additional opportunity for the fine correction of a compressed output pulse shape. In Fig. 15 the input and output pulses of the 14-GHz VPM-2 are

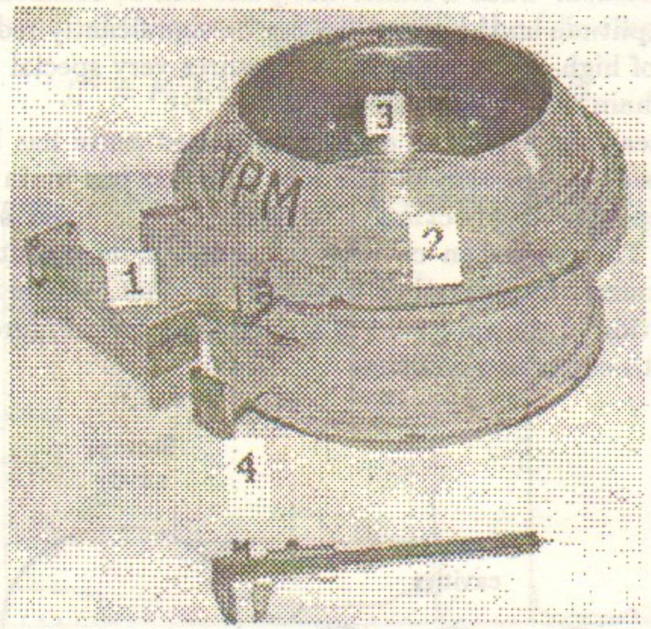

Figure 14: General view of two-cavity.

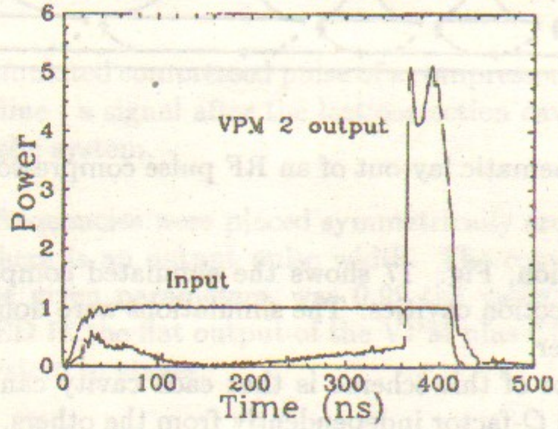

Figure 15: Low power VPM-2 14-GHz VPM. waveforms.

shown. For the same parameters of a storage cavity the compression efficiency of the VPM-2 is the same as for a single-cavity VPM.

Obviously, for further improvement of the pulse shape, more cavities in the chain are needed. Then a rather flat pulse can be realized as the ripples period and amplitude on the pulse top can be significantly reduced. But the large number of high-Q coupled cavities requires very special tuning of each cavity in the chain during operation.

Another means of achieving a flat compressed pulse has been proposed at BINP (Russia) by Kazakov[23]. His idea is to use one main storage cavity and several separate **Correction Cavities** (CC) coupled sequentially by a waveguide. The correction cavities are tuned independently at different frequencies around the operating frequency so that, taken together, they simulate a portion of the spectrum of a long delay line. Figure 16 shows the compressor with correction cavities.

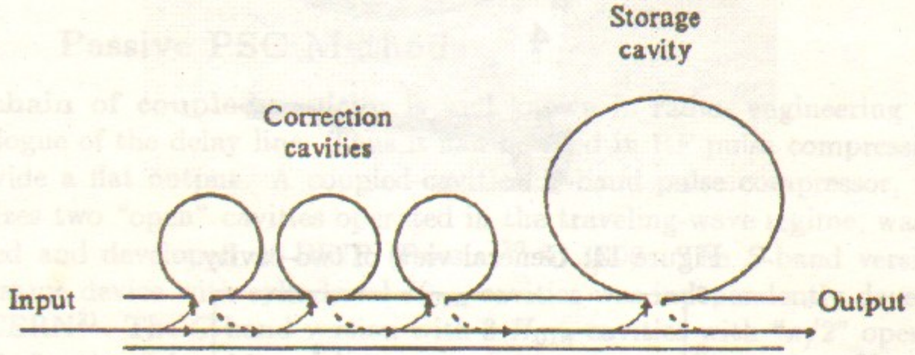

Figure 16: The schematic lay-out of an RF pulse compressor with correction cavities.

As an illustration, Fig. 17 shows the simulated compressed pulse of a VPM with 16 correction cavities. The simulations were done for the VLEPP RF pulse parameter.

The significance of this scheme is that each cavity can be tuned in frequency and loaded Q-factor independently from the others. This means that not only a flat pulse can be constructed, but also a pulse of a given shape, so that the necessary spectrum can be formed. The other important feature of the scheme is that the correction cavities contribution is needed only during the compressed pulse. Thus, compared to the storage cavity Q-factor, the unloaded Q-factor of such cavities can be reduced by a factor equal to

the compression ratio. For example, the following parameters were used for the simulation in Fig.17: for the storage cavity the unloaded Q-factor $Q_{sc} = 2 \times 10^5$, and for the correction cavities $Q_{cc} = 2.5 \times 10^4$, which is smaller by a factor of 8. To avoid parasitic phase deviations of the output pulse, the spectrum of the system was formed in the following way:

$$f_i^{cc} = F_0 \pm i \times 1/T_{out}, i = 1, 2, .., N_{cc}/2 \tag{16}$$

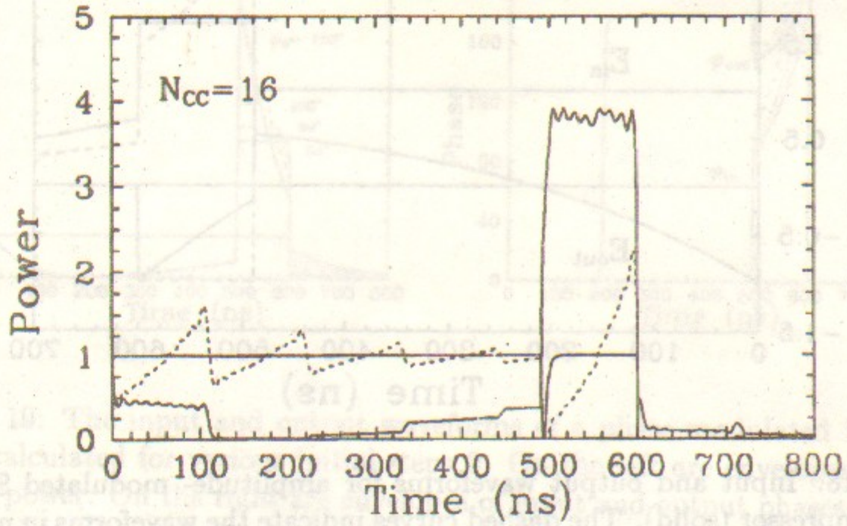

Figure 17: The simulated compressed pulse of a compressor with 16 correction cavities. Dotted line - a signal after the last correction cavity. Solid line - an output signal of the system.

The cavities frequencies were placed symmetrically around the operating frequency. T_{out} here is an output pulse width. The compression efficiency, calculated for the given parameters, was 0.99 the value for a single-cavity VPM. As for SLED II, the flat output of the VPM plus CC makes it possible to cascade the system in stages.

3.2 Active PSC Methods

Amplitude-modulated SLED, theoretically, is the simplest method for achieving a constant amplitude output pulse from an ordinary SLED cavity[24]. The shape of the input pulse may be tailored so that the exponential dive of the emitted field is canceled by a rise in the direct, or reflected wave. If we

need a flat output pulse, the required input modulation is as shown in Fig. 18, where a negative field indicates a π phase shift with respect to the initial input. The standard SLED waveforms are also shown for comparison. The calculations were done for VLEPP pulse parameters.

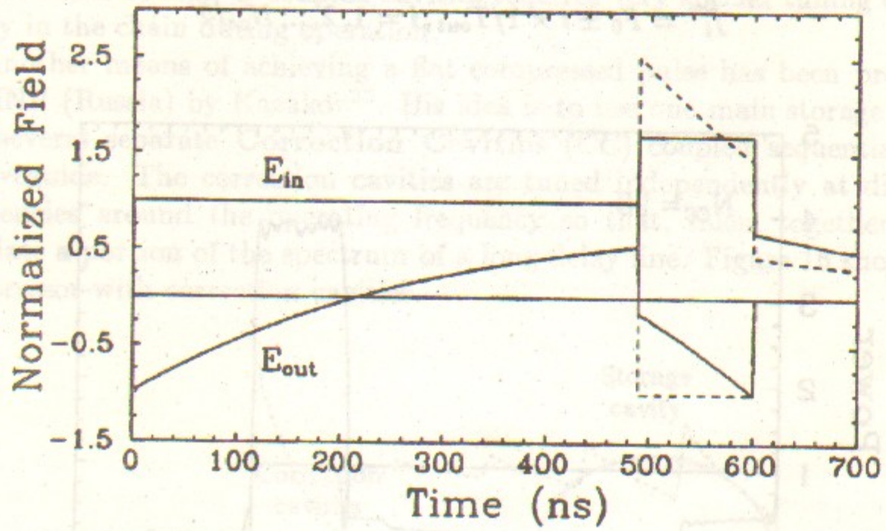

Figure 18: Input and output waveforms for amplitude- modulated SLED-type compressor (solid). The dashed curves indicate the waveforms in normal SLED operation.

The maximal normalized amplitude of the modulated input pulse in Fig. 18 does not exceed 1. This has a practical consideration as usually an RF power source operates below its saturation, or maximum output, level. This limiting condition for the VPM (VLEPP) case brings the efficiency down to 0.6 from 0.72 of standard SLED operation. Thus we see that a heavy price is paid for a flat output pulse. While perhaps of some theoretical interest, amplitude- modulated SLED operation is probably impractical with current microwave source technology.

Phase-modulated SLED is another approach to flattening the output pulse of a SLED-type compressor[24–26]. If we replace the phase switch by a continuous phase modulator, we can try to control the phase of the klystron voltage such that the magnitude of the reflected wave remains constant. In fact, this can be done by starting with a phase step smaller than 180°, which yields a smaller reflected voltage, and then raising the phase continuously until 180° is reached (Fig. 19). After this, of course, the voltage will decay

as in the former case. The length of this flat top depends on its amplitude and on the coupling and Q-factor of the storage cavities. If it is made as long as the compressed pulse, a fully usable rectangular shape is achieved.

The simulation was done for the VPM (VLEPP) parameters. The compression efficiency, for the case of an initial step equal to 90°, was 0.64 (without modulation, 0.72), with 80% fully flat pulse top.

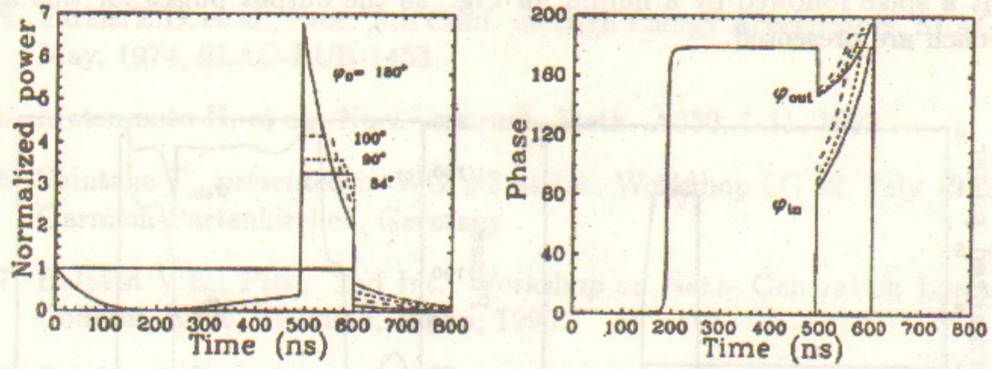

Figure 19: The input and output waveforms of a phase-modulated 14-GHz VPM calculated for various initial steps 0. On the left are envelopes of RF output power. On the right are envelopes of input and output phases. Input phase behavior in is optimized to produce the flat top of a compressed pulse.

Another problem with this approach is that the phase of the output pulse also varies, whereas accelerator applications generally call for a constant phase. Since a constant rate of phase slippage is equivalent to a lowered frequency, the linear part of this variation may be compensated by using a SLED-type system of slightly higher frequency[25]. This frequency shift for the phase slippage amplitude of the compressed pulse $\Delta_{\varphi_{max}}$ is expressed as

$$\Delta f = \Delta F \sin\theta_0 \sin\frac{\Delta\varphi_{max} D}{2L}, \qquad (17)$$

where ΔF is a passband of the acceleration structure, θ_0 is phase advance per cell, D and L are structure period and structure length. For the 14-GHz VLEPP structure for the case of a phase-modulated VPM with initial phase step 90°, the desired frequency shift is $\Delta f = 1.45$ MHz. This reduces the total phase variation from 45° to less than 8°.

Further optimization might improve the situation slightly, but it is clear that the efficiency and feasibility of this method depend strongly on how much amplitude droop and phase variation can be tolerated for a given application.

Finally we will introduce the **Hybrid method**, which combines the features of passive and active PSC approaches. As an example we present a phase-modulated two-cavity VPM[27]. In this case the phase modulation is applied to linearize not a sharp exponential dive of the compressed pulse, but a spike followed by a hump. in Fig. 20 the output pulses for this approach are presented.

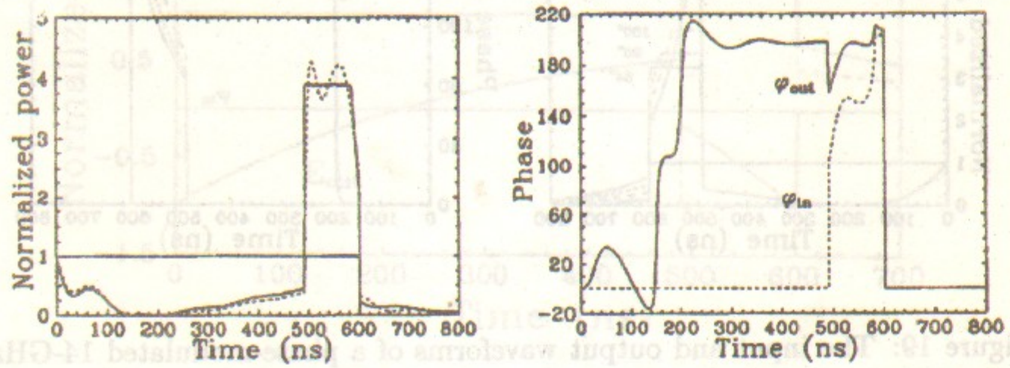

Figure 20: The amplitude and phase waveforms of the two-cavity phase-modulated VPM.

The compression efficiency of this method is 0.69, 3% less than for a single-cavity VPM without modulation. Using frequency-shifting as in the previous method, the phase variation of the output was suppressed to less than 5°.

A hybrid method with an amplitude-modulated three-cavity SLED-type compressor is intended to be used in C-band JLC (KEK, Japan) in order to tune the shape of the compressed pulse in a special way[22].

Acknowledgments

The author would like to thank Prof. V.E. Balakin for stimulating discussions and S. Kazakov for reading the manuscript.

Bibliography

1. Caryotacis G., Proc. Int. Work-shop RF 96, April 1996, Hayama, Kanagawa, Japan (to be published).
2. Brix D.L. and Scalapino D.J., IEEE Trans. Magn. MAG- 15, 33, 1979.
3. Alvarez R.A. et al, J. Part. Acc. 11, 125-130,1981.
4. Farkas Z.D. et al., Proc. 9th Conf. on High Energy Accelerators, SLAC, May, 1974, SLAC-PUB-1453.
5. Matsumoto H. et al., Nucl. Instrum. Meth. A330, 1-11, 1993.
6. Shintake T., presented in WG #3 at Int. Workshop LC 92, July 1992, Garmish-Partenkirchen, Germany.
7. Balakin V.E., Proc. 2nd Int. Workshop on Next- Generation Linear Collider, KEK, Tsukuba, Japan, 1990.
8. Balakin V.E. and Syrachev I.V., Proc. 3rd Int. Workshop on Next Generation Linear Collider, Branch INP, Protvino, Russia, 1991, pp. 145-156.
9. Vainstein L.A., High Power Electronics 3, pub. "Nauka", 170-215, 1964, (in Russian).
10. Syrachev I.V., Vogel V.F., Mizuno H., Odajiri J., Otake Y., and Tokumoto S., Proc. Int. Conf. Linac-94, Tsukuba, Japan, 1994, pp. 475-477.
11. Yamaguchi S. et al., Proc. Int. Conf. Linac-94, Tsukuba, Japan, 1994, pp. 478-480.
12. Fiebig A. and Schieblich Ch., Proc. European Part. Accel. Conf., Rome, Italy,1988, pp. 1075-1077.
13. Wilson P.B., Farkas Z.D. and Ruth R.D., Proc. Linear Accel. Conf., Albuquerque, NM, 1990, SLAC-PUB-5330.
14. Vlieks A.E. et al., Proc. 6th Int. Workshop LC95, March 1995,Tsukuba, Japan, pp. 1049-1058.
15. Vlieks A.E. et al., Proc. 6th Int. Workshop LC95, March 1995,Tsukuba, Japan, pp. 1059-1065.

16. Tantawi S.G. et al., SLAC-PUB-95-6827, 1995.

17. Farkas Z.D., SLAC-PUB-3694, 1985.

18. Lavine T.L. et al., SLAC-PUB-5451, 1991.

19. Mizuno H. and Otake Y., Proc. 17th Int. Linac Conf., Tsukuba, Japan, 1994, pp. 463-465.

20. Balakin V.E. and Syrachev I.V., Proc. 3rd European Part. Accel. Conf., Berlin, Germany, 1992, pp. 1173-1175.

21. Fiebig A., CERN, PS/RF/Note. 91-12, 1991.

22. Shintake T., Proc. Int. Workshop RF 96, April 1996, Hayama, Kanagawa, Japan (to be pubished).

23. Kazakov S.Yu., Proc. 3rd European Part. Accel. Conf., Berlin, Germany, 1992, pp. 1247-1248.

24. Nantista C.D., SLAC-Report-95-455, pp. 155-163, 1995.

25. Fiebig A. and Schieblich Ch., Proc. 2nd European Part. Accel. Conf., Nice, France, 1990, pp. 937-939.

26. Syrachev I.V., Proc. 4th European Part. Accel. Conf., London, UK, 1994, pp. 375-379.

27. Syrachev I.V., Proc. 1st Int. Workshop on Pulsed RF Sources for Linear Colliders, Dubna, Russia, 1993, pp. 351- 356.

ОБЪЕДИНЕННАЯ USA–CERN–JAPAN
УСКОРИТЕЛЬНАЯ ШКОЛА –
ВЧ ТЕХНИКА ДЛЯ УСКОРИТЕЛЕЙ
(9–18 сетября 1996 г., Япония)

ЛЕКЦИИ, ПРОЧИТАННЫЕ СОТРУДНИКАМИ
ИЯФ СО РАН

Ответственный за выпуск А.М. Кудрявцев
Работа поступила 10.07.1997 г.

Сдано в набор 20.07.1997 г.
Подписано в печать 10.08.1997 г.
Формат бумаги 60×90 1/16 Объем 5.8 печ.л., 4.6 уч.-изд.л.
Тираж 150 экз. Бесплатно. Заказ N 66.

Обработано на IBM PC и отпечатано на
ротапринте ГНЦ РФ "ИЯФ им. Г.И. Будкера СО РАН",
Новосибирск, 630090, пр. академика Лаврентьева, 11.